Physical Layer Network Coding for M-QAM MIMO Systems

Bismark Okyere

School of Computer Science and Electronic Engineering
University of Essex

This dissertation is submitted for the degree of
Doctor of Philosophy

CSEE August 2022

I would like to dedicate this thesis to my family

Declaration

I hereby declare that this thesis is my own work and has not been submitted in any form for another degree or diploma at any university or other institute of higher education.

I certify that to the best of my knowledge, the intellectual content of this thesis is the product of my own work and that all the assistance received in preparing this thesis and sources have been acknowledged.

Bismark Okyere

August 2022

Acknowledgements

I would like to thank my supervisor, Prof. Leila Musavian, for giving me the opportunity to work with her on this interesting topic. I have learnt a lot doing research under her guidance and I will not be at this stage of the PhD work without her relentless support. I would also like to acknowledge my co-supervisor, Prof. Shahid Mumtaz, for his mentorship in an EU project I had the opportunity to be involved in.

Through this PhD program, I have had the opportunity to collaborate with other top researchers from other institutes and universities and I would like to thank all of you for your support, the experience and the knowledge shared.

Last, but not least, I celebrate my family for the emotional support in difficult times of the thesis, coupled with the stress that came along with COVID-19 pandemic. My daughter was born around the time I had enrolled in the PhD program and seeing her grow everyday always reminds me of how I far I have come in the PhD work. She has been a constant inspiration for me.

Thank you.

Abstract

The aim of this thesis is to design, implement and assess a practical Physical Layer Network Coding (PNC) scheme in multi-user massive Multiple-Input Multiple-Output (MIMO) systems utilizing M-ary Quadrature Amplitude Modulation (M-QAM). PNC is a new technology that is gradually becoming one of the most sought after, as it has the potential to increase network capacity, whilst ensuring that the spectrum is also efficiently used. One of the design goals is to ascertain if combining PNC and massive MIMO is even possible. In accomplishing this goal in a multi-user cellular system with a centralized base station relaying bi-directional communication of M-QAM symbols among user equipment (UEs), a formulation of PNC mapping scheme as a function of clusters of sum and difference (SD) of transmitted symbols from the antennas of the UE pairs is pursued. The simulation results reveal that the proposed PNC scheme achieves twice the spectral efficiency in massive MIMO, without altering the latter's underlying framework and without any degradation in the bit-error-rate (BER).

Having established the feasibility of combining PNC and massive MIMO, an evaluation of the proposed scheme against jamming attack is carried out and the simulation results reveal the resilience of the scheme against a barraging jamming noise signal, yet with an increase in spectral efficiency (SE). In addition, extension of the proposed PNC scheme together with Index modulation (IM), a physical layer technique that increases energy efficiency (EE) by utilizing fewer resources to transmit, is designed, implemented and evaluated. The simulation results reveal that combining PNC and IM creates a good balance between EE and SE.

Table of contents

List of figures

List of tables

Nomenclature

Acronyms / Abbreviations

5G 5th Generation

AoD Angle of Departure

AWGN Additive White Gaussian Noise

B5G Beyond 5G

BER Bit Error Rate

bpcu Bits per Channel Unit

bps Bits per Second

BPSK Binary Phase-Shift Keying

CSI Channel State Information

DoS Denial of Service

EE Energy Efficiency

FEC Forward Error Correction

GHz Giga Hertz

IM Index Modulation

ISI Inter-Symbol Interference

LLR Log-Likelihood Ratio

LoS Line of Sight

LUE Legitimate UEs

M-QAM M-ary QAM

MAP Maximum Aposteriori

MIMO Multiple-Input Multiple-Output

MISO Multiple Input Single Output

MLE Maximum Likelihood Estimator

ML Maximum Likelihood

MMSE Minimum-Mean Square Error

nLoS None Line of Sight

OFDM Orthogonal Frequency Division Modulation

PHY Physical Layer

PLS Physical Layer Security

PNC Physical Layer Network Coding

QAM Qaudrature Amplitude Modulation

QPSK Quadrature Phase Shift Keying

RF Radio-frequency

SD Sum Difference

SE Spectral Efficiency

SIMO Single Input Multiple Output

SINR Signal-to-Interference plus Noise Ratio

SISO Single Input Single Output

SJNR Signal-to-Jamming plus Noise Ratio

SJR Signal-to-Jamming Noise Ratio

SM Spatial Modulation

SNR Signal to Noise Ratio

STC Space-Time Coding

SVD Singular Value Decomposition

TWRC Two-Way Relay Channel

UE User Equipment

ULA Uniform Linear Array

ZF Zero-Forcing

Chapter 1

Introduction

1.1 Motivation

An insatiable demand for network capacity to support high data rate services such as high speed internet and multimedia applications has led to the evolution of the wireless communication systems. These evolved systems must provide solutions for constraints not only limited to capacity and data rate but also existing key performance indicators (KPI), such as, network coverage, reliability, energy efficiency (EE), latency and spectral efficiency (SE). Some of these challenges can be addressed through the use of massive Multiple-Input Multiple-Output (MIMO) and Beamforming [1, 2].

The wireless communication era beyond 5G (B5G) is expected to be augmented by novel enabling technologies. However, because it takes time to research into new technologies, develop, test and deploy, in the interim or even long term, a mix of existing technologies would still be sought after to satisfy the crunching requirements beyond 5G. The wireless medium is expected to continue to be interference limited. Beyond 5G, there will be a plethora of transmission technologies coexisting and efficiently using the existing sub-6GHz spectrum and the new spectrum such as the millimeter-Wave (mmWave) and the Terahertz (THz) bands. New technologies would have to have interference mitigation mechanisms as part of their underlying architectures in order to coexist with other technologies. This makes Physical Layer Network Coding (PNC) [3], a physical-layer technique that operates

without any interference mitigation by leveraging on the decoding techniques that isolate the individual symbols from interfered symbols, key beyond 5G.

Most of the interference in the current wireless systems are what would be termed "friendly" interference. These are interference that occur as a result of multiple communication entities trying to use the wireless medium at the same time. The intent is though, not to sabotage the communication systems. However, there are some interference in the wireless medium, and their intent are to prevent any communication system from operating normally - meaning, making it difficult for the receiving nodes in the communication system to properly decode messages received from peer nodes. Such uncontrolled interference fall into the category of denial-of-service (DoS) attack and is often referred to as radio-frequency (RF) jamming [4, 5]. RF jamming is a malicious attempt to overwhelm a wireless communication system with the objective of sabotaging the normal operation of the network. Again, PNC is a key physical layer technique that has the potential to withstand jamming attack.

Although PNC addresses SE, allowing multiple nodes to transmit at the same time without any interference mitigation, EE is rather over overlooked. Forexample, massive MIMO is poised to offer high SE, as massive number of antennas at the base station are able to accommodate large number of communications from a multitude of devices, ensuring that the spectrum is utilized efficiently and massively. In the case of Ultra-reliable low-latency communications (URLLC), which is an important usecase introduced in 5G to cater for services that require high reliability and very low end-to-end latency, EE may not always be ensured. URLLC applications that include mission-critical applications such as industrial automation, remote surgery, intelligent transportation systems, smart grids, just to name a few would have miniature devices or sensors, whose life span extends whenever they are not always powered on. Therefore, there is the need to ensure their source of energies are efficiently utilized. Besides reliability and latency, the performance of a URLLC based system is driven by these two KPIs: SE and EE. A highly performing URLLC communication system should undoubtedly have high values of these KPIs. Unfortunately, these two KPIs are conflicting. An increase in EE compromises the SE and the vice versa. Finding a good balance between these two metrics is therefore challenging. However, this challenge

can be tackled with Index Modulation (IM) technique [6]. In IM, only a subset of the communication resources (time/frequency/space/code sequence) is activated to transmit information by conventional modulations, whilst the resource activation pattern also carries further information. Using only part of the resources to transmit, yet conveying more information increases EE.

Considering that both massive MIMO and PNC ensure high SE and IM offering high EE, the lingering question is whether these three physical layer techniques can be accommodated into a single solution to provide a good balance between EE and SE, or even provide high EE beyond what the individual techniques would have offered. Incorporating PNC means that interference mitigation mechanisms might not be required. Integrating this into a massive MIMO system will yield high capacity gain, and with IM, few resources in the massive MIMO system would be utilized, including resources available to the device, and therefore their energies could be efficiently managed. A major research question here is if an integrated system of massive MIMO and PNC and/or IM is even feasible and if feasible, whether the error performance will be as a good as what the individual schemes offer.

1.2 Thesis Contributions

The aforementioned challenges above are now factored into the following key objectives for this thesis:

1. To design and develop a practical joint massive MIMO and PNC scheme that allows PNC to be deployed in massive MIMO systems and furthermore, analyse the performance of the combined massive MIMO and PNC, hereinafter, referred to as massive MIMO PNC;

2. To design and develop a joint massive MIMO PNC and IM and analyse its error performance;

3. And to ascertain the extent to which massive MIMO PNC shields a communication system against a barraging jamming attack.

PNC has traditionally been researched along the lines of point-to-point relay communication systems between a relay and two communication nodes and most of the PNC mapping schemes have been proposed along these lines. Because PNC in MIMO or massive MIMO systems is fairly new, the contributions in the thesis work in addressing the aforementioned objectives are the following:

1) Designed a PNC mapping scheme that is tailored to the complexity of increasing the number of antennas at the base station as well as the communication nodes, henceforth, called user equipment (UEs). Here, we propose of an extension of a scheme presented in [7]. In [7], the authors presented a basic PNC mapping scheme, that is based on the summation and difference of the constellation values of the Binary Phase-shift keying (BPSK) modulated symbols in a 2×2 MIMO system. We affirm that the summation and difference constellation symbols lead to unique set of PNC symbols. However, if we were to demonstrate the full potential of PNC in MIMO systems, then the log-likelihood ratio (LLR) algorithm used in [7] will not work in systems with large number of antennas and with nodes transmitting high order modulation symbols, such as the M-ary Quadrature Amplitude Modulation (M-QAM). Instead, we use Maximum Aposteriori (MAP) estimation to derive the summation and difference of the interfered symbols contributed by the large number of receiving antennas at the base station.

The publication addressing this contribution is the following:

- **B. Okyere**, L. Musavian and R. Mumtaz, "Performance Analysis of Physical Layer Network Coding in Massive MIMO Systems With M-QAM Modulations," in IEEE Transactions on Vehicular Technology, vol. 70, no. 5, pp. 4631-4645, May 2021.

2) Developed a generalized PNC mapping scheme for any number of antennas and any order of the M-QAM and further simplified the derived mathematical formulations for the mapping functions. This work is concluded by assessing the bit-error-rate (BER) of the detection of the summation and difference of the received symbols using Zero-Forcing (ZF) and Minimum-Mean Square Error (MMSE) detection schemes.

The publications addressing this contribution are the following:

- **B. Okyere**, L. Musavian and R. Mumtaz, "Performance Analysis of Physical Layer Network Coding in Massive MIMO Systems With M-QAM Modulations," in IEEE Transactions on Vehicular Technology, vol. 70, no. 5, pp. 4631-4645, May 2021.

- **B. Okyere**, L. Musavian and R. Mumtaz, "Multi-User Massive MIMO and Physical Layer Network Coding," 2019 IEEE Globecom Workshops (GC Wkshps), 2019, pp. 1-6.

3) We then explored further on determining how resilient a PNC communication system is to jamming attack. We propose of a MIMO PNC system model that includes a jammer. The jammer sends a barraging jamming signals of noise with the intent of circumventing the capability of the legitimate users' to correctly decode received symbols. Through Monte-Carlo simulation, the error performance is evaluated between our massive MIMO PNC scheme and a jammer and the traditional MIMO with jammer. The results depict that our proposed PNC scheme performed considerable well in the midst of jamming noise signals, as opposed to the traditional MIMO.

The publications addressing this contribution are the following:

- **B. Okyere**, L. Musavian and R. Mumtaz, "Performance Analysis of Physical Layer Network Coding in Massive MIMO Systems With M-QAM Modulations," in IEEE Transactions on Vehicular Technology, vol. 70, no. 5, pp. 4631-4645, May 2021.

- **B. Okyere**, L. Musavian, B. Özbek, S. A. Busari and J. Gonzalez, "The Resilience of Massive MIMO PNC to Jamming Attacks in Vehicular Networks," in IEEE Transactions on Intelligent Transportation Systems, vol. 22, no. 7, pp. 4110-4117, July 2021.

- **B. Okyere**, L. Musavian, R. Mumtaz and J. Gonzalez, "The Resilience of MIMO Based Physical Layer Network Coding to Jamming Attack," 2020 IEEE International Conference on Communications Workshops (ICC Workshops), 2020, pp. 1-5.

4) The last contribution in this work is the fusion of MIMO-PNC and IM. Index Modulation's capability to enable a subset of the communication resources, which include transmit

antennas, spectrum sub-carriers, time slot, among others, and conveying additional information just from detecting the indices of the activated subset of radio resources, whilst saving some energy, makes it a compelling physical layer technique that efficiently uses the spectrum. Since MIMO-PNC provides some degree of EE, a robust fusion of PNC and IM, goes a greater degree to strike a good balance between EE and SE. In our contribution, we combined our proposed massive MIMO-PNC scheme with IM and the performance was quite good. However, further research is needed on the decoding part of the combined PNC-IM in order to elevate the performance to be as close as possible to practically being used in real communication systems. But the combination of these two physical layer techniques are feasible, as we have proved, and with improved error performance, B5G usescases and applications such as URLLC could be developed in energy efficient way.

The publication addressing this contribution is the following:

- **B. Okyere**, L. Musavian, B. Özbek, S. A. Busari and J. Gonzalez, "A Novel Joint Index Modulation and Physical Layer Network Coding Mechanism for Beyond 5G," in IEEE Communications Standards Magazine, vol. 5, no. 2, pp. 100-105, June 2021.

1.3 Thesis Outline

Chapter 2 introduces the core concept of the thesis. It starts by introducing multi-antenna systems, outlining the revolution from MIMO to massive MIMO. The multiplexing and diversity techniques of MIMO are illustrated and comparisons are made among different antenna configurations such as Single Input Single Output (SISO), Single Input Multiple Output (SIMO) and Multiple Input Single Output (MISO). Multi-user MIMO is also introduced briefly to lay down the foundation for massive MIMO. In the end, linear detection techniques for massive MIMO, the advantages and disadvantages are also presented. These linear detectors are the underlying detection techniques for the proposed work described in Chapter 3.

Chapter 3 describes the design of the proposed massive MIMO PNC scheme. A multi-user system model is identified and the detection of the sum and difference of the transmitted

symbols from the interfered symbols using ZF and MMSE is formulated and the PNC mapping functions, based on the order of the M-QAM are presented and simplified. Simulation results based on a multi-user massive MIMO PNC system is presented and the results show that our proposed scheme, besides achieving twice the spectral efficiency of the MIMO system, has a better error performance compared to the traditional massive MIMO.

In Chapter 4, we present the assessment of the jamming attack on a PNC system, with our proposed MIMO-PNC scheme as the underlying framework. This contribution was primarily simulation work, so the system model is presented and the simulation approach is outlined. The results are analysed and presented. The results show that our proposed MIMO-PNC scheme withstood the barraging jamming attack. We considered both sub-6GHz (Rayleigh fading) and mmWave.

Chapter 5 describes the approach of the fusion of MIMO-PNC and IM. In this work, we focus on Spatial Modulation (SM), and therefore, a system model with this as a requirement is presented. The building blocks of the system model are described in detail. Simulation results are presented and the error performance is analysed. As presented in the contribution section above, the performance could further be improved by implementing an IM detector that is closely aligned with the fusion of MIMO-PNC and IM.

We end the thesis with a conclusion chapter. In Chapter 6, we summarize the various contributions, the rationale, goals and the benefits as well as the proposed future derivative works.

1.4 Publications

Journal papers

1. **B. Okyere**, L. Musavian, B. Özbek, S. A. Busari and J. Gonzalez, "The Resilience of Massive MIMO PNC to Jamming Attacks in Vehicular Networks," in IEEE Transactions on Intelligent Transportation Systems, vol. 22, no. 7, pp. 4110-4117, July 2021.

2. **B. Okyere**, L. Musavian and R. Mumtaz, "Performance Analysis of Physical Layer Network Coding in Massive MIMO Systems With M-QAM Modulations," in IEEE Transactions on Vehicular Technology, vol. 70, no. 5, pp. 4631-4645, May 2021.

3. **B. Okyere**, L. Musavian, B. Özbek, S. A. Busari and J. Gonzalez, "A Novel Joint Index Modulation and Physical Layer Network Coding Mechanism for Beyond 5G," in IEEE Communications Standards Magazine, vol. 5, no. 2, pp. 100-105, June 2021.

Conference papers

1. **B. Okyere**, L. Musavian and R. Mumtaz, "Multi-User Massive MIMO and Physical Layer Network Coding," 2019 IEEE Globecom Workshops (GC Wkshps), 2019, pp. 1-6.

2. **B. Okyere**, L. Musavian, R. Mumtaz and J. Gonzalez, "The Resilience of MIMO Based Physical Layer Network Coding to Jamming Attack," 2020 IEEE International Conference on Communications Workshops (ICC Workshops), 2020, pp. 1-5.

Chapter 2

The Fundamentals of the Core Concepts

2.1 MIMO

MIMO, is a multi-antenna [8–10] physical layer technology, that refers to a collection of signal processing techniques that use multiple antennas at the transmitter, receiver, or both to improve on the performance of the wireless communication systems by either combating or exploiting multi-path propagation in the communications medium between the transmitter and receiver [11]. Multiple antennas at the transmitter and receiver introduce spatial degrees of freedom, and this can be exploited either through diversity or multiplexing [12]. Creating diversity in the spatial domain can facilitate in combating against multi-path propagation fading issues. Therefore the study of MIMO has always been on the lines of spatial diversity and spatial multiplexing techniques.

Although the motivation of multi-antenna technology was founded based on spatial multiplexing, the antenna diversity at either the transmitter or the receiver has paved way in overcoming multi-path propagation issues, such as fading [13]. Due to the scattering of signals in the propagation medium, the transmitted signal tends to split up into different replicates and each moving across independent fading channels. When multiple replicas of the same information are sent across independently fading channels, the intensity of the fading experienced by each replica of the transmitted signal is different. The different replicas, but the same signal, arrive at the receiver at different times and with different phases

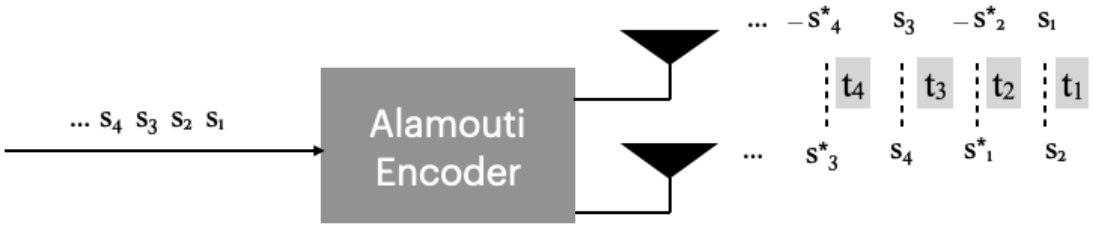

Fig. 2.1 Alamouti STBC

and also different angle of arrival. Since the signal strength of each of the replicas would have deteriorated over some distance to the receiver, having multiple of them at the receiver, and with effective combining techniques, the replicas could be constructively combined for the actual transmitted signal to be detected. This guarantees that at least one of the replicas will suffer less fading compared to the rest. Thus, the chance of properly receiving the transmitted data increases because of the diversity. Notable combining techniques include selection combining, maximal ratio combining, and equal-gain combining [14]. MIMO's spatial diversity leverages on the multi-path propagation phenomenon by artificially transmitting the same signals on different antennas. At the receiver, even in non-rich scattering environment, the replicated signals on the different antennas traverse over independent fading channels increasing the reliability of detecting the original signal from the replicas. Space-Time Coding (STC) allows the same information to be transmitted at the same time from different transmit antennas, and as a result, attain transmit diversity. It is a coding technique that is performed in both spatial and temporal domains to create replicas of signals transmitted from various antennas at different time slots. The spectrum can still be efficiently utilized, whilst using STC to achieve transmit diversity and power gain over spatially uncoded systems. Space-Time Trellis Codes (STTCs) and Space-Time Coding Codes (STBCs) are some of the notable STC schemes. STTC is a coding technique that promises full diversity and significant coding gain, however at the cost of high decoding complexity. Alamouti coding was introduced under STBC to overcome the decoding complexity and is well known for being one of the few STC schemes that achieve full diversity and full data rate for two antenna system. Depending on the time slot, the Alamouti encoder takes M-ary modulated

symbols as depicted in Fig. 2.1. The Alamouti encoded symbol is transmitted from the two transmit antennas over two time slots. In the first time slot, t_1, the symbols s_1 and s_2 on the first and second antennas respectively are transmitted. In the second time slot, t_2, the same symbols, but this time, the negative conjugate of s_2, $-s_2^*$, and the conjugate of s, s_1^* are respectively transmitted on antennas 1 and 2. This can be represented as a matrix as follows:

$$\mathbf{S}(\textbf{Alamouti}) = \begin{bmatrix} s_1 & s_2 \\ -s_2^* & s_1^* \end{bmatrix}_{2\times 2}. \tag{2.1}$$

Evidently, the encoding is performed on both spatial and temporal domains, with the rows of the matrix representing the time slots and the columns representing the symbols transmitted at each time slot. The rows and columns of $\mathbf{S}$ are orthogonal, and i.e. $\mathbf{S}\mathbf{S}^H = \alpha\mathbf{I}_2$. As a result of the orthogonality, linear signal processing equalizers can be deployed at the receiver to detect s_1 and s_2.

Multiplexing of transmitted signals in wireless communication system is founded on the concept of dividing data streams into layers and transmitting each layer through independent space. Spatial multiplexing is based on this concept. In MIMO systems, when the information bits are modulated into symbols, based on the number of antennas at the transmitter, the symbols are grouped into blocks accordingly. Spatial multiplexing leverages on the differences in the channels between transmitting and receiving antenna pairs to create multiple independent streams between the transmitting and receiving antennas, increasing throughput by sending different data over parallel streams. At the receiver, each of the received signals at each antenna consists of the sum of the transmitted signals from all of the transmit antennas. However, in spatial multiplexing, and in the scattering rich transmission environment, several independent sub-channels are generated in the same spectrum. In this regard, the multiplexing gain comes at no additional cost on bandwidth or power. The degree of freedom is often synonymous to the multiplexing gain in the signal space constellation [15]. If M is the number of transmit antennas and N, the number of receive antennas, then the number of degrees of freedom in this multiple antenna configuration is equal to $min(M,N)$. The degree of freedom influences the overall capacity of the system. Fig. 2.2 a) - Fig. 2.2

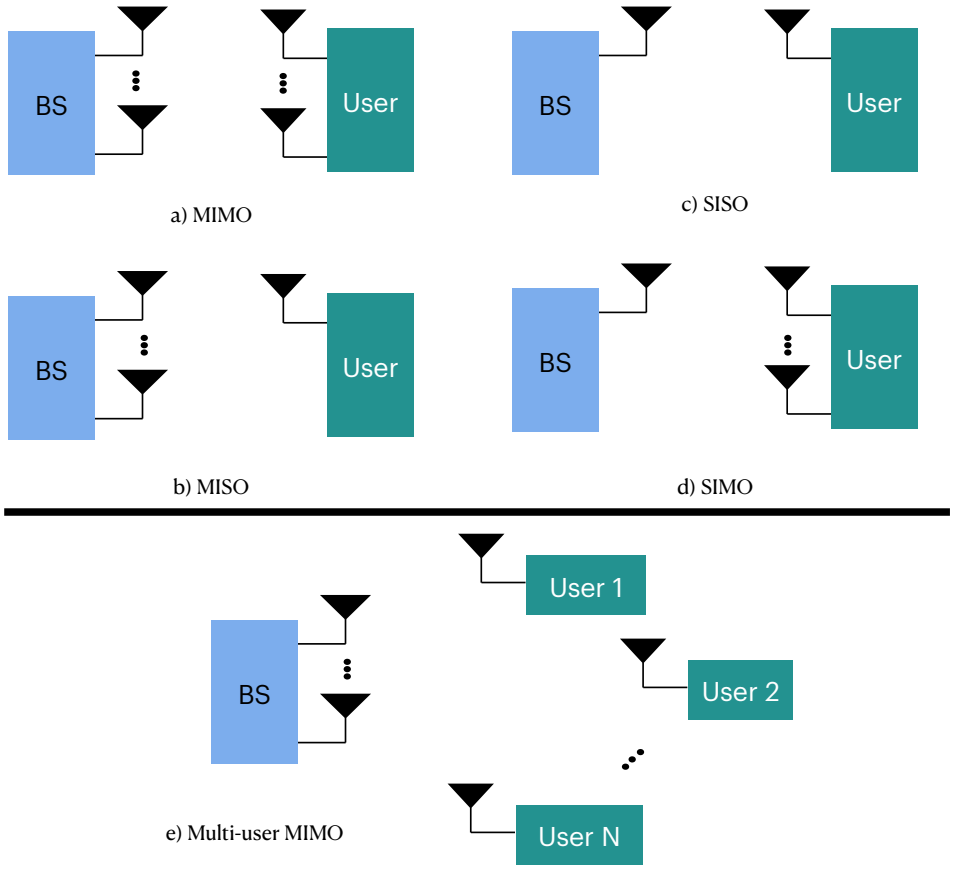

Fig. 2.2 Antenna configurations

d) depict the various antenna configurations that multi-antenna systems can adopt. Each of these configurations achieve different diversities and multiplexing or capacity gains. Among the different configurations, the Single Input Single Output (SISO) in Fig. 2.2 c), exhibits the worst of the diversity gains. The capacity of such a system is given by [16]

$$C(\text{SISO}) = \log_2(1 + SNR|h|^2) \text{ bps/Hz}, \tag{2.2}$$

where SNR is the signal to noise ratio and h, the complex channel gain between the transmit and the receive antennas. There is no receive or transmit diversity gain. However, in the case of the Single Input Multiple Output (SIMO) in Fig. 2.2 d), where there is a single antenna at the transmitter and multiple antennas at the receiver, the receiver diversity gain increases, and the capacity is given as [15]

$$C(\text{SIMO}) = \log_2(1 + SNR\sum_{i=1}^{\text{N}}|h_i|^2) \text{ bps/Hz}, \tag{2.3}$$

where h_i, the complex channel gain between the transmit antenna and each of the receive antennas. The main difference between the SISO and SIMO antenna configurations is that the latter's capacity is dependent on the logarithmic of the number of antennas at the receiver, leading to a high capacity gain than the SISO. It also has a higher receive diversity gain.

It is also possible to have a diversity at the transmitter as shown in the configuration for the Multiple Input Single Output (MISO), depicted in Fig. 2.2 b). The transmitter can then send multiple but different streams at the same time to a single receive antenna. A detector at the receiver should be able to isolate the different streams in the equalizer. The capacity of a MISO system is given as [15]

$$C(\text{MISO}) = \log_2(1 + SNR\sum_{i=1}^{\text{M}}|h_i|^2) \text{ bps/Hz}. \tag{2.4}$$

The MISO unfortunately, does not have any multiplexing gain, but does have a higher diversity gain at the transmitter.

The MIMO configuration in Fig. 2.2 a) rather overcomes the limitations of the other antenna configurations by having many antennas at the transmitter as well as the receiver, providing enough diversity as much as multiplexing gain. The capacity of such a system is given as [15]

$$C(\text{MIMO}) = \log_2 \left[\det(\mathbf{I}_N + \frac{SNR}{M} \boldsymbol{H}\boldsymbol{H}^{\text{H}}) \right] \text{ bps/Hz}, \tag{2.5}$$

where $\mathbf{I}_N$ is the identity matrix of dimension $N \times N$ and $\boldsymbol{H}$, an i.i.d complex channel matrix of dimension $M \times N$ and $(\cdot)^{\text{H}}$, the conjugate transpose. The capacity can be computed by decomposing the vector channel into a set of parallel, independent scalar Gaussian sub-channels using singular value decomposition (SVD). If the diagonal element of the SVD decomposed $\boldsymbol{H}$ has the same eigenvalues, then MIMO capacity is reduced to [15]

$$C(\text{MIMO}) = \min(M,N)\log_2(1+SNR) \text{ bps/Hz}. \tag{2.6}$$

Equation (2.6) is an important one, because it shows that the MIMO capacity as a factor of the minimum between the transmit and and receive antennas, and is higher than the capacity of the SISO or MISO antenna configurations.

2.1.1 Multi-user MIMO

The multi-antenna configurations in Fig. 2.2a) - 2.2d) are largely point-to-point and just between two entities, one as the transmitter and one as the receiver. In practical communication networks such as cellular networks [17], a base station could serve multiple users making such point-to-point antenna configurations impractical. The configuration that typifies the services provided by cellular network is the Multi-user MIMO [14, 18, 19]. The strategy of using several antennas at the base station to serve multiple users is called Multi-user MIMO communications. This communication system exploits the spatial degree of freedom in order to multiplex multiple users simultaneously and utilizing the same spectrum. This is achieved by having multiple number of antennas at the base station and this strategy leads to significant

gains in capacity and diversity as multiple antennas can be used to transmit many streams of information, but for different users, at the same time or in most cases where the channel is compromised with lower bit error rate, the same stream of information is repeated several times on the different antennas.

2.1.2 Massive MIMO

Although the spatial domain is utilized by MIMO, it has not been extensively exploited as it should be. To extensively utilize the spatial domain is to have a large swath of antennas. This is termed massive MIMO. Massive MIMO is basically the extension of MU-MIMO, by deploying a large array of antennas at the base station to serve a sizeable number of users. Since its conception [20], it has received significant amount of attention [21–23], because its large array of antennas increases the multiplexing gain, allowing many number of users to be served at the same time. The multiplexing gain increases throughput and the capacity of the system. In 5G, massive MIMO is one of the key technologies [1, 24], and it will continue to pave way for services that require high throughput, even beyond 5G, as depicted in Fig. 2.3. In the shorter wavelength of the electromagnetic spectrum, such as mmWave [25], not only would the base station be able to stack up large number of antennas together, but also in the user device, which traditionally, has had limited number of antennas. The mmWave spectrum facilitates stacking up large number of miniature antennas together to form a giant array antenna.

Energy efficiency is another relevant benefit of massive MIMO [26]. Beamforming is a spatial filtering technique that enhances transmitted signals to a desired direction and suppresses noise and interference to other directions [27–29]. Beamforming is achieved by controlling the phase and the relative amplitude of the signal at each transmit antenna in order to create constructive and destructive interference in the wavefront. The goal is to make the constructive part as directional as possible with the strongest beam, whereas the destructive has significantly lower power. The larger the number of antennas, there more localised the transmitted beam and the less interference transmitted signals impose on the communication

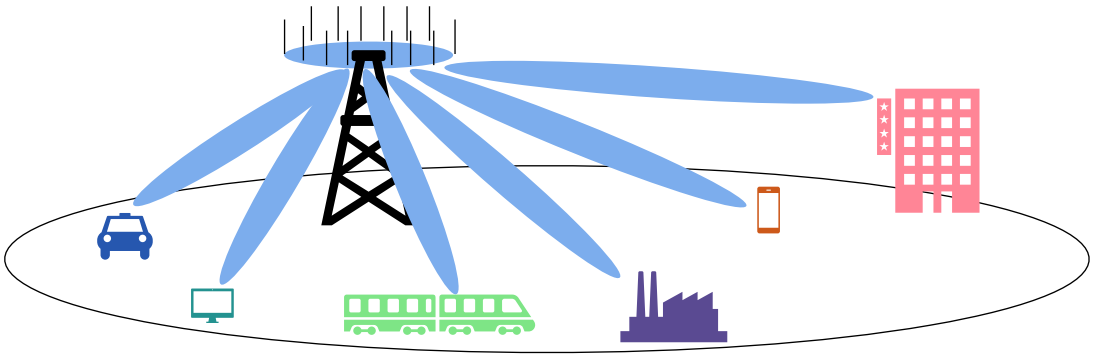

Fig. 2.3 MU Massive MIMO

in the desired direction. Therefore, not only does beamforming make massive MIMO energy efficient, it also contributes to the interference mitigation.

Besides the large capacity that massive MIMO offers at the base station, spatial diversity can also be further exploited. The entire system can achieve higher reliability with large number of antennas. The high reliability in massive MIMO systems is as result of the so called channel hardening effect. With a large number of transmit antennas, the effect of small scale fading [30] can be mitigated or completely eliminated by exploiting channel hardening effect. With channel hardening, fast-fading decreases and the channel starts to exhibit deterministic behavior, one that is deemed a stable capacity. The rigorousness and the complexity of channel estimation reduces and also power allocation, since the small-scale fading decreases, leaving only the large-scale fading to be dealt with. Besides high reliability, channel hardening phenomenon might turn detection schemes of low-complexity to good performing schemes for massive MIMO systems [31].

2.1.3 MIMO Detection Techniques

One of the design goals of any wireless communication system, in an interference and noise limited environment, is for receivers to correctly detect or decode [32] the transmitted symbols. In a multi-user cellular communication systems where multiple users are communicating via a base station concurrently, the received symbols at the intended receiver will be

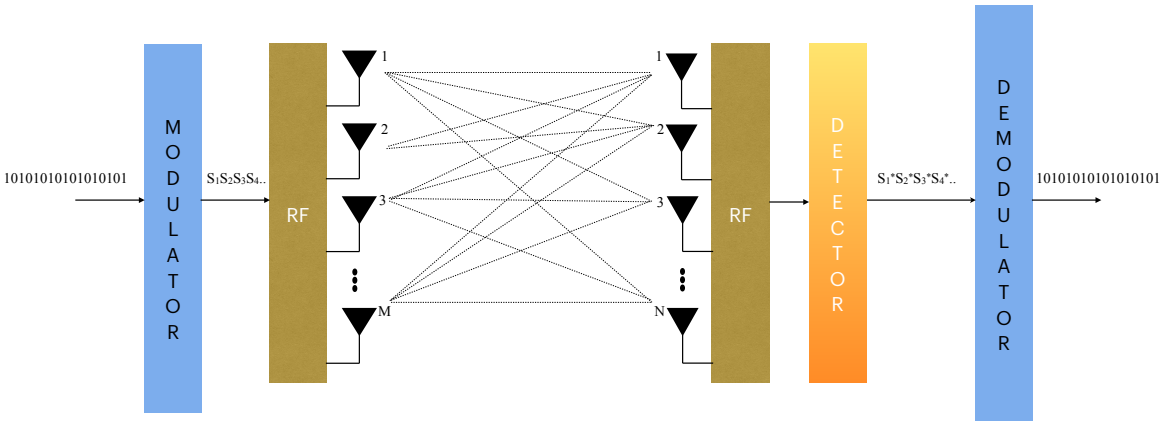

Fig. 2.4 Detection of transmitted symbols over MIMO

a mix of symbols from the intended transmitter and symbols from unintended transmitters. Unlike MIMO's spatial diversity, the spatially multiplexed MIMO technique transmits different signals on each of the transmit antennas with the purpose of increasing data throughput, utilizing the same frequency band and transmission power.

Considering the point-to-point $M \times N$ spatially multiplexed MIMO system in Fig. 2.4, the channel matrix, $\boldsymbol{H}$, is represented as in (2.7), where the channel gain between the m^{th} transmit antenna and the n^{th} received antenna is h_{nm}, $m = 1,\ldots,M$ and $n = 1,\ldots,N$.

$$\boldsymbol{H} = \begin{bmatrix} h_{1,1} & h_{1,2} & \ldots & h_{1,n} \\ h_{2,1} & h_{2,2} & \ldots & h_{2,n} \\ \vdots & \vdots & \ddots & \vdots \\ h_{m,1} & h_{m,2} & \ldots & h_{m,n} \end{bmatrix}_{M \times N} . \tag{2.7}$$

Let $\boldsymbol{r}$, $\boldsymbol{s}$ and $\boldsymbol{z}$ denote, respectively, the received symbols vector, the transmit symbols vector and additive white Gaussian noise at the receiver.

$$\boldsymbol{r} = \boldsymbol{H}\boldsymbol{s} + \boldsymbol{z}, \tag{2.8}$$

A MIMO detector should be able to correctly estimate $\boldsymbol{s}$ from $\boldsymbol{r}$. A Maximum Likelihood (ML) detector is the optimal detector that can be deployed in MIMO systems to estimate transmitted symbols. The goal of an ML detection scheme is to determine the set of

transmitted symbols that minimizes the Euclidean distance between the received symbols vector and all possible symbols that can be considered for the transmit symbols vector. The ML estimator has to satisfy (2.9).

$$\widehat{\boldsymbol{s}}_{\mathrm{ML}} = \underset{s}{\operatorname{argmin}} \|\boldsymbol{r} - \boldsymbol{H}\boldsymbol{s}\|^2, \tag{2.9}$$

where $\widehat{\boldsymbol{s}}_{\mathrm{ML}}$ is the estimated symbol.

The need to search through all the constellation values of the transmitted symbols in order to determine the value that minimises (2.9) creates an exponential complexity in executing such a function. Therefore, ML is relevant in comparing sub-optimal detection techniques, but it is not a practical detector for real life MIMO systems. Zero Forcing (ZF) and Minimum Mean Square Error (MMSE) are some of the well known practical linear detectors deployed in MIMO systems. Linear receivers (ZF and MMSE) can reduce the decoding complexity but they typically suffer from noise enhancement.

ZF is a linear equalizer whose objective is to remove inter-symbol interference (ISI) of the received symbols. Successfully alleviating the received symbols off from the ISI, the desired transmitted symbols will be detected. It operates on the assumption that noise plays little factor at the receive antennas. Let the received symbol at the n^{th} receive antenna be given as

$$r_n = h_{n,k}s_k + \sum_{j=1, j\neq k}^{N} h_{n,j}s_k + z_n, \tag{2.10}$$

where the first component of the summation is the desired transmitted symbols and the corresponding channel gain, and the second component and the rest representing the contributions from the interference. To mitigate the interference components, ZF equalizes the received transmitted symbols with weight as follows

$$\widehat{\boldsymbol{s}}_{\mathrm{ZF}} = \boldsymbol{G}^{\mathrm{ZF}}\boldsymbol{r} = \boldsymbol{G}^{\mathrm{ZF}}\boldsymbol{H}\boldsymbol{s} + \boldsymbol{G}^{\mathrm{ZF}}\boldsymbol{z}, \tag{2.11}$$

$$= \boldsymbol{s} + \boldsymbol{G}^{\mathrm{ZF}}\boldsymbol{z}, \tag{2.12}$$

where, $\boldsymbol{G}^{\mathrm{ZF}}$ is given as

$$\boldsymbol{G}^{\mathrm{ZF}} = (\boldsymbol{H}^{\mathrm{H}}\boldsymbol{H})^{-1}\boldsymbol{H}^{\mathrm{H}} , \tag{2.13}$$

where $(\cdot)^{-1}$ is the inverse of a matrix. As shown in (2.12), the noise, $\boldsymbol{z}$, can be significantly enhanced by a factor of $\boldsymbol{G}^{\mathrm{ZF}}$.

MMSE removes ISI and noise by minimizing the mean squared error of the received symbols from the transmitted symbols. To mitigate against the noise factor ignored by ZF detector, the relation for the MMSE detection is rather

$$\boldsymbol{G}^{\mathrm{MMSE}} = (\boldsymbol{H}^{\mathrm{H}}\boldsymbol{H} + \sigma^2\boldsymbol{I})^{-1}\boldsymbol{H}^{\mathrm{H}} , \tag{2.14}$$

where σ^2 is the variance of the additive white Gaussian noise.

2.1.4 State of the art of MIMO

The use of multiple antennas first came to light in the following seminal papers [15, 33–35] and have since gained a lot of interest. Foschini, whilst at Bell Laboratories, showed that the communication capacity enabled by a system with M transmit and N receive antennas, under the assumption that the transmit radio knows nothing about the multi-antenna transfer function $\boldsymbol{H}$ from the transmitter to the receiver, is given by the classic formula in (2.5). Telatar did confirm the postulation from Foschini by providing alternative way of estimating the capacity of the the MIMO system using information theory. The introduction of space-time codes [34, 36] allowed the spatial diversity to be efficiently exploited, although in the Alamouti's [36], only 2×1 was considered. In [34] , Tarokh generalized it to a higher number of transmit antennas.

As highlighted in the previous sections, there are two types of STC: STTC and STBC. Although STTC has a better performance, it is not practical and cost effective. STTC was introduced in [33] as a coding technique that promises full diversity and substantial coding gain at the price of quite high decoding complexity, as a result of using ML at the

receiver. STBC, on the other hand has been developed on the lines of Alamouti's [36]. STBC is designed to allow for increased performance of wireless transmissions, knowing each signal may be delayed or experience different SNR. STBC compensates for the added noise and other additional losses through spatial channels and can help reduce bit-error rates. It combines the benefit of the Forward-Error-Correction (FEC) and Diversity.

Having established the MIMO linear detectors in the previous sections, it is worth mentioning that, there are other sub-optimal detectors that are also used in MIMO systems. In [37], a survey of massive MIMO detection techniques were comprehensively studied and presented. Low complexity massive MIMO detection algorithms with optimal performance, in the last decade, have garnered a lot of attention. The authors presented an extensive review of the milestones in the development of optimal and near-optimal linear detection algorithms specifically designed for massive MIMO systems such as detectors based on a local search, belief propagation and box detection. They also briefly explored several nonlinear low-dimension antenna based MIMO detectors and their applicability in massive MIMO systems. In addition, they presented recent advances of detection algorithms which are mostly based on machine learning or sparsity based algorithms context.

There have been other comprehensive surveys addressing many facets of the use of massive MIMO. In [25], a survey of the mmWave massive MIMO system challenges and benefits were introduced. User throughput, spectral efficiency, and energy efficiency of massive MIMO systems were also addressed. Furthermore, effects of the modulation scheme, the signal waveform, the multiple access technique, user scheduling algorithm, the front-haul design, the antenna array architecture, and the precoding algorithm were outlined. This survey also presents a holistic view of beamforming techniques for mmWave communication. The underlying principle of beamforming mechanism is briefly explained, and the evolution of beamforming systems for mmWave communications along with the contemporary developments is described. With ultra dense networks poised to be a distinct possibility for future generation of wireless communications, mmWave technology is envisaged to be the key enabler to support and leverage data rates in excess of 10 Gbps. Massive MIMO systems have clearly outlined the importance of beamforming along with spatial multiplexing techniques

to enhance data rates, increase network capacity and mitigate interference. In achieving the desired performance for mmWave MIMO systems, hybrid beamforming methods, comprising of baseband precoding with limited number of RF chains and constant amplitude analog phase shifters, are shown to be effective. To reduce the hardware cost, the precoding can be jointly designed in both analog and digital domains to reduce the required number of RF chains. The survey concluded that the performance of mmWave massive MIMO system in practical scenarios and real-life applications is still under intense research, although greater strides have been made in recent times

2.2 Physical Layer Network Coding

2.2.1 Core Concept

Physical Layer Network Coding (PNC), an important physical layer technique, tolerates interference. Built on the concept of the well-known network-layer Network Coding, orthogonality in uplink transmission is relaxed in the sense that multiple nodes can transmit in parallel. Orthogonality would have mandated that either in the time-domain, the nodes transmit sequentially, or in the frequency-domain, the bandwidth is divided among the nodes for transmission. Although the transmissions from the nodes in uplink interfere, with PNC, only a function of the superimposed signals is extracted by the receiving nodes. Extracting a function of the interfered signals, where a new signal is generated with constellations conforming to that of the input, is often referred to as PNC mapping. PNC Mapping is one of the most challenging aspects of developing PNC schemes. Since PNC allows transmitting nodes to transmit in parallel, in a relay system, there is a boost in network capacity and throughput, making PNC, a plausible physical layer technique that can address some of the challenges in interference-limited network. The realization of the PNC scheme is closely related to the demodulation mapping. Consider the relay system in Fig. 2.5, where two nodes, Node 1 and Node 2 communicate with each other through a relay, R. This is often referred to as a two-way relay channel (TWRC) system model. The first system model shown in Fig. 2.5(a) is without network coding. Node 1 and Node 2 are not allowed to transmit at the

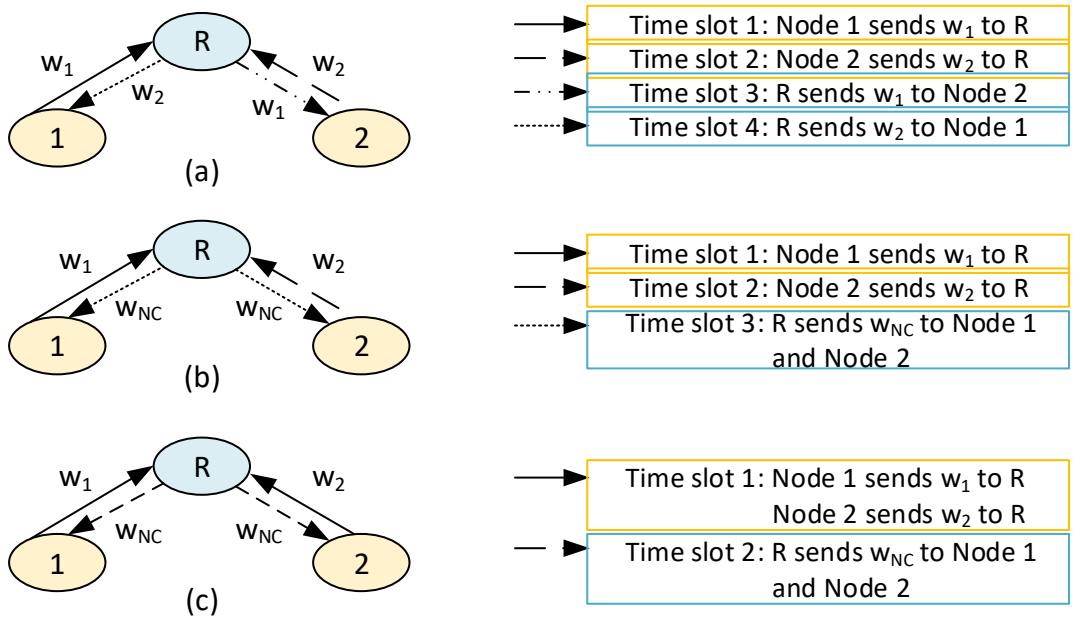

Fig. 2.5 Network Coding in TWRC

same time, and therefore, it takes four time slots for messages, w_1 and w_2, to be exchanged. In Fig. 2.5(b), Node 1 and Node 2, much like in Fig. 2.5(a), transmit at orthogonal times. However, the relay, R, generates a combined message, w_{NC}, using w_1 and w_2, and sends w_{NC} in a single time slot back to Node 1 and Node 2. The bitwise XOR is typically the operation that generates w_{NC}, i.e., $w_{NC} = w_1 \oplus w_2$. In downlink (DL), each of these nodes performs a similar operation on w_{NC} by XOR'ring that with a copy of what was sent previously, i.e., $w_1 \oplus W_{NC}$ for Node 1, and $w_2 \oplus W_{NC}$ for Node 2, to extract the actual packet sent by the other node. In Fig. 2.5(c), Node 1 and Node 2 can transmit at the same time. Since messages w_1 and w_2 interfere at R, decoding or separating each from the other may not be possible. This is the reason wireless communication systems employ orthogonal multiple access schemes either in time, frequency or space to reduce the effects of interference. However, this interference becomes trivial through network coding at the physical layer since it generates or maps interfered symbols to network-coded symbols. The network-coded symbols are chosen such that there is no ambiguity for each node to recover its intended messages from others. Upon receiving the DL broadcast NC symbols, each node performs a similar operation, to retrieve

the symbols sent by the other transmitting nodes. Irrespective of the chosen modulation scheme at the physical layer, the constellation of the superimposed signals at the relay may go out-of-range, if compared to the constellation of the modulated signals at the transmitting nodes. Therefore, a key challenge in PNC is the development of unambiguous PNC mapping algorithms that map superimposed constellations at the relay to the constellations that can be decoded by the nodes. The toleration of interference in PNC leads to capacity boost, as time slots required to have end-to-end communication in a relay system is reduced by half.

2.2.2 State of the art of PNC

The seminal work of Ahliswede et al in [38] did spearhead a new wave of techniques that exploits the efficient usage of the network resources - a technique termed Network Coding. Due to its potential to improve the efficiency of wireless networks, there has been considerable amount of interest in understanding its theory and application in the wireless network. Many theories have been presented in the lines of network coding that includes, but not exclusively to [39, 40].

Applying the network coding technique at the physical layer became increasingly important in the wireless communication system, because compared to the traditional way of communication, the total number of time slots of end-to-end communication reduces from four to two in a relay system [41]. The quest for applying network coding in wireless systems and at the physical layer started off with the work presented in [41], although along the same time, other group of researchers had proposed different designs [42, 43]. However, the work of [41], although based on two way relay system and transmission scheme of Binary Phase Shift Keying (BPSK), has often been the benchmark for other derivative works around PNC.

It is fair to state that a lot of spin-off works have focused on the simple three-node TWRC system, where two nodes communicate concurrently through a central relay system. A good network coding function allows the relay to effectively compute the corresponding network coded information. The authors in [44] optimally designed a practical compute-and-forward based Linear PNC (LPNC) scheme for fading TWRCs, where the channel state information (CSI) is not available at the transmitters. Using a defined Euclidean distance for LPNC, they

derived an explicit expression on an optimized integer coefficients that minimizes the error probability. They noted that the LPNC framework are not limited to TWRCs, rather could widely be applied to more comprehensive wireless networks, e.g., distributed MIMO and multiple-access relay channels.

In [7], the authors proposed a linear detection based scheme using log-likelihood ratio (LLR) and selective combining. The relay utilizes the summation and difference of the two end packets, and then converts them to an NC symbol. The focus of [7] was only a 2×2 MIMO with BPSK modulation. This work was then extended in [45] to a 4×4 MIMO relay system, where the relay is equipped with four antennas and two UEs, each equipped with two antennas. A multiplexing gain is observed when the number of antennas at both the relay and the two UEs increased in [45].

In [46], the authors proposed a space-time (ST) coded multiple-input multiple-output (MIMO) linear physical-layer network coding (LPNC) scheme that promises full-rate and full-diversity, while achieving the maximum coding gain of LPNC. An eigen-direction alignment precoding scheme is proposed in [47] and [48] for MIMO TWRCs, where multiple independent PNC streams are created over aligned eigenmodes. Although [3] did not focus on MIMO and PNC, they touched on combining channel coding and PNC to ensure network reliability, a key technique for practical deployment of MIMO and PNC. Therefore, in order for any proposed PNC scheme to be deployed in real systems, integrating channel coding [49][50] is of utmost importance and further research is needed to ascertain the PNC performance.

In [51], analog network coding based MIMO TWRC was investigated. However, this is known to propagate noise from a node to another, and therefore, its performance, is not as good as the schemes, where each node tries to detect the NC symbols from the noisy received symbols[52]. On the other hand, in [53–55], it was shown that, in a MIMO PNC scheme, when a user selects the strongest transmit antenna, it significantly outperforms space-time block codes. A channel-quantized PNC, that converts K received signals at the relay into two signals by a QR matrices decomposition in a MIMO TWRC, where Q is an orthogonal matrix and R, an upper triangular matrix, is proposed in [56], which showed that PNC technique

can achieve full diversity gain of K. A Full-duplex TWRC in massive MIMO together with a lattice-based PNC was investigated in [57], which showed that their proposed scheme requires just a single timeslot to exchange information across TWRC using full-duplexing, where transmission and reception can occur at the same time in a single node. However, most practical communication systems still operate in half-duplexing mode. Looking at the previous works, none has produced any result for a joint multi-user massive MIMO and PNC, with more than two UEs and where each UE can have multiple number of antennas.

2.3 Index Modulation

2.3.1 Core Concept

The next generation of wireless communication systems are expected to strike a good balance between SE and EE. To satisfy the requirement of SE mandates that communication resources are efficiently utilized, and to satisfy the EE, requires that only the relevant but few resources are utilized at any point in time. Index Modulation (IM) [58] is a physical layer technology that has received considerable amount of attention lately [59], thanks to its capability to use limited communication resources to convey information beyond the conventional means of realizing end-to-end communication. IM, in essence, constitutes a group of modulation schemes that depend on the turning on and off of communication resources such as sub-carrier, time slot, antennas, among others, and using indices of the active resources to convey further information in addition to the actual information transmitted on the active resources.

The dimensions exploited by IM are similar to conventional modulation schemes, which include space, spectrum and time. The spatial dimension is one that has received considerable attention and touted to be considered in B5G wireless systems. Therefore, and coupled with the massive MIMO, this will be the main focus of this sub-section. Spatial Modulation (SM) [60] is a variant of IM used in systems with multiple antennas, where only a single RF chain and for that matter, a single antenna is required to transmit. However, the selection of the antenna can implicitly convey message bits that can be inferred by the receiver if the selected transmit antenna can be decoded by the receiver. SM has proven to strike a favorable trade-off

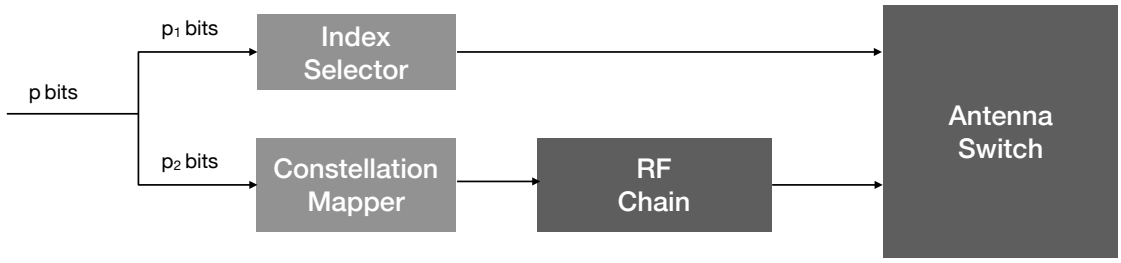

Fig. 2.6 SM Architecture

between EE and SE [61]. Fig. 2.6 depicts the architecture of the transmission process of SM. In this figure, the information bits to be transmitted is divided into two streams: one is the the actual information bits that undergo conventional modulation, using schemes such as Quadrature Amplitude Modulation (QAM) and the other bit stream selects which antenna to be switched on for the transmission. The achievable rate of transmission using SM, R_{SM}, can be derived from the generalized SM (GSM) as follows

$$R_{\text{GSM}} = p_1 + p_2 \tag{2.15}$$

$$= \lfloor \log_2 \binom{M}{k} \rfloor + k \log_2(Q) \text{ [bpcu]}, \tag{2.16}$$

where $\binom{M}{k}$ is the Binomial coefficient of the number of ways to choose k from M, $\lfloor . \rfloor$, floor of the estimated value within, M and k being the total number of antennas and number of antennas to activate respectively, and Q the cardinality of the modulation scheme to modulate the bit streams to be transmitted on the activated antennas. If we assume that the number of active antennas at any point is one, then (2.16) reduces to

$$R_{SM} = \lfloor \log_2(M) \rfloor + \log_2(Q) \text{ [bpcu]}, \tag{2.17}$$

where bpcu is bits per channel use.

This is how SM Works. In Fig. 2.7, the bit stream needs to be transmitted using SM scheme, where a single antenna out of the four can be switched on at any point in time. The

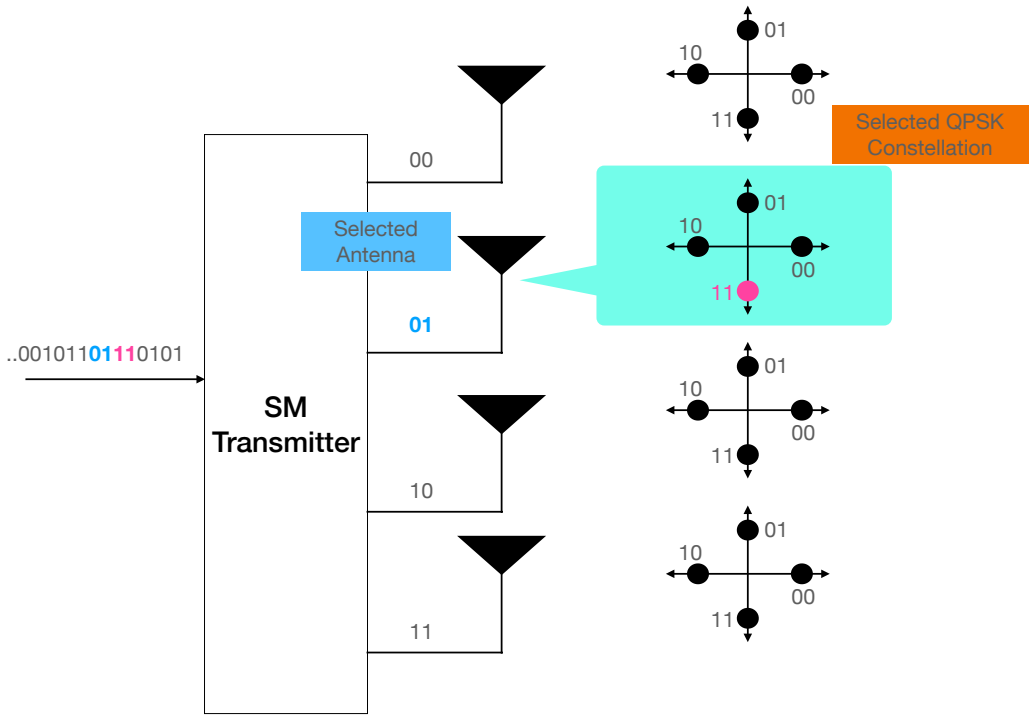

Fig. 2.7 How SM-MIMO works

modulation scheme for the transmission of the bit stream is QPSK or 4-QAM. Since there are only four antennas, two bits are needed in selecting at most a single antenna at any point in time. Similarly, since the modulation scheme is QPSK, groups of two bits in the bit stream would be considered for modulation. Looking at the figure, forexample, if "0111" have to be transmitted, "01" selects the second antenna, whilst "11" maps to the constellation complex value through the constellation mapper. Such an SM transmission architecture will lead to a rate of 4 bpcu.

2.3.2 State of the art of IM

As already indicated in the beginning of this sub-section, IM has evolved beyond SM. Although SM is the primary focus of this thesis work, it is worth highlighting some of the notable works in the evolution of the IM. There are few comprehensive surveys on IM and the reader can be referred to these two pertinent ones [58, 59].

IM schemes have evolved around the dimensions of space, time and frequency of the wireless communication systems. Unlike the conventional modulation schemes that utilizes the full capacity of each of these dimensions to convey information over the communication medium, IM utilizes a fraction of the resources to transmit and in addition convey further information by letting the receiver decode which of the resources were active and implicitly inferring which information bits has been used by the transmitter to select those active resources. This goes without saying that IM does work better together with the conventional modulation schemes such as PSK, M-QAM and etc.

Orthogonal frequency division modulation (OFDM) has been one of the key modulation schemes deployed in Long-Term Evolution (LTE) and beyond [62, 63]. This two-dimensional modulation scheme divides the frequency domain of the spectrum into narrowband sub-carriers and the time domain into time slots, allowing the spectrum to be efficiently used. By dividing the spectrum into narrowband flat fading sub-channels, OFDM becomes more resistant to frequency selective fading. An OFDM-IM scheme proposed in [64] allows a subset of all the available sub-carriers to be used for transmission and at the receiving end, the receiver decoding the active subarriers by inferring the symbols or information bits used to select those subcarriers. This would be the additional information transferred implicitly without any energy consumption. This scheme falls under the frequency domain IM. Other notable OFDM-IM schemes include the Subcarrier-Index modulation OFDM (SIM-OFDM) and the Enhanced SIM-OFDM (ESIM-OFDM). SIM-OFDM [65] uses On-Off Key (OOK) modulation scheme to modulate the bits that decide which sub-carriers in an OFDM sub-block will be active, whilst the rest of bits are modulated on the other modulation schemes are transferred on the active sub-carriers. The performance of SIM-OFDM is rather undesirable due to error propagation, hence, the introduction of ESIM-OFDM [66]. In this enhancement, the OFDM sublock is split into two, and each with only two sub-carriers, where a single sub-carrier is activated at a time. This avoids error propagation and improves the performance. In essence, these two have now evolved into the generalized SIM-OFDM (GSIM-OFDM) [64], or what is now referred to as IM-OFDM or OFDM-IM. In GSIM-OFDM, multiple

sub-carriers are enabled to increase the spectrum efficiency. In increasing the SE, combining GSIM-OFDM with MIMO is proposed here [67, 68].

Influenced by the frequency domain IM schemes, the following are some of the notable proposed schemes in the time domain: single carrier IM (SC-IM) [69], Dual-mode single carrier with index modulation (DM-SCIM) [70] among a few. In the SC-IM, IM is applied on the time slots at each transmit opportunity. The transmit symbols in the time slots are, hitherto, divided into active and inactive. The inactive symbols would incur no energy consumption, however, the indices of the active symbols will carry further information, in addition to the actual symbols occupied by the information bits. DM-SCIM, on the other hand improves on the SE the SCIM by using two QAM constellations for the active symbols, whose index would carry further information. The SE can even be boosted further by combining this with MIMO as proposed here [71].

As has been reiterated above, the focus of this thesis work is on the SM variant of the IM and chapters below describe a novel scheme where we combine massive MIMO-PNC and SM.

Chapter 3

Massive MIMO PNC

3.1 Introduction

The core concepts for massive MIMO and the detection schemes, as well as PNC have been introduced in Chapter 2. In this section, we present a generic approach where PNC can be deployed in massive MIMO systems that utilizes any variant of M-QAM and without changing the underlying MIMO framework. This further allows existing detection schemes such as ZF and MMSE to be used without any modification. In line with this goal, we formulate a generalized PNC mapping function, for which its inputs are the detected sum-difference (SD) symbols from clusters derived from the SD transformation of the channel and equalization of the received superimposed symbols. Furthermore, we derive and optimize a specialization of the generalized PNC mapping function and demonstrate that with a few variants of the M-QAM. A generalized PNC mapping function is then formulated. The generalized PNC mapping functions 1) provide a common platform for any M-QAM modulation scheme to be investigated and utilized, and 2) understand the complexity and optimizations required for the PNC mapping functions, particularly, for higher order modulation schemes. Finally, we evaluate the bit-error-rate (BER) of the detection of the SD symbols with ZF and MMSE and the PNC mapping performance of this scheme.

The next subsections provide in-depth details of this proposed scheme.

3.2 Proposed massive MIMO and PNC Scheme

In this section, we delve deeper into our proposed scheme that combines massive MIMO and PNC. The system model and its architecture will be described to show how PNC can be deployed in a massive MIMO systems, with the underlying transmission scheme being M-QAM modulations. We present the mathematical formulations in modeling the proposed scheme and then provide the simulation results. The simulation results are then analysed and presented and the conclusion sub-section explains our assessment of the proposed scheme based on the simulation analysis.

We consider a single cell massive MIMO system, in which N user equipment (UEs) exchange information through a relay or a base station, as in Fig. 3.1. Each of the N UEs is equipped with up to K antennas, and the base station with M antennas. This is a typical multi-user MIMO system with the UEs equipped to have more than a single antenna. The communication among all UEs is done in the same time-frequency resource, and therefore, interference is expected, which is a common assumption in massive MIMO systems, even without network coding. It is assumed that $M \geq 64$, $M \gg N$, $M \gg K$ in order to fulfil the universal antenna requirements of massive MIMO, where $\gg$ denotes far greater than. The system model is also assumed to operate in half-duplex, in the sense that, each UE cannot transmit and receive at the same time. Therefore, each round of information exchange consists of two phases, namely, uplink (UL) and downlink (DL) phases. In the DL phase, the mapped PNC symbols are delivered to the UEs.

3.2.1 System Model

Asynchronisation of transmission and reception of the interfered symbols is one of the major issues in PNC. It is also one of the main research areas with respect to PNC. Loss in synchronisation impacts the performance in estimating the PNC symbols, as most PNC algorithms assume that all transmitted symbols will arrive at the same time at the receiver. However, for the sake of simplicity, in our work, we assume synchronous transmission, hence, in the UL phase, all users transmit to the base station simultaneously in the same frequency

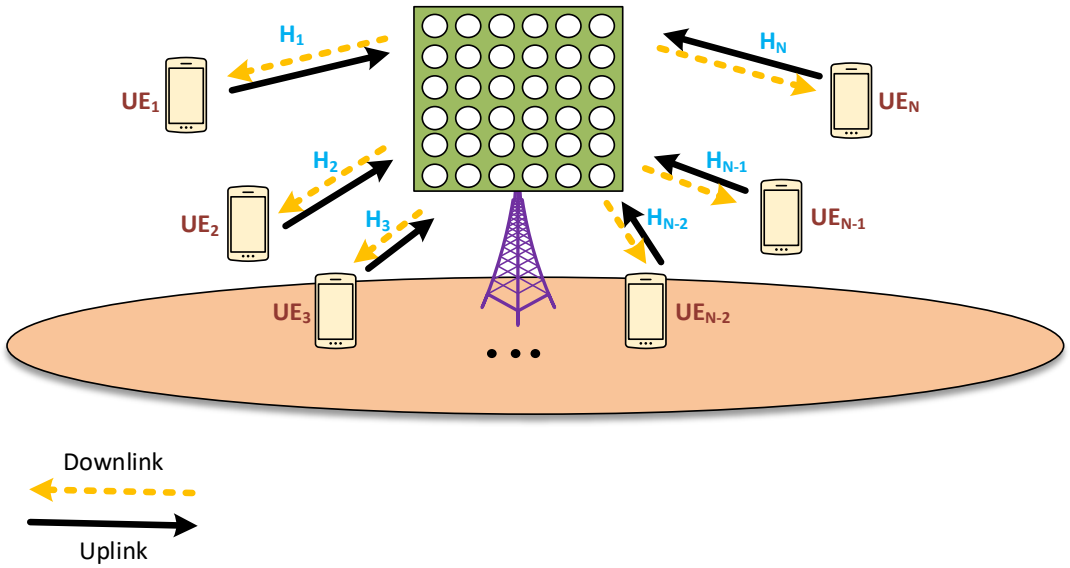

Fig. 3.1 System Model for massive MIMO and PNC

band and at the same time. We also did not consider channel coding in this work for the sake of simplicity, considering there already have been some works [3, 72] in combining channel coding and PNC, as previously stated in the introduction section. In essence, channel coding is essential for improving the reliability of the PNC scheme in practical systems. It is already established that if the sources transmitting in the UL phase use a uniform channel code, then the codeword as a result of XOR'ing of the sources symbols is still valid. Although there is no direct XOR'ing in our proposed scheme, we believe some of the existing joint channel coding PNC schemes can be tailored and extended to our proposed PNC scheme.

If $\boldsymbol{H}$ is the overall channel between the base station and the multi-antenna UEs in the multi-user massive MIMO system, as depicted in Fig. 3.1, $\boldsymbol{H}$ can be re-formulated as

$$\boldsymbol{H} = \Big[\boldsymbol{H}(1) \quad \boldsymbol{H}(2) \quad \dots \quad \boldsymbol{H}(N)\Big]_{\mathrm{M}\times\mathrm{L}}, \tag{3.1}$$

where $L = K \times N$, and $\boldsymbol{H}(n)$ for $n = 1, \ldots, N$, is the $M \times K$ channel matrix between the base station and the n^{th} UE and can be expressed as

$$\boldsymbol{H}(n) = \begin{bmatrix} h(n)_{1,1} & h(n)_{1,2} & \ldots & h(n)_{1,k} \\ h(n)_{2,1} & h(n)_{2,2} & \ldots & h(n)_{2,k} \\ \vdots & \vdots & \ddots & \vdots \\ h(n)_{m,1} & h(n)_{m,2} & \ldots & h(n)_{m,k} \end{bmatrix}_{\mathrm{M}\times\mathrm{K}}, \tag{3.2}$$

where $h(n)_{m,k} \in \mathbb{C}$, for $m = 1, \ldots, M$ and $k = 1, \ldots, K$, denotes the complex channel gain between m^{th} antenna of base station and k^{th} antenna of the n^{th} UE. The entries of $h(n)_{m,k}$ are assumed to be identically and independently distributed (i.i.d.) complex Gaussian, distributed with zero mean and unit variance, presented by $\mathscr{CN}(0,1)$. The received signal vector at the base station, $\boldsymbol{r}$, is given by (2.8). The complex vectors of $\boldsymbol{r}$ and $\boldsymbol{z}$ are of the dimension $M \times 1$. Indeed, $\boldsymbol{z}$ is the vector of additive white Gaussian noise (AWGN) at the receive antennas of the base station, with zero mean and variance of σ^2, i.e., $\mathscr{CN}(0,\sigma^2)$, $\boldsymbol{s}$ is the overall transmitted symbols vector from all the UEs of dimension $M \times 1$.

$$\boldsymbol{s} = \begin{bmatrix} \boldsymbol{s}(1) & \boldsymbol{s}(2) & \ldots & \boldsymbol{s}(n) \end{bmatrix}^{\mathrm{T}}_{1\times\mathrm{L}}, \tag{3.3}$$

where $\boldsymbol{s}(n) = \begin{bmatrix} s_1 & s_2 & \ldots & s_K \end{bmatrix}^{\mathrm{T}}_{1\times\mathrm{K}}$ represents a vector of K symbols from the n^{th} UE.

In general, a MIMO detector is required to estimate transmitted symbols vector $\boldsymbol{s}$ from the received symbols vector $\boldsymbol{r}$. Linear detectors such as ZF and MMSE are known to have desirable computational complexity, but suffer from an ample performance loss in comparison to the Maximum Likelihood (ML), and they are, therefore, considered sub-optimal compared to ML. However, they both have been proven to perform well in massive MIMO [73]. This goes without saying that the performance loss using these linear detectors compared to ML is not considered in this section. We are convinced, by looking at our algorithm, that these linear detectors can be replaced by other high performing sub-optimal detectors, and the performance of our PNC scheme will scale accordingly.

Applying the aforementioned linear detectors with an $L \times M$ detection matrix $\boldsymbol{G}$ to the received signal vector $\boldsymbol{r}$, the estimate of the transmit symbols vector $\boldsymbol{s}$ can be expressed as

$$\widehat{\boldsymbol{s}} = \boldsymbol{G}\boldsymbol{r} \,, \tag{3.4}$$

where $\boldsymbol{G}$, respectively, for ZF and MMSE, are given in (2.13) and (2.14). It has to be noted that in practice, the noise variance varies from one antenna to the other in the same node. Also, for the sake of simplicity, we assume that there is a perfect channel state information (CSI) at the receiver, and therefore, $\boldsymbol{H}$ is known at the base station.

The goal now is to derive NC symbols from the received superimposed transmitted symbols at the base station, without decoding them individually. The massive MIMO system model fairly tolerates interference, a key requirement for PNC, and therefore, moving the network coding to the physical layer is a means to gaining advantages of both approaches, by jointly performing PNC and massive MIMO detection. Furthermore, in order for PNC to be deployed in mainstream cellular massive MIMO systems, it is essential that it supports M-QAM modulation. Adaptive modulation and coding, which based on the channel quality, the base station assigns a suitable modulation and coding scheme to the UEs, is a key transmission scheme in cellular systems. The chosen adaptive modulation and coding scheme has to have the desired balance of spectral efficiency and error resilience for the link state as observed by the device. The most important criteria for PNC is that the PNC mapping function, $f_{\text{PNC}}(.)$, used at the base station, should generate PNC symbols that can be decoded by the UEs without any ambiguity in recovering the symbols from the other users.

Each of the antennas at the massive MIMO base station receives superimposed symbols that constitute transmitted symbols from each of the multi-antenna UEs. The constellation for the received interfered symbols, depending on the modulation scheme used at the UEs, may lead to ambiguities if they are mapped to NC symbols, which follow the same constellation as the transmitted symbols. A practical solution in alleviating this network coding ambiguity in massive MIMO systems is, by creating clusters, which constitute of a few transmitted symbols and whose superposition are independently passed on to $f_{\text{PNC}}(.)$, to generate the

NC symbols. An SD matrix transformation of the massive MIMO channel is a plausible means of creating these kind of clusters. In order to support all variants of M-QAM, a top-down approach is employed, where the scheme is first, generalized, and then based on the modulation scheme of interest, further optimizations are embarked upon.

The approach is not to precode the user signals before they are transmitted. Rather, at the receiver, after receiving the transmitted symbols, and knowing the channel matrix, the receiver will transform the channel matrix with an SD matrix to an SD channel matrix. The mathematical formulation is as follows. Let the SD matrix be

$$\boldsymbol{P}_{\text{sd}} = \begin{bmatrix} \boldsymbol{I}_{\text{Q}} & \boldsymbol{I}_{\text{Q}} \\ \boldsymbol{I}_{\text{Q}} & -\boldsymbol{I}_{\text{Q}} \end{bmatrix}_{\text{L}\times\text{L}}, \tag{3.5}$$

where $Q = \frac{1}{2}L$ and $\boldsymbol{I}_{\text{Q}}$ denoting a $Q \times Q$ square Identity Matrix, then the inverse, $\boldsymbol{P}_{\text{sd}}^{-1}$, is related to $\boldsymbol{P}_{\text{sd}}$ as $\boldsymbol{P}_{\text{sd}}^{-1} = \frac{1}{2}\boldsymbol{P}_{\text{sd}}$. In order for the receiver to preserve $\boldsymbol{r}$ in (2.8), both $\boldsymbol{H}$ and $\boldsymbol{s}$ have to be transformed. The transformation is formulated as

$$\boldsymbol{r} = (\boldsymbol{H}{\boldsymbol{P}_{\text{sd}}}^{-1})(\boldsymbol{P}_{\text{sd}}\boldsymbol{s}) + \boldsymbol{z} \tag{3.6}$$

$$= \boldsymbol{H}_{\text{sd}}\boldsymbol{s}_{\text{sd}} + \boldsymbol{z}\,, \tag{3.7}$$

where $\boldsymbol{H}_{\text{sd}} = \frac{1}{2}\boldsymbol{H}\boldsymbol{P}_{\text{sd}}$, is the linear transformation of the massive MIMO channel with a massive SD matrix, and $\boldsymbol{s}_{\text{sd}} = \boldsymbol{P}_{\text{sd}}\boldsymbol{s}$, clusters of SD symbols, whose estimates at the base station, are then mapped to the PNC symbols. In essence, without changing anything about the massive MIMO transmission, the receiver is pretending $\boldsymbol{H}_{\text{sd}}$ is the channel matrix, in order to estimate the sum and difference of the transmitted symbols. This is possible, thanks to the linear relationship between $\boldsymbol{P}_{\text{sd}}^{-1}$ and $\boldsymbol{P}_{\text{sd}}$. This facilitates the adoption of ZF and MMSE without any modification, to detect the sum and difference symbols directly from the received symbols vector, $\boldsymbol{r}$. Each pair of the detected SD symbols forms a cluster and this cluster becomes the input to the PNC mapping function, $f_{\text{PNC}}(.)$, to generate the corresponding PNC

symbols. The pair of estimated SD symbols in each cluster, is then passed on to the PNC mapping function, $f_{\text{PNC}}(.)$, to generate the corresponding PNC symbols.

Since $\boldsymbol{r}$, the received symbols vector, in either (2.8) or (3.7) is assumed to be received over a fading channel, it is imperative that $\boldsymbol{s}_{\text{sd}}$ is estimated. Leveraging on massive MIMO linear detectors such as, ZF and MMSE, the estimate of $\boldsymbol{s}_{\text{sd}}$, at the base station, by extending (3.4), is expressed as

$$\widehat{\boldsymbol{s}}_{\text{sd}} = \boldsymbol{G}_{\text{sd}}\boldsymbol{r}\ , \tag{3.8}$$

where $\boldsymbol{G}_{\text{sd}}$ is the SD equalization matrix. The SD equalization matrix is based on the massive SD-transformed channel matrix, $\boldsymbol{H}_{\text{sd}}$, and for ZF and MMSE, it is expressed as

$$\boldsymbol{G}_{\text{sd}} = \begin{cases} (\boldsymbol{H}_{\text{sd}}^{\text{H}}\boldsymbol{H}_{\text{sd}})^{-1}\boldsymbol{H}_{\text{sd}}^{\text{H}}, & \text{for ZF} \\ (\boldsymbol{H}_{\text{sd}}^{\text{H}}\boldsymbol{H}_{\text{sd}} + \sigma^2\text{I})^{-1}\boldsymbol{H}_{\text{sd}}^{\text{H}}, & \text{for MMSE} \end{cases} . \tag{3.9}$$

Upon receiving $\boldsymbol{r}$ from multiple UEs, knowing $\boldsymbol{H}$, the base station can determine $\boldsymbol{G}_{\text{sd}}$, and then, use that to estimate the $L \times 1$ clusters of SD of the transmitted symbols. The clusters of the estimated SD symbols at the base station is expressed as

$$\widehat{\boldsymbol{s}}_{\text{sd}} = \begin{bmatrix} \widehat{s}_{\text{sd},1} \\ \widehat{s}_{\text{sd},2} \\ \vdots \\ \widehat{s}_{\text{sd},\text{Q}} \\ \widehat{s}_{\text{sd},\text{Q+1}} \\ \vdots \\ \widehat{s}_{\text{sd},2\text{Q}} \end{bmatrix} = \begin{bmatrix} \widehat{s_1 + s_{\text{Q+1}}} \\ \widehat{s_2 + s_{\text{Q+2}}} \\ \vdots \\ \widehat{s_{\text{Q}} + s_{2\text{Q}}} \\ \widehat{s_1 - s_{\text{Q+1}}} \\ \vdots \\ \widehat{s_{\text{Q}} - s_{2\text{Q}}} \end{bmatrix}_{\text{L}\times 1} , \tag{3.10}$$

where for example, $\widehat{s}_{\text{sd},1}$ or $\widehat{s_1 + s_{\text{Q+1}}}$ and $\widehat{s}_{\text{sd},\text{Q+1}}$ or $\widehat{s_1 - s_{\text{Q+1}}}$, are respectively, the estimated summation and difference of the transmitted symbols, s_1 and $s_{\text{Q+1}}$. This pair of SD symbols constitutes a cluster, that is then, passed on to the PNC mapping, $f_{\text{PNC}}(.)$. For these clusters

of summation and difference symbols to be created as in (3.10), the base station has to view the multi-user massive MIMO system model as a giant point-to-point massive MIMO between itself and a black box of many multi-antenna UEs. The dimension of the massive SD-transformed channel matrix, $\boldsymbol{H}_{\mathrm{sd}}$, is assumed to be a square matrix, for the sake of simplicity.

Finally, a vector of the PNC symbols, $\widehat{\boldsymbol{s}}_{\mathrm{PNC}}$, is generated from the PNC mapping function, $f_{\mathrm{PNC}}(.)$, through the relation

$$\widehat{\boldsymbol{s}}_{\mathrm{PNC}} = f_{\mathrm{PNC}}(\widehat{\boldsymbol{s}}_{\mathrm{sd}}) \tag{3.11}$$

$$= \begin{bmatrix} f_{\mathrm{PNC}}(\widehat{s}_{\mathrm{sd},1}, \widehat{s}_{\mathrm{sd},\mathrm{Q}+1}) \\ f_{\mathrm{PNC}}(\widehat{s}_{\mathrm{sd},2}, \widehat{s}_{\mathrm{sd},\mathrm{Q}+2}) \\ \vdots \\ f_{\mathrm{PNC}}(\widehat{s}_{\mathrm{sd},\mathrm{Q}}, \widehat{s}_{\mathrm{sd},2\mathrm{Q}}) \end{bmatrix}_{\mathrm{Q}\times 1} . \tag{3.12}$$

The next section will describe the underlying scheme for the PNC mapping function, $f_{\mathrm{PNC}}(.)$.

3.2.2 Generalization of the PNC Mapping Scheme

The goal of the PNC mapping scheme is to derive the set of PNC symbols, $\widehat{\boldsymbol{s}}_{\mathrm{PNC}}$, from the estimated massive SD transmitted symbols, $\widehat{\boldsymbol{s}}_{\mathrm{sd}}$. The derived PNC symbols, $\widehat{\boldsymbol{s}}_{\mathrm{PNC}}$, must not lead to any ambiguity of decoding, if broadcast in DL to the UEs. If the probability distribution function of the sum and difference function is known, Maximum a Posteriori (MAP) decoder can be employed to derive $\widehat{\boldsymbol{s}}_{\mathrm{PNC}}$. By definition,

$$\mathrm{Posteriori} = \frac{\mathrm{Likelihood} \times \mathrm{Prior}}{\mathrm{Observation}} . \tag{3.13}$$

Assuming the unknown or the parameter to be estimated is θ, and x, the observed data, then (3.13) can be expressed in these variables as

$$P(\theta|x) = \frac{P(x|\theta)P(\theta)}{P(x)} , \tag{3.14}$$

where $P(\theta|x)$ is the posteriori or the conditional probability of the unknown, θ, given the observation, x, whereas $P(x|\theta)$ is the likelihood or the conditional probability of the observation given the unknown, and $P(\theta)$ and $P(x)$ are respectively, the marginal distribution functions for the unknown and the observation.

A MAP decoder is based on (3.14), and can be formulated as determining the value of the parameter, θ, that maximizes the posteriori, $P(\theta|x)$. This can be expressed as

$$\widehat{\theta}_{\text{MAP}} = \underset{\theta}{\text{argmax}}\ P(\theta|x) \tag{3.15}$$

$$= \underset{\theta}{\text{argmax}}\ \frac{P(x|\theta)P(\theta)}{P(x)}\ . \tag{3.16}$$

Since $P(x)$ is not a function of θ, it can be ignored, and therefore, the $\widehat{\theta}_{\text{MAP}}$ can be approximated to

$$\widehat{\theta}_{\text{MAP}} \approx \underset{\theta}{\text{argmax}}\ P(x|\theta)P(\theta)\ . \tag{3.17}$$

Again, $P(\theta)$ can be ignored if the expected values of θ that maximizes the posteriori distribution function are each equally likely. Hence, $P(\theta)$ becomes a constant, and therefore, can be ignored, leading (3.17) to further be approximated as

$$\widehat{\theta}_{\text{MAP}} \approx \underset{\theta}{\text{argmax}}\ P(x|\theta) = \widehat{\theta}_{\text{MLE}}\ , \tag{3.18}$$

where $\widehat{\theta}_{\text{MLE}}$ is the Maximum Likelihood Estimator (MLE). When the cardinality of θ is 2, hypothesis testing using LLR is plausible. If the cardinality is more than 2, then LLR is not the appropriate approach.

Having defined the MAP decoder, we can now employ it in our PNC Mapping scheme in massive MIMO systems in estimating the NC symbols at the physical layer. In (3.10), clusters of estimated SD symbols that are mapped to PNC symbols are expressed as $\{(\widehat{s}_{\text{sd,i}}, \widehat{s}_{\text{sd,Q+i}}) \mid 1 \leq i \leq Q\}$. We assume that the corresponding set of clusters of transmitted input symbol, $\{(s_i, s_{Q+i}) \mid 1 \leq i \leq Q,\ s_i, s_{Q+i} \in \Theta\}$, are modulated symbols from the constel-

lation, represented by Θ. Then, the likelihood of obtaining the PNC symbol, $\widehat{s_i \oplus s_{Q+i}} = v$, such that $v \in \Theta$ is expressed as in (3.19),

$$\begin{aligned} L(\widehat{s_i \oplus s_{Q+i}} = v | \widehat{s}_{\mathrm{sd,i}}, \widehat{s}_{\mathrm{sd,Q+i}}) &= \sum_{v \in \Theta} P(\widehat{s}_{\mathrm{sd,i}}, \widehat{s}_{\mathrm{sd,Q+i}} | \widehat{s_i \oplus s_{Q+i}} = v) \\ &= \sum_{v \in \Theta} P(\widehat{s}_{\mathrm{sd,i}} | \widehat{s_i \oplus s_{Q+i}} = v) P(\widehat{s}_{\mathrm{sd,Q+i}} | \widehat{s_i \oplus s_{Q+i}} = v) \, . \end{aligned} \tag{3.19}$$

Since the noise in (2.8) and (3.7) is assumed to be AWGN, the likelihood function can be assumed to be Gaussian. Using the Gaussian probability density function, $P(Y) = \frac{1}{\sqrt{2\pi\sigma^2}} e^{-\frac{(y-\mu)^2}{2\sigma^2}}$, where y is the received symbol, μ the expected value of the combined input symbols and σ^2, the noise variance, (3.19) can be expressed further as

$$L(\widehat{s_i \oplus s_{Q+i}} = v | \widehat{s}_{\mathrm{sd,i}}, \widehat{s}_{\mathrm{sd,Q+i}}) = \sum\nolimits_{v \in \Theta} \frac{1}{2\pi\sqrt{\sigma_i^2 \sigma_{Q+i}^2}} e^{-\frac{\left(\widehat{s}_{\mathrm{sd,i}} - s_{\mathrm{sd,i}}\right)^2}{2\sigma_i^2}} e^{-\frac{\left(\widehat{s}_{\mathrm{sd,Q+i}} - s_{\mathrm{sd,Q+i}}\right)^2}{2\sigma_{Q+i}^2}} , \tag{3.20}$$

where σ_i^2 and σ_{Q+i}^2 are respectively, the noise variances of the i^{th} and $(Q+i)^{th}$ streams upon estimation of their corresponding sum and difference symbols, and where ${\sigma_x}^2 = \{\boldsymbol{G}_{\mathrm{sd}}^{\mathrm{H}} \boldsymbol{G}_{\mathrm{sd}}\}_{x,x} \sigma^2$. If $\{\boldsymbol{G}_{\mathrm{sd}}^{\mathrm{H}} \boldsymbol{G}_{\mathrm{sd}}\}_{x,x} = \mathrm{I}$, then the noise variances are identical.

Knowing the general likelihood's function for the set of all clusters, $L(\widehat{s_i \oplus s_{Q+i}} = v | \widehat{s}_{\mathrm{sd,i}}, \widehat{s}_{\mathrm{sd,Q+i}})$, the MAP estimator in (3.17) can be employed to determine the PNC symbol of each cluster as follows

$$\begin{aligned} &(\widehat{s_i \oplus s_{Q+i}} = v)_{MAP} \\ &\quad \approx \underset{\widehat{s_i \oplus s_{Q+i}}}{\operatorname{argmax}} \, L(\widehat{s_i \oplus s_{Q+i}} = v | \widehat{s}_{\mathrm{sd,i}}, \widehat{s}_{\mathrm{sd,Q+i}}) P(\widehat{s}_{\mathrm{sd,i}}, \widehat{s}_{\mathrm{sd,Q+i}}). \end{aligned} \tag{3.21}$$

The overall set of estimated PNC symbols is expressed as

$$\widehat{s}^{i}_{\text{PNC}} = f_{\text{PNC}}(\widehat{s}_{\text{sd,i}}, \widehat{s}_{\text{sd,Q+i}}) \tag{3.22}$$

$$= \{(s_i \oplus \widehat{s_{Q+i}} = v)_{\text{MAP}} \mid 1 \leq i \leq Q,\ v \in \Theta\}. \tag{3.23}$$

In the next section, we will provide details into how the generalized MAP-based PNC mapping function in (3.19) - (3.23) is applied to a few variants of the M-QAM modulation scheme.

3.2.3 Specialization of the PNC Mapping scheme for 4-QAM

Table 3.1 PNC Mapping Of I/Q-Component Of 4-QAM, Based On SD Scheme

$\boldsymbol{s}_i$	$\boldsymbol{s}_{Q+i}$	$\boldsymbol{s}_{\text{sd,i}}$	$\boldsymbol{s}_{\text{sd,Q+i}}$	$\boldsymbol{s}^{i}_{\text{PNC}}$
1	1	2	0	-1
1	-1	0	2	1
-1	1	0	-2	1
-1	-1	-2	0	-1

This section describes the application of the PNC Mapping scheme in subsection 3.2.2 to massive MIMO system where the transmissions from the UEs use lower-order modulation, such as 4-QAM. We will demonstrate by focusing on a single cluster of estimated SD symbols, $\widehat{\boldsymbol{s}}_{\text{sd,i}}$ and $\widehat{\boldsymbol{s}}_{\text{sd,Q+i}}$, derived from the equalization of the received symbol vector $\boldsymbol{r}$, using massive SD equalization matrix (see (3.8)-(3.9)). For the sake of simplicity, we will focus on only the in-phase (I) component constellation of QPSK. However, since quadrature (Q) component of QPSK is similar to the I-component and independently modulated or demodulated, the PNC mapping of the I-component is equally applicable to the Q-component. Table 3.1 shows how SD symbols, $\boldsymbol{s}_{\text{sd,i}}$ and $\boldsymbol{s}_{\text{sd,Q+i}}$, of the transmitted symbols, $\boldsymbol{s}_i$ and $\boldsymbol{s}_{Q+i}$, are mapped to the PNC symbols, $\boldsymbol{s}^{i}_{\text{PNC}}$. Having $\boldsymbol{s}_{\text{sd,i}}$ and $\boldsymbol{s}_{\text{sd,Q+i}}$ in Table 3.1 as the expected SD symbols, $f_{\text{PNC}}(.)$

function presented in subsection 3.2.2, can then be used to estimate the PNC symbols from the estimated SD symbols, $\widehat{\boldsymbol{s}}_{\mathrm{sd,i}}$ and $\widehat{\boldsymbol{s}}_{\mathrm{sd,Q+i}}$ as follows:

$$\begin{aligned} LLR(s_i \oplus s_{Q+i}) &= \ln\left[\frac{L(\widehat{s_i \oplus s_{Q+i}} = +1|\widehat{s}_{\mathrm{sd,i}}, \widehat{s}_{\mathrm{sd,Q+i}})P(\widehat{s}_{\mathrm{sd,i}}, \widehat{s}_{\mathrm{sd,Q+i}})}{L(\widehat{s_i \oplus s_{Q+i}} = -1|\widehat{s}_{\mathrm{sd,i}}, \widehat{s}_{\mathrm{sd,Q+i}})P(\widehat{s}_{\mathrm{sd,i}}, \widehat{s}_{\mathrm{sd,Q+i}})}\right] \\ &= \ln\left[\frac{P(\widehat{s}_{\mathrm{sd,i}}|s_{\mathrm{sd,i}} = 0)P(\widehat{s}_{\mathrm{sd,Q+i}}|s_{\mathrm{sd,Q+i}} = -2) + P(\widehat{s}_{\mathrm{sd,i}}|s_{\mathrm{sd,i}} = 0)P(\widehat{s}_{\mathrm{sd,Q+i}}|s_{\mathrm{sd,Q+i}} = +2)}{P(\widehat{s}_{\mathrm{sd,Q+i}}|s_{\mathrm{sd,Q+i}} = 0)P(\widehat{s}_{\mathrm{sd,i}}|s_{\mathrm{sd,i}} = -2) + P(\widehat{s}_{\mathrm{sd,Q+i}}|s_{\mathrm{sd,Q+i}} = 0)P(\widehat{s}_{\mathrm{sd,i}}|s_{\mathrm{sd,i}} = +2)}\right] \\ &= LL_{Q+i}(s_i \oplus s_{Q+i} = +1) - LL_i(s_i \oplus s_{Q+i} = -1)\,, \end{aligned} \tag{3.24}$$

where

$$LL_{Q+i}(s_i \oplus s_{Q+i} = +1) = \ln\left(e^{\frac{2\widehat{s}_{\mathrm{sd,Q+i}} - 2}{\sigma^2_{Q+i}}} + e^{-\frac{2\widehat{s}_{\mathrm{sd,Q+i}} - 2}{\sigma^2_{Q+i}}}\right)\,, \tag{3.25}$$

and

$$LL_i(s_i \oplus s_{Q+i} = -1) = \ln\left(e^{\frac{2\widehat{s}_{\mathrm{sd,i}} - 2}{\sigma^2_i}} + e^{-\frac{2\widehat{s}_{\mathrm{sd,i}} - 2}{\sigma^2_i}}\right)\,. \tag{3.26}$$

To reduce the computational complexity, (3.25) and (3.26) can be approximated using the log sum of exponential property [74], i.e. $\ln(e^x + e^y) \approx \max(x,y) + \ln(1 + e^{-|x-y|})$, where $\max(x,y)$ is the maximum value of the two variables, x and y. Equations (3.25) and (3.26) are, hence, approximated as in (3.27) and (3.28), respectively.

$$LL_i(s_i \oplus s_{Q+i} = -1) \approx \max\left(\frac{2\widehat{s}_{\mathrm{sd,i}} - 2}{\sigma_i^2}, -\frac{2\widehat{s}_{\mathrm{sd,i}} - 2}{\sigma_i^2}\right) + \ln\left(1 + e^{-\left|\frac{4\widehat{s}_{\mathrm{sd,i}}}{\sigma_i^2}\right|}\right). \quad (3.27)$$

$$LL_{Q+i}(s_i \oplus s_{Q+i} = +1) \approx \max\left(\frac{2\widehat{s}_{\mathrm{sd,Q+i}} - 2}{\sigma_{Q+i}^2}, -\frac{2\widehat{s}_{\mathrm{sd,Q+i}} - 2}{\sigma_{Q+i}^2}\right) + \ln\left(1 + e^{-\left|\frac{4\widehat{s}_{\mathrm{sd,Q+i}}}{\sigma_{Q+i}^2}\right|}\right). \quad (3.28)$$

By definition, $LLR(s_i \oplus s_{Q+i}) \geq 0$, and therefore the estimated PNC symbols is expressed as in (3.29).

$$\widehat{s_i \oplus s_{Q+i}} = \begin{cases} +1, LL_{Q+i}(s_i \oplus s_{Q+i} = +1) \geq LL_i(s_i \oplus s_{Q+i} = -1) \\ -1, LL_{Q+i}(s_i \oplus s_{Q+i} = +1) < LL_i(s_i \oplus s_{Q+i} = -1) \end{cases}. \quad (3.29)$$

3.2.4 Specialization of the PNC Mapping for 16-QAM

Table 3.2 PNC Mapping Of I/Q-Component Of 16-QAM, Based On SD Scheme

s_i	s_{Q+i}	$s_{\mathrm{sd,i}}$	$s_{\mathrm{sd,Q+i}}$	s^i_{PNC}
1	1	2	0	-3
1	-1	0	2	3
1	3	4	-2	-1
1	-3	-2	4	1
-1	1	0	-2	3
-1	-1	-2	0	-3
-1	3	2	-4	1
-1	-3	-4	2	-1

s_i	s_{Q+i}	$s_{\mathrm{sd,i}}$	$s_{\mathrm{sd,Q+i}}$	s^i_{PNC}
3	1	4	2	-1
3	-1	2	4	1
3	3	6	0	-3
3	-3	0	6	3
-3	1	-2	-4	1
-3	-1	-4	-2	-1
-3	3	0	-6	3
-3	-3	-6	0	-3

Having already presented the PNC Mapping scheme for 4-QAM modulation in massive MIMO system, this section will focus on relatively a higher order modulation scheme, such as 16-QAM. The constellation for each of I/Q component of 16-QAM is $\Theta_{16-QAM} = \{-3,-1,1,3\}$. As in previous section, the goal is to estimate PNC symbols, $\widehat{\boldsymbol{s}}^{i}_{\text{PNC}}$, from the estimated SD symbols, $\widehat{\boldsymbol{s}}_{\text{sd,i}}$ and $\widehat{\boldsymbol{s}}_{\text{sd,Q+i}}$, and the expected SD symbols, $\boldsymbol{s}_{\text{sd,i}}$ and $\boldsymbol{s}_{\text{sd,Q+i}}$, in Table 3.2, using the $f_{\text{PNC}}(.)$ function, assuming that the transmitted symbols are based on 16-QAM.

Since the cardinality of Θ_{16-QAM} is more than two, LLR is not the appropriate approach in estimating the PNC symbols, contrary to the approach for 4-QAM in subsection 3.2.3, where the cardinality is two. The estimated PNC symbol, based on MAP decoder, for each cluster is given in generalized equation (3.21). In this equation, the prior joint probability distribution, $P(\widehat{s}_{\text{sd,i}}, \widehat{s}_{\text{sd,Q+i}})$, of estimated SD symbols, $\widehat{s}_{\text{sd,i}}$ and $\widehat{s}_{\text{sd,Q+i}}$, is equally likely, and therefore the (3.21) approximates to an MLE i.e.

$$(\widehat{s_i \oplus s_{Q+i}} = v)_{MAP} = (\widehat{s_i \oplus s_{Q+i}} = v)_{MLE} \tag{3.30}$$

$$\approx \underset{\widehat{s_i \oplus s_{Q+i}}}{\text{argmax}}\, L(\widehat{s_i \oplus s_{Q+i}} = v | \widehat{s}_{\text{sd,i}}, \widehat{s}_{\text{sd,Q+i}}) \,. \tag{3.31}$$

The 16-QAM PNC symbol, $v \in \Theta_{16-QAM}$, given the estimated SD symbols, $\widehat{s}_{\text{sd,i}}$ and $\widehat{s}_{\text{sd,Q+i}}$, that maximizes the likelihood function, $L(\widehat{s_i \oplus s_{Q+i}} = v | \widehat{s}_{\text{sd,i}}, \widehat{s}_{\text{sd,Q+i}})$, becomes the estimated PNC symbol, $(\widehat{s_i \oplus s_{Q+i}} = v)_{MAP}$. Given the expected SD symbols and the PNC symbols that they are mapped to in Table 3.2, the log-likelihood of PNC symbol of -3, given that the

cluster has the estimated SD symbols, $\widehat{s}_{\mathrm{sd,i}}$ and $\widehat{s}_{\mathrm{sd,Q+i}}$, is expressed as in (3.32).

$$
\begin{aligned}
LL(s_i \oplus s_{Q+i} = -3) &= \ln\left[L(\widehat{s_i \oplus s_{Q+i}} = -3|\widehat{s}_{\mathrm{sd,i}}, \widehat{s}_{\mathrm{sd,Q+i}})\right] \\
&= \ln\Big[P(\widehat{s}_{\mathrm{sd,i}}|s_{\mathrm{sd,i}} = +2)P(\widehat{s}_{\mathrm{sd,Q+i}}|s_{\mathrm{sd,Q+i}} = 0) + P(\widehat{s}_{\mathrm{sd,i}}|s_{\mathrm{sd,i}} = -2)P(\widehat{s}_{\mathrm{sd,Q+i}}|s_{\mathrm{sd,Q+i}} = 0) \\
&+ P(\widehat{s}_{\mathrm{sd,i}}|s_{\mathrm{sd,i}} = +6)P(\widehat{s}_{\mathrm{sd,Q+i}}|s_{\mathrm{sd,Q+i}} = 0) + P(\widehat{s}_{\mathrm{sd,i}}|s_{\mathrm{sd,i}} = -6)P(\widehat{s}_{\mathrm{sd,Q+i}}|s_{\mathrm{sd,Q+i}} = 0)\Big] \\
&= \ln\left[\frac{1}{2\pi\sqrt{\sigma_i^2\sigma_{Q+i}^2}} e^{-\frac{\widehat{s}_{\mathrm{sd,Q+i}}^2}{2\sigma_{Q+i}^2}} \left(e^{-\frac{\left(\widehat{s}_{\mathrm{sd,i}}-2\right)^2}{2\sigma_i^2}} + e^{-\frac{\left(\widehat{s}_{\mathrm{sd,i}}+2\right)^2}{2\sigma_i^2}} + e^{-\frac{\left(\widehat{s}_{\mathrm{sd,i}}-6\right)^2}{2\sigma_i^2}}\right.\right. \\
&\left.\left. + e^{-\frac{\left(\widehat{s}_{\mathrm{sd,i}}+6\right)^2}{2\sigma_i^2}}\right)\right] \\
&= \ln\left[\frac{1}{2\pi\sqrt{\sigma_i^2\sigma_{Q+i}^2}} e^{-\left(\frac{\widehat{s}_{\mathrm{sd,Q+i}}^2}{2\sigma_{Q+i}^2} + \frac{\widehat{s}_{\mathrm{sd,i}}^2+4}{2\sigma_i^2}\right)} \left(\cosh\left(\frac{2\widehat{s}_{\mathrm{sd,i}}}{\sigma_i^2}\right) + \cosh\left(\frac{6\widehat{s}_{\mathrm{sd,i}}}{\sigma_i^2}\right) e^{-\frac{16}{\sigma_i^2}}\right)\right].
\end{aligned}
\tag{3.32}
$$

The log-likelihood of PNC symbol of -1, given $\widehat{s}_{\mathrm{sd,i}}$ and $\widehat{s}_{\mathrm{sd,Q+i}}$, is expressed as in (3.33).

$$
\begin{aligned}
LL(s_i \oplus s_{Q+i} = -1) &= \ln\left[L(\widehat{s_i \oplus s_{Q+i}} = -1|\widehat{s}_{\mathrm{sd,i}}, \widehat{s}_{\mathrm{sd,Q+i}})\right] \\
&= \ln\Big[P(\widehat{s}_{\mathrm{sd,i}}|s_{\mathrm{sd,i}} = +4)P(\widehat{s}_{\mathrm{sd,Q+i}}|s_{\mathrm{sd,Q+i}} = -2) + P(\widehat{s}_{\mathrm{sd,i}}|\widehat{s}_{\mathrm{sd,i}} = -4)P(\widehat{s}_{\mathrm{sd,Q+i}}|s_{\mathrm{sd,Q+i}} = +2) \\
&+ P(\widehat{s}_{\mathrm{sd,i}}|s_{\mathrm{sd,i}} = +4)P(\widehat{s}_{\mathrm{sd,Q+i}}|s_{\mathrm{sd,Q+i}} = +2) + P(\widehat{s}_{\mathrm{sd,i}}|s_{\mathrm{sd,i}} = -4)P(\widehat{s}_{\mathrm{sd,Q+i}}|s_{\mathrm{sd,Q+i}} = -2)\Big] \\
&= \ln\left[\frac{1}{2\pi\sqrt{\sigma_i^2\sigma_{Q+i}^2}} e^{-\left(\frac{\widehat{s}_{\mathrm{sd,i}}^2+16}{2\sigma_i^2} + \frac{\widehat{s}_{\mathrm{sd,Q+i}}^2+4}{2\sigma_{Q+i}^2}\right)} \cosh\left(\frac{4\widehat{s}_{\mathrm{sd,i}}}{\sigma_i^2}\right) \cosh\left(\frac{2\widehat{s}_{\mathrm{sd,Q+i}}}{\sigma_{Q+i}^2}\right)\right].
\end{aligned}
\tag{3.33}
$$

The log-likelihood of PNC symbol of +1, given $\widehat{s}_{\mathrm{sd,i}}$ and $\widehat{s}_{\mathrm{sd,Q+i}}$, is expressed as in (3.34).

$$\begin{aligned}
LL(s_i \oplus s_{Q+i} = +1) &= \ln\left[L(\widehat{s_i \oplus s_{Q+i}} = +1|\widehat{s}_{\mathrm{sd,i}}, \widehat{s}_{\mathrm{sd,Q+i}})\right] \\
&= \ln\Big[P(\widehat{s}_{\mathrm{sd,i}}|s_{\mathrm{sd,i}} = -2)P(\widehat{s}_{\mathrm{sd,Q+i}}|s_{\mathrm{sd,Q+i}} = +4) + P(\widehat{s}_{\mathrm{sd,i}}|s_{\mathrm{sd,i}} = +2)P(\widehat{s}_{\mathrm{sd,Q+i}}|s_{\mathrm{sd,Q+i}} = -4) \\
&+ P(\widehat{s}_{\mathrm{sd,i}}|s_{\mathrm{sd,i}} = +2)P(\widehat{s}_{\mathrm{sd,Q+i}}|s_{\mathrm{sd,Q+i}} = +4) + P(\widehat{s}_{\mathrm{sd,i}}|s_{\mathrm{sd,i}} = -2)P(\widehat{s}_{\mathrm{sd,Q+i}}|s_{\mathrm{sd,Q+i}} = -4)\Big] \\
&= \ln\left[\frac{1}{2\pi\sqrt{\sigma_i^2\sigma_{Q+i}^2}} e^{-\left(\frac{\widehat{s}_{\mathrm{sd,Q+i}}^2 + 16}{2\sigma_{Q+i}^2} + \frac{\widehat{s}_{\mathrm{sd,i}}^2 + 4}{2\sigma_i^2}\right)} \cosh\left(\frac{4\widehat{s}_{\mathrm{sd,Q+i}}}{\sigma_{Q+i}^2}\right) \cosh\left(\frac{2\widehat{s}_{\mathrm{sd,i}}}{\sigma_i^2}\right)\right].
\end{aligned} \tag{3.34}$$

Finally, the log-likelihood of PNC symbol of +3, given $\widehat{s}_{\mathrm{sd,i}}$ and $\widehat{s}_{\mathrm{sd,Q+i}}$, is expressed as in (3.35).

In all of these, four sets of the sum, $\widehat{s}_{\mathrm{sd,i}}$ and the difference, $\widehat{s}_{\mathrm{sd,Q+i}}$, influenced the Gaussian distribution function for the corresponding LL. So for example, to estimate the PNC Symbol +3, the following sets of $\{\widehat{s}_{\mathrm{sd,i}}, \widehat{s}_{\mathrm{sd,Q+i}}\} = \{0,2\},\{0,-2\},\{0,6\},\{-6,0\}$ were utilized in LL as shown in (3.35). This approach has to be repeated in estimating the rest of the PNC symbols.

$$\begin{aligned}
LL(s_i \oplus s_{Q+i} = +3) &= \ln\left[L(\widehat{s_i \oplus s_{Q+i}} = +3|\widehat{s}_{\mathrm{sd,i}}, \widehat{s}_{\mathrm{sd,Q+i}})\right] \\
&= \ln\Big[P(\widehat{s}_{\mathrm{sd,i}}|s_{\mathrm{sd,i}} = 0)P(\widehat{s}_{\mathrm{sd,Q+i}}|s_{\mathrm{sd,Q+i}} = +2) + P(\widehat{s}_{\mathrm{sd,i}}|s_{\mathrm{sd,i}} = 0)P(\widehat{s}_{\mathrm{sd,Q+i}}|s_{\mathrm{sd,Q+i}} = -2) \\
&+ P(\widehat{s}_{\mathrm{sd,i}}|s_{\mathrm{sd,i}} = 0)P(\widehat{s}_{\mathrm{sd,Q+i}}|s_{\mathrm{sd,Q+i}} = +6) + P(\widehat{s}_{\mathrm{sd,i}}|s_{\mathrm{sd,i}} = 0)P(\widehat{s}_{\mathrm{sd,Q+i}}|s_{\mathrm{sd,Q+i}} = -6)\Big] \\
&= \ln\left[\frac{1}{2\pi\sqrt{\sigma_i^2\sigma_{Q+i}^2}} e^{-\left(\frac{\widehat{s}_{\mathrm{sd,i}}}{2\sigma_i^2} + \frac{\widehat{s}_{\mathrm{sd,Q+i}} + 4}{2\sigma_{Q+i}^2}\right)} \left(\cosh\left(\frac{2\widehat{s}_{\mathrm{sd,Q+i}}}{\sigma_{Q+i}^2}\right) + \cosh\left(\frac{6\widehat{s}_{\mathrm{sd,Q+i}}}{\sigma_{Q+i}^2}\right) e^{-\frac{16}{\sigma_{Q+i}^2}}\right)\right].
\end{aligned} \tag{3.35}$$

3.3 Numerical Results

In this section, we present Monte-Carlo system simulation results to evaluate the performance of the proposed PNC mapping scheme for massive MIMO systems. The goal of the simulation is to evaluate the bit-error-rate (BER) of the MAP-based PNC mapping functions derived in sub-section 3.2.3 and sub-section 3.2.4, using linear detectors, such as ZF and MMSE, to estimate the clusters of SD symbols.

3.3.1 Simulation Setup

Simulation parameters are listed in Table 3.3. The simulation scenario consists of a single cell, with a base station, which is located at the center of the cell. The UEs are uniformly distributed in the cell. The base station and the UEs have multiple antennas, M, for the base station and K, for each UE, however, the base station has far more antennas than each of the UEs. For the sake of simplicity, K is assumed to be the same for all UEs. The focus of the simulations is uplink. In each time slot, each UE transmits a fixed number of symbols. The channel paths among the UEs are uncorrelated, and so are the individual antenna paths per UE. For each SNR, Monte Carlo simulations are performed over 10K iterations.

We simulated three major use-cases over this setup: conventional massive MIMO (without any network coding), massive MIMO with network layer NC and massive MIMO with physical layer NC. We present the results for different variants of the M-QAM over these three use-cases in 3.3.2.

3.3.2 Performance Analysis

In the analysis, we compare the BER of the three use-cases of conventional massive MIMO, massive MIMO with NC and massive MIMO with PNC. Comparing the BER of the conventional massive MIMO to our work on massive MIMO and PNC is necessary in order to ascertain if the former's decoding performance is sacrificed at the expense of incorporating PNC into massive MIMO. To reiterate, ZF and MMSE were adopted without any modifica-

Table 3.3 Simulation Parameters

Parameters	***Values***
No. antennas at relay, M	[4, 64, 120]
No. antennas per UE, K	[2, 4, 10]
No. UEs, N	[2, 16, 12]
Channel, H	i.i.d Rayleigh
SNR in dB	$0 \ldots 50$
Modulation	4-QAM, 16-QAM, 64-QAM
No. iterations	10^4
Channel Coding	Uncoded
Linear Detectors	ZF, MMSE

tion in our PNC scheme, and therefore BER of the massive MIMO and PNC is expected not to be worse than that of the conventional massive MIMO.

In Fig. 3.2, we compare the BER of conventional massive MIMO, massive MIMO with NC and massive MIMO with PNC, where the detection scheme is ZF, and with the following parameters: $M = 64$, $N = 16$, $K = 4$, and the modulation schemes are 4-QAM, 16-QAM, and 64-QAM. The mathematical derivations for the MAP-based PNC mapping function for 64-QAM are included in the Appendix. The figure reveals that, irrespective of the modulation scheme, the BER of massive MIMO and PNC was better than the conventional massive MIMO, exceeding our expectation. This can be attributed to the fact that the ZF linear detector does not have to detect the individual transmitted symbols, rather a sum and difference of the transmitted symbols will be detected, and then, soft decoding into the PNC symbols using the MAP decoder are implemented. Looking closely at varying M-QAM across all usecases, the plots reveal relatively progressive error performance as SNR increases, which is higher for higher order dimension, e.g. 64-QAM. Although diversity gain has increased upon having huge number of antennas at the base station, so has interference and noise at the receive antennas. As interference and noise accumulate at the receive antennas, it is difficulty

to correct erroneously detected symbols of a higher order modulation scheme. Hence, ZF detection may not be suitable for massive MIMO and PNC for higher order modulations schemes such as 64-QAM, due to its inability to address noise accumulations.

Fig. 3.3 considers the same simulation parameters as in Fig. 3.2, except the linear detector is MMSE-based. Again, in this figure, the BER of massive MIMO and PNC is lower than the BER of conventional massive MIMO, closely aligning with the results in Fig. 3.2. The plots also show that as the SNR approaches 25dB, the BER of massive MIMO and PNC for 4-QAM decreases sharply compared to massive MIMO and PNC for 16-QAM and 64-QAM. The modulation scheme of 4-QAM appears to be the preferred transmission scheme in the lower SNRs and when throughput is small. However, 64-QAM may be the preferred modulation scheme for massive MIMO and PNC as SNR increases. In general, if the noise variance at the receive antennas can be easily determined, then MMSE-based massive MIMO and PNC is preferred, when the number of base station antennas is big.

The simulation setup for Fig. 3.4 and Fig. 3.5 are, respectively, the higher order antenna dimension of Fig. 3.2 and Fig. 3.3. The simulation parameters are: $M = 120$, $N = 30$, $K = 4$. Modulation 4-QAM, 16-QAM, and 64-QAM are deployed in both Fig. 3.4 and Fig. 3.5, with the former using ZF and the latter, MMSE linear detection. Again, in both figures, the BER of our massive MIMO and PNC scheme peformed better than conventional massive MIMO, exceeding our expectations. The plots in Fig. 3.4 reveal that massive MIMO with PNC utilizing 4-QAM performs better than those with 16-QAM and 64-QAM, but requires higher SNR to achieve that performance. Again, ZF may not be the appropriate the detection scheme for the lower SNRs. Fig. 3.5, on the other hand, reveals that massive MIMO and PNC with 64-QAM performs better in the higher SNRs, making it the ideal setup for higher throughput requirements.

In Fig. 3.6, our proposed scheme using MMSE and ZF was bench-marked against an optimal detector in ML, in MIMO system with just 4 antennas at the base station and two users, each with two antennas. Evidently, our proposed scheme with ML detector performed way better than that of the ZF and MMSE and this trend of performance will be similar for higher order dimension of antennas and the higher order of the QAM. ML is

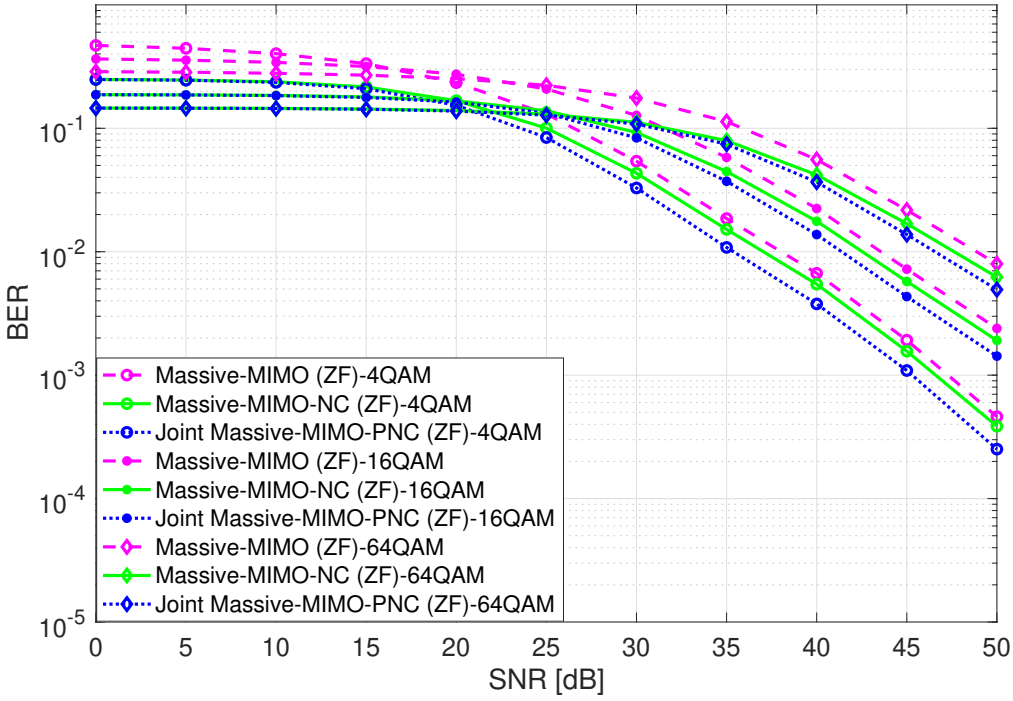

Fig. 3.2 Uplink BER performance comparison between i) conventional multi-user MIMO ii) multi-user MIMO with network layer NC and iii) multi-user MIMO with PNC), all using ZF detector, for M=64, N=16 and K=4.

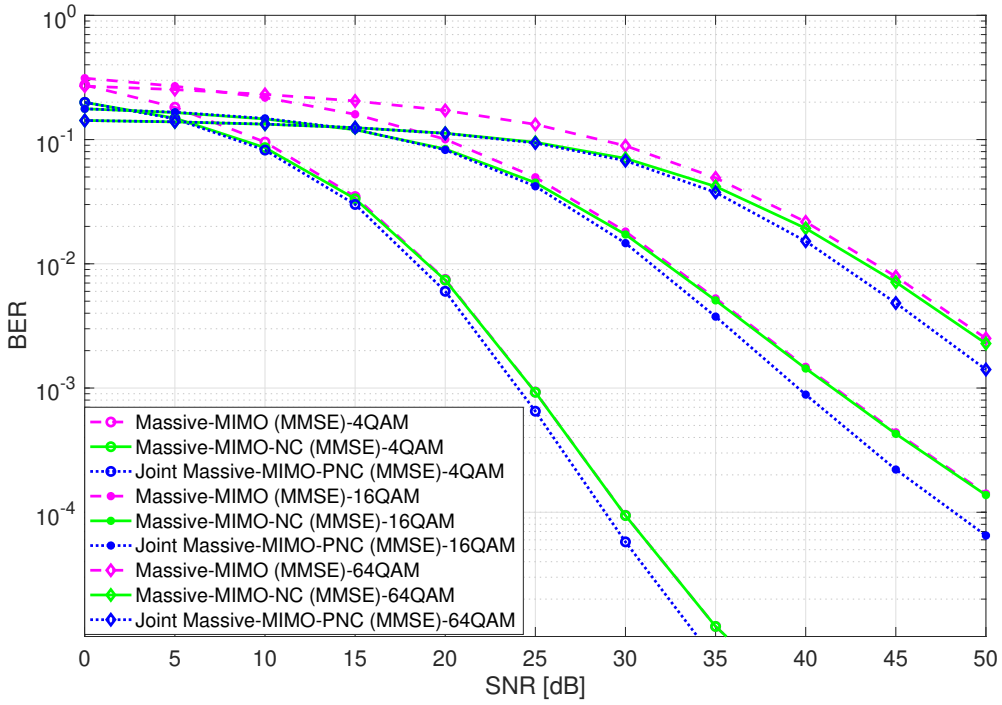

Fig. 3.3 Uplink BER performance comparison between i) conventional multi-user MIMO ii) multi-user MIMO with network layer NC and iii) multi-user MIMO with PNC), all using MMSE detector, for M=64, N=16 and K=4.

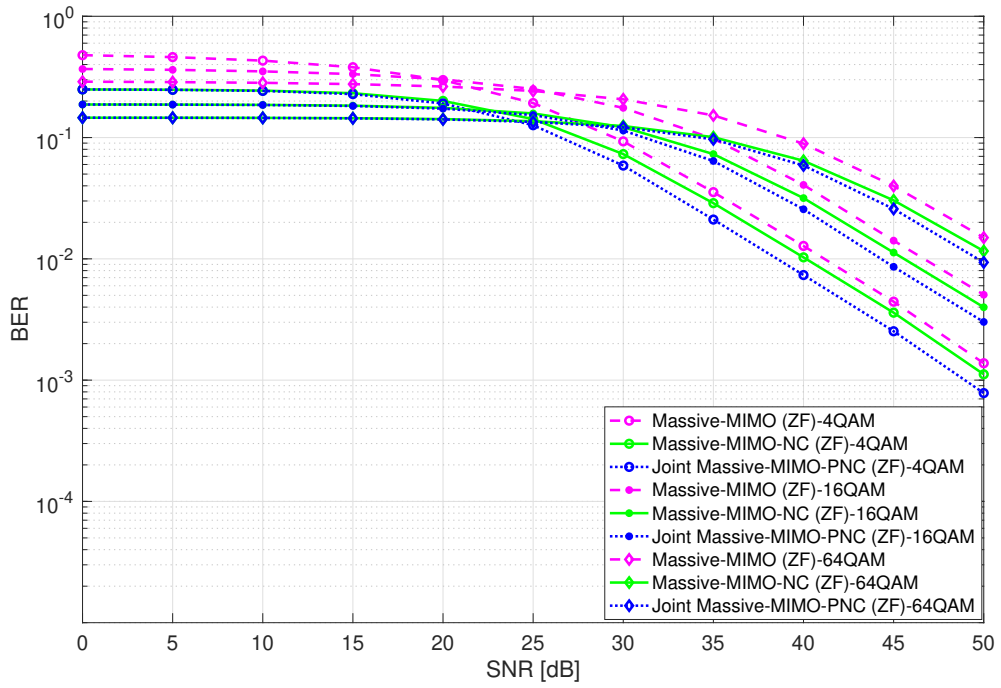

Fig. 3.4 Uplink BER performance comparison between i) conventional multi-user MIMO ii) multi-user MIMO with network layer NC and iii) multi-user MIMO with PNC), all using ZF detector, for M=128, N=16 and K=8.

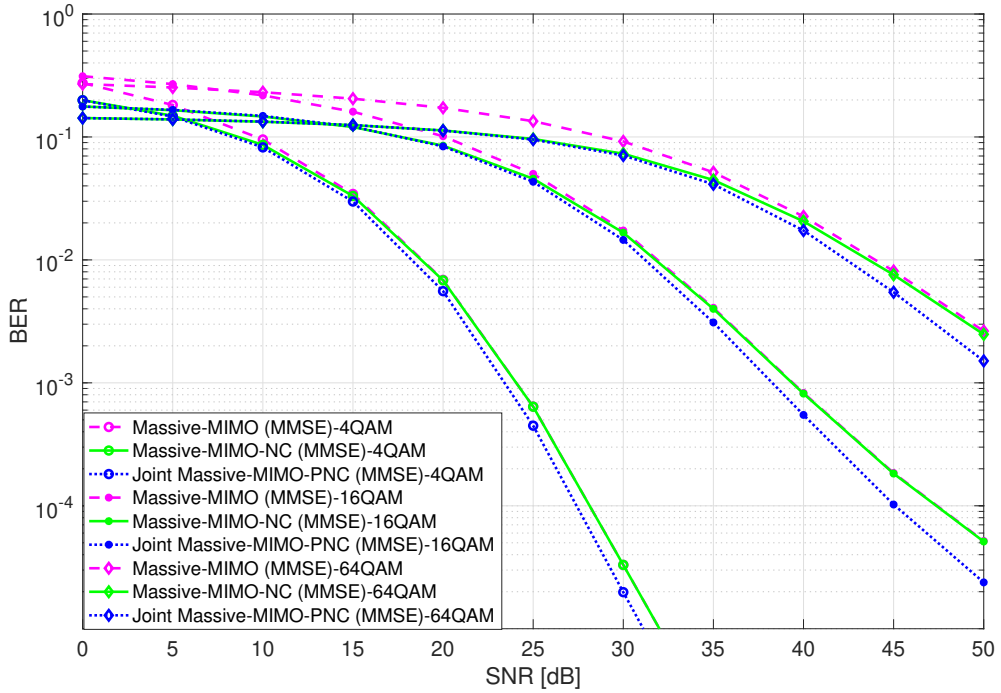

Fig. 3.5 Uplink BER performance comparison between i) conventional multi-user MIMO ii) multi-user MIMO with network layer NC and iii) multi-user MIMO with PNC), all using MMSE detector, for M=128, N=16 and K=8.

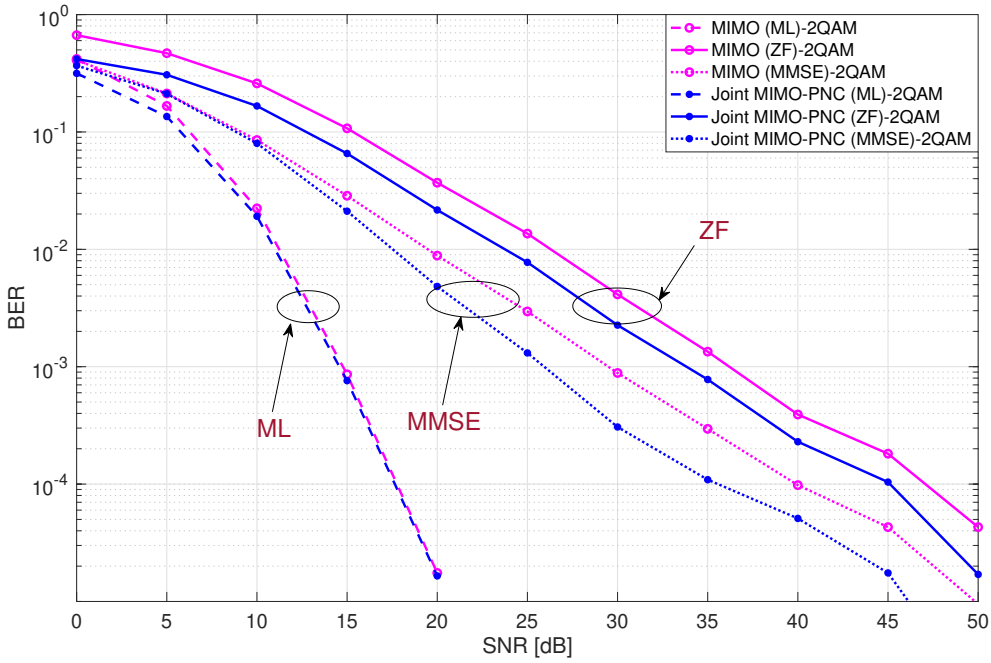

Fig. 3.6 Uplink BER performance comparison between i) conventional multi-user MIMO and ii) multi-user MIMO with PNC), all using ZF, MMSE detector and ML, for M=4, N=2 and K=2.

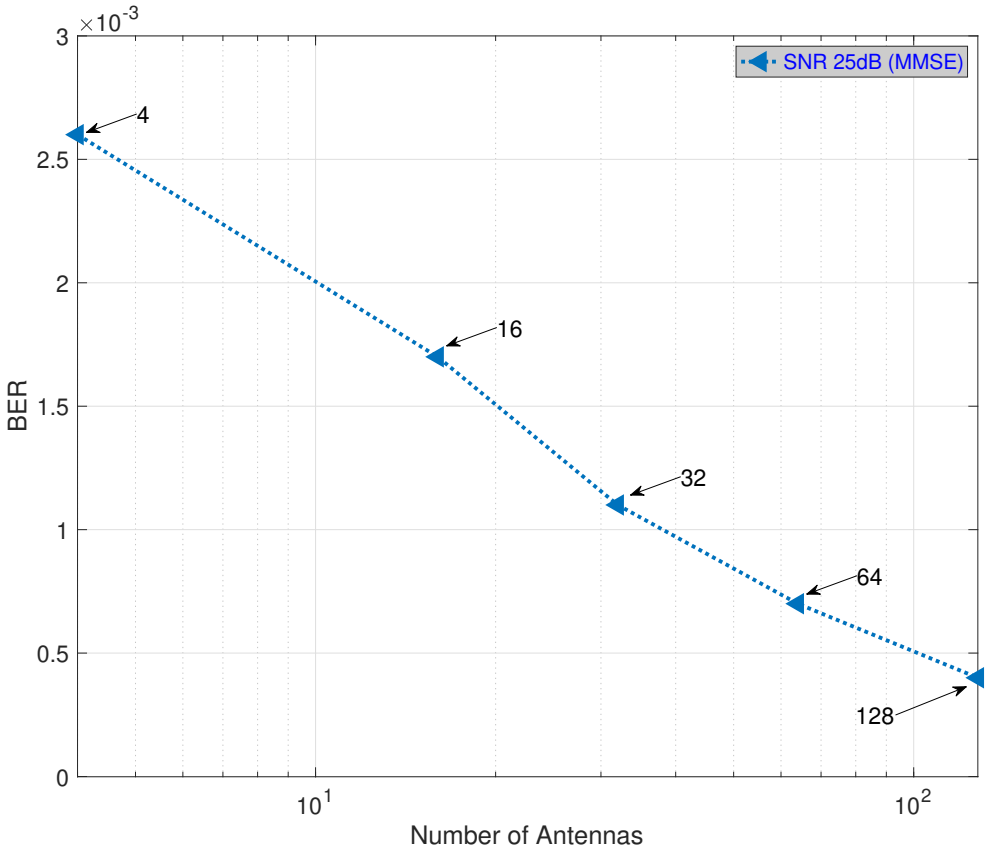

Fig. 3.7 BER of proposed M-MIMO PNC scheme against the number of antennas

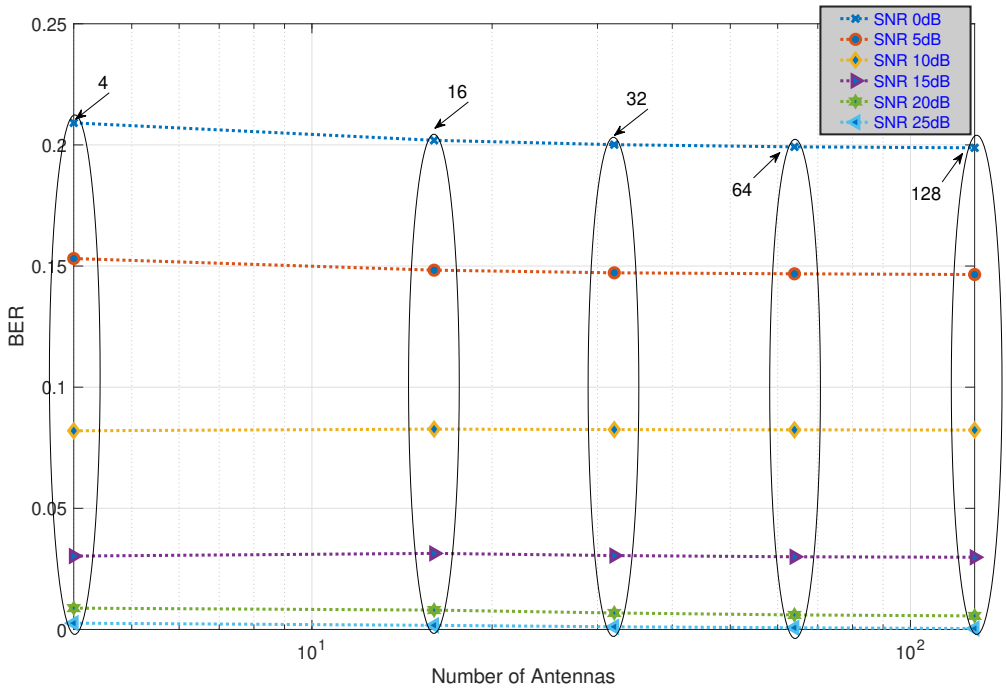

Fig. 3.8 BER of proposed M-MIMO PNC scheme against the number of antennas at different SNR's

not practical enough because of the exponential computational complexity as the number of antenna increases and also as the order of dimension of the QAM increases. However, the result asserts the notion that ZF and MMSE can be replaced with other higher performance sub-optimal detectors, and our proposed scheme's performance will scale accordingly.

Our proposed PNC scheme's decoding complexity lies on the product of the number of users and number antennas that each user has. The larger the cumulative number of the transmit antennas, the higher complexity in correctly estimating the PNC symbols. However, in practical systems, user devices may not be equipped with large number of antennas as opposed to the massive number of antennas at the base station. The order of dimension of the QAM also plays a role in the PNC decoding complexity. Much like having large number of antennas, the higher the order of the M-Ary QAM, the more constellation values, the more the sum and difference symbols, and the higher the complexity in decoding.

The performance of our proposed scheme can also be explained utilizing the minimum distance concept [75]. The goal is to characterize the minimum distance between two NC symbols. However, in our proposed scheme, because we derive the PNC symbols from the SD symbols, the minimum distance among the SD symbols is rather pertinent. Taking 4-QAM for example, the constellation values of the independent I/Q phases are {+1, -1}, leading SD symbols to be {2, 0, -2} as shown in Table 3.1. It is evident that the minimum distance of the SD symbols is no different than the minimum distance of the transmitted symbols. It means, rather detecting the transmitted symbols and deriving the NC symbols, if we detect the SD symbols, the decoding performance of the latter is expected not to be much worse or better than the former. However, considering Table 3.1, for example, mapping the detected SD symbols to PNC symbol of +1, does not require that both the sum and difference are decoded correctly. If the detected sum is zero, without detecting that the difference is either +2 or -2, a +1 PNC symbol can be assumed. Similar approach goes for mapping detected SD symbols to PNC symbol of -1. This approach seems to lower the probability of error in correctly decoding the PNC symbol allowing our proposed scheme to perform slightly better than the conventional M-MIMO, where the decision region is definite in detecting the individual transmitted symbols.

Our proposed scheme also benefits from the law of large numbers as much as underlying massive MIMO systems. In Fig. 3.7, we plotted the BER of our proposed scheme against variation of number of antennas, whilst fixing the SNR and the modulation scheme, respectively at 25 dB and QPSK. In the figure, one can notice that as the number of antennas increases, the BER of our proposed scheme decreases exponentially till a point where the channel starts to harden, where the noise starts to average out causing the impact of fading to diminish, leading to lower probability of error. The plot in Fig. 3.7 is extended by varying the SNR and Fig. 3.8 shows the corresponding results. As in Fig. 3.7, each of the plots decreases exponentially till at a certain number of antennas, when their BER start to decrease steadily. Among the individual BER plots, the one with the 25dB SNR has the lowest BER. The steady part of the BER in both figures can be attributed to the phenomenon of the law of large numbers.

It is also evident from the results that the performance was presented with respect to UL. Our proposed scheme is applicable at the interference point, which is the UL. This is where PNC is performed by the base station. In essence, the base station receives interfered symbols, apply our proposed scheme and then generate the PNC symbols. In DL, the base station transmits the derived PNC symbols to respective UEs in a way similar to how conventional massive MIMO operates in DL. Therefore, the performance evaluation in DL is similar to those for the conventional massive MIMO in the literature.

3.4 Conclusions

A practical approach for deploying PNC in M-QAM massive MIMO systems has been described in this chapter. A proposed PNC mapping scheme based on clusters of estimated SD of the transmitted symbols from user pairs was developed to enable using PNC in massive MIMO systems. Utilizing existing linear detectors, such as ZF and MMSE and using an SD linearly transformed channel matrix, the SD symbols are detected. Employing MAP soft decoding, we mapped the detected SD symbols to the PNC symbols. The simulation results reveal that, using existing MIMO detection schemes, our proposed scheme achieves twice

the spectral efficiency of conventional massive MIMO. The BER of our scheme was slightly better than the conventional massive MIMO, indicating that our proposed PNC scheme can be deployed without sacrificing the BER of the conventional massive MIMO. Furthermore, the results also revealed that for lower throughput and at low SNR, 4-QAM appears to be the preferred modulation scheme, whereas 64-QAM or higher is the preferred scheme in higher SNR, satisfying a higher throughput requirement. Further research is however needed in order to make this a reality in deployed systems. For example, research in integrating channel coding is needed to improve on the error performance and get the proposed scheme closer to real systems. Research in users transmitting with different QAM modulation schemes is also needed to get the proposed scheme close to real systems. Also, dealing with asynchronous transmission by multiple sources with our proposed scheme as the underlying PNC system requires further research.

Chapter 4

Jamming Attacks in Massive MIMO PNC

4.1 Introduction

The broadcast nature of the wireless medium has undoubtedly propelled some significant innovations that allow users to access network resources from nearly any convenient location. These innovations enable mobile users to access real-time information whilst on the move, allowing increase in coverage and scalable deployment of network resources. Interference has been one of the main challenges to deal with in such an open air interface in wireless communication, where signals from multiple sources arrive simultaneously at a receiver. Although, there is no interference that is friendly, some forms of interference can be controlled by regulating the transmission of the interference sources. Unfortunately, some forms of interference are intentional and uncontrollable. They fall into the category of denial-of-service (DoS) attack and are often referred to as radio-frequency (RF) jamming. RF jamming is a malicious attempt to overwhelm a wireless communication system with the objective of sabotaging the normal operation of the network [76].

Jamming attack in itself is considered under the umbrella of active attack in physical layer security (PLS) [77]. The broadcast nature of the wireless medium makes the physical layer the most vulnerable layer. PLS solutions approach security issues from information theoretic perspective, by leveraging on the randomness, interference and other characteristics as observed by the PHY. However, some attacks, particularly those categorised under

active attacks, might require countermeasure approaches that include PHY algorithms and techniques that can withstand the attack with little or no degradation. The countermeasure approaches address the proactive types of jamming attacks [78, 77], where the attacker's main objective is to thwart the normal operation of a wireless system by persistently sending jamming signals. One of the most prevailing jamming technique is deploying noise.

Noise jamming techniques reduce the cumulative received SNR by increasing the thermal noise level at the receiver. Barrage jamming, spot jamming and sweep jamming are the three most common types of noise jamming [78, 77]. These noise jamming techniques, respectively, focus the transmit power on multiple frequencies at the same time, a fleet of frequencies and a single frequency. A number of jamming attacks research in radar systems have focused on the Barrage jamming where the entire bandwidth of the transmission is targeted with noise. The adverse effect of jamming has been extensively studied, as outlined in [79]. The effect of jamming in millimeter-wave (mmWave) communications has been examined in [80, 81]. For the mmWave massive MIMO systems, a reinforcement learning based power control strategy, based on the signal-to-interference-plus-noise ratio (SINR) of the signals and the jamming strength has been considered in [80], while a hybrid beamforming design to cancel the interference coming from jamming signal has been presented in [81].

In the previous section, we outlined a practical approach for deploying PNC in multi-user massive MIMO systems, utilizing M-QAM modulation scheme. In this massive MIMO PNC work, we formulated a Maximum a Posteriori (MAP) based PNC mapping scheme, leveraging on the existing MIMO's linear detectors such as Zero-Forcing (ZF) and Minimum Mean Square Error (MMSE). The transmissions were over the Rayleigh fading channel with additive-white Gaussian noise (AWGN) at the receive antennas and the performance evaluation revealed that in the lower SNR regime, our PNC scheme outperformed conventional massive MIMO in those structured noisy and interfered channels. The lingering question now is if such a robust PNC scheme can withstand uncontrolled jamming signals from a jammer.

In this section, we study a multi-user massive MIMO system, where a base station's capacity to perform PNC is challenged by an active jammer that persistently transmits

jamming signals. We anaylse the error performance of the base station's capability to estimate the PNC symbols amid the active jamming signals.

4.2 Jamming Attack to our Proposed Massive-MIMO PNC System

The system model shown in Fig. 4.1 depicts a single cell massive MIMO with centralized base station, through which legitimate users (LUEs) communicate. The goal in this setup is for each of the LUEs to communicate and receive symbols from every other LUEs. The LUEs transmit their symbols in the uplink, the base station estimates the PNC symbols from the aggregated received symbols and then broadcasts the PNC symbols back in the downlink to the respective LUEs. In the same system model, there is a jammer whose objective is to sabotage the correctness of the PNC symbols estimation by sending jamming signals. The jammer has a few degrees of freedom in adversely influencing the estimation of the PNC symbols by the base station. These include the transmit power of the jamming signal and number of antennas to transmit the jamming signals. In essence, it is assumed that the jammer has multiple number of transmit antennas. The jammer's position is assumed to be outside of the cell in which the LUEs are communicating through the base station. The channel between the base station and the jammer is assumed not to be known by the base station and communications between these two entities are independent of the communications between the base station and LUEs. The jamming technique can be assumed to be any of those mentioned in Section 4.1.

In this single cell massive MIMO scenario, M denotes the number of antennas through which the base station receives UL messages from the LUEs, N denotes the number of LUEs which are equipped with K number of antennas, and $L = K \times N$ input antennas. As depicted in Fig. 4.1, the received symbols vector at the base station is given by

$$\boldsymbol{r} = \boldsymbol{H}\boldsymbol{s} + \boldsymbol{J}\boldsymbol{z} + \boldsymbol{n}\,, \tag{4.1}$$

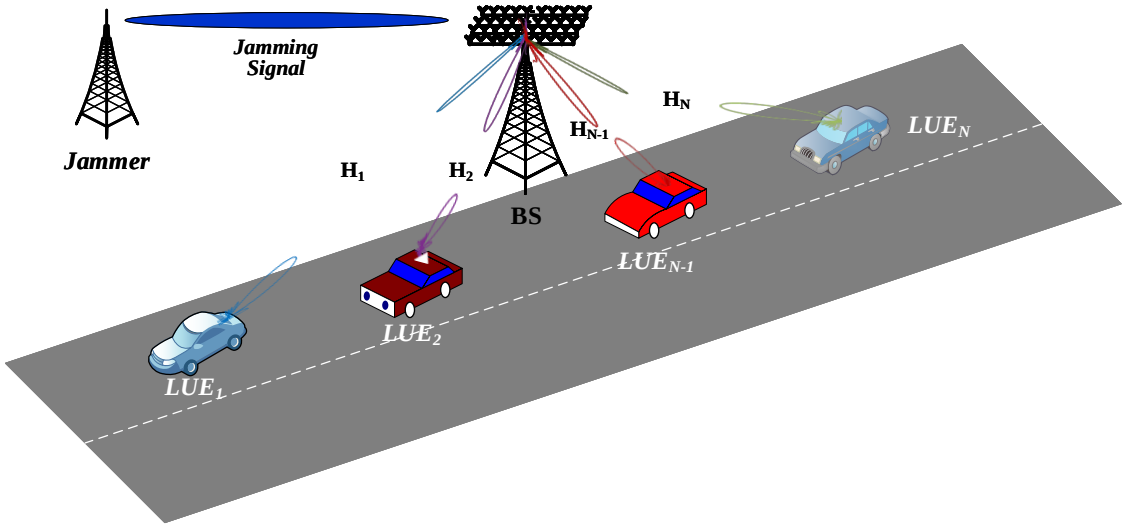

Fig. 4.1 A System Model for a Multi-user Massive MIMO Vehicular Network under Jamming Attack.

where $\boldsymbol{J} \in \mathbb{C}^{M \times J}$ is the jammer to base station complex channel matrix. We assume that the transmitted symbols are Gray-scale M-ary Quadrature Amplitude Modulation (QAM) and the average transmitted energy per symbol is $\mathbb{E}[|s_i|^2] = E_s / L$, where E_s is the M-ary QAM symbol energy at each antenna.

We consider linear detectors to estimate the transmitted symbols from the received symbols at the receive antennas of the base station. ZF and MMSE linear detectors are the main focus. They are known to have desirable computational complexity and are proven to perform well in massive MIMO networks. We also assume that there is a perfect channel state information (CSI) at the base station (i.e., the channel matrix $\boldsymbol{H}$ is known at the receiver (base station)). The estimated complex symbols vector, $\widehat{\boldsymbol{s}}$, is given as

$$\widehat{\boldsymbol{s}} = \boldsymbol{G}\boldsymbol{r}, \tag{4.2}$$

where $\boldsymbol{G}$ is the complex detection matrix, which is also expressed, respectively, for ZF and MMSE, as

$$\boldsymbol{G}^{\mathrm{ZF}} = (\boldsymbol{H}^{\mathrm{H}}\boldsymbol{H})^{-1}\boldsymbol{H}^{\mathrm{H}}\,, \tag{4.3}$$

$$\boldsymbol{G}^{\mathrm{MMSE}} = (\boldsymbol{H}^{\mathrm{H}}\boldsymbol{H} + \sigma_n^2\mathrm{I})^{-1}\boldsymbol{H}^{\mathrm{H}}, \tag{4.4}$$

where σ_{n}^2 is AWGN noise variance at the received antennas. As shown in (4.3) and (4.4), $\boldsymbol{G}^{\mathrm{ZF}}$ and $\boldsymbol{G}^{\mathrm{MMSE}}$ are both dependent on the complex channel matrix, $\boldsymbol{H}$.

In section 3.2, we described a massive MIMO PNC algorithm, where a multi-antenna base station estimates PNC symbols from received interfered symbols, which are composed of superimposed transmitted symbols from multi-user multi-antenna UEs. The concept is based on a linear transformation of the channel between the base station and the UEs, using a sum-difference (SD) matrix, under the assumption that channel is known to the base station. The SD matrix ensures that the transmitted symbols are grouped into clusters of transmit antennas, from the UEs that intend to communicate with each other. The base station then estimates a sum and difference of the transmitted symbols in the cluster, from the received symbols using linear detectors such as ZF and MMSE. The detection matrix is based on the SD transformed channel matrix. Therefore, the distinction here is that for conventional massive MIMO, the complex detection matrix is dependent on the original complex channel matrix, whereas the complex detection matrix for the massive MIMO PNC is dependent on the transformed complex channel matrix.

Considering (2.8), the system model in 4.1 can be expressed, mathematically, as

$$\boldsymbol{r} = (\boldsymbol{H}{\boldsymbol{P}_{\mathrm{sd}}}^{-1})(\boldsymbol{P}_{\mathrm{sd}}\boldsymbol{s}) + \boldsymbol{J}\boldsymbol{z} + \boldsymbol{n} \tag{4.5}$$

$$= \boldsymbol{H}_{\mathrm{sd}}\boldsymbol{s}_{\mathrm{sd}} + \boldsymbol{J}\boldsymbol{z} + \boldsymbol{n}, \tag{4.6}$$

where $\boldsymbol{P}_{\mathrm{sd}}$ is the SD matrix, $\boldsymbol{H}_{\mathrm{sd}} = \frac{1}{2}\boldsymbol{H}\boldsymbol{P}_{\mathrm{sd}}$, is the linear transformation of the MIMO channel with a SD matrix, and $\boldsymbol{s}_{\mathrm{sd}} = \boldsymbol{P}_{\mathrm{sd}}\boldsymbol{s}$, clusters of SD symbols, whose estimates at the base station, are then mapped to the PNC symbols. Although the term $\boldsymbol{J}\boldsymbol{z}$ in (4.5) is missing in

the corresponding equation in (3.7), the estimation of the $\boldsymbol{s}_{\text{sd}}$, SD symbols, also remains the same. Utilizing the same following equalization matrix

$$\boldsymbol{G}_{\text{sd}} = \begin{cases} (\boldsymbol{H}_{\text{sd}}^{\text{H}}\boldsymbol{H}_{\text{sd}})^{-1}\boldsymbol{H}_{\text{sd}}^{\text{H}}, \text{ for ZF} \\ (\boldsymbol{H}_{\text{sd}}^{\text{H}}\boldsymbol{H}_{\text{sd}} + \sigma_n^2\text{I})^{-1}\boldsymbol{H}_{\text{sd}}^{\text{H}}, \text{ for MMSE} \end{cases}, \tag{4.7}$$

the estimated SD symbols is still given as

$$\widehat{\boldsymbol{s}}_{\text{sd}} = \boldsymbol{G}_{\text{sd}}\boldsymbol{r}. \tag{4.8}$$

4.3 Channel Modelling

In this section, we will describe the channel models for both sub-6 GHz and mmWave frequencies.

4.3.1 Sub-6 GHz Model

The channel model for the sub-6 GHz has been one of the well researched fields. Until recent progress in mmWave, the radio propagation in the sub-6 GHz was perceived as the most favorable radio propagation channel. It is still the most reliable spectrum for radio propagation, amid the scarcity of bandwidth for future wireless communication systems.

In this sub-section, we assume a multi-path propagation medium with worse-case of line-of-sight (LoS), making Rayleigh fading channel the prime focus. Given that $\boldsymbol{H}$ in (2.8) is assumed to be a Rayleigh fading complex channel matrix, its distribution can be modeled as a joint probability distribution of its in-phase and quadrature components. The complex entries of $\boldsymbol{H}$, i.e. h_{ij}, where i is the receive antenna index and j, the transmit antenna index, are i.i.d. Gaussian random variables of zero mean and a unit variance.

The effect of the jamming signal at the base station antennas is modelled as an additive noise. In the presence of a jammer, the term $\boldsymbol{Jz}$ in (2.8) is assumed to dominate over the AWGN, $\boldsymbol{n}$. The signal-to-jamming plus noise ratio (SJNR) is expressed as SJNR =

$L \times E_{\mathrm{s}} / (\sigma_{\mathrm{n}}^2 + \sigma_{\mathrm{z}}^2)$, where σ_{z}^2 is the jamming noise variance. The signal-to-jamming ratio (SJR) is given as $\mathrm{SJR} = J \times E_{\mathrm{z}} / \sigma_{\mathrm{z}}^2$. In the absence of a jammer, the signal-to-noise ratio is given as, $\mathrm{SNR} = L \times E_{\mathrm{s}} / \sigma_{\mathrm{n}}^2$. The effect of the term $\boldsymbol{Jz}$ in (4.6), is the prime focus of this investigation. Treating the jamming signal, $\boldsymbol{z}$, as additive noise, then the lower bound of the performance of the system model is achieved since the worst case jamming signal is Gaussian when the transmitted signal is considered to be Gaussian [82]. Therefore, in our system model, the jamming term is modeled as Gaussian for sub-6 GHz. If the jamming does not dominate the AWGN, $\boldsymbol{n}$, then the decoding performance is expected to be similar to the results in the previous section. Therefore, the target is to evaluate the error performance of the system model when the jamming term, $\boldsymbol{Jz}$, dominates $\boldsymbol{n}$.

4.3.2 mmWave Model

The mmWave system consists of a base station equipped with M antennas having uniform linear array (ULA) antenna structure and M radio frequency (RF) chains, communicating with N legitimate single-antenna users in a single cell. The mmWave channel model is composed of the LoS and the non-LoS (nLoS) components [83], [84].

The channel matrix of the n^{th} user, $\mathbf{H}_n \in \mathbb{C}^{M \times 1}$, is given as

$$\mathbf{H}_n = \mathbf{H}_n^{\mathrm{LoS}} + \mathbf{H}_n^{\mathrm{nLoS}}, \tag{4.9}$$

where $\mathbf{H}_n^{\mathrm{LoS}}$ and $\mathbf{H}_n^{\mathrm{nLoS}}$, respectively, denote the LoS component and the nLos components of the mmWave channel and they are respectively, defined as

$$\mathbf{H}_n^{\mathrm{LoS}} = \alpha_n^{\mathrm{LoS}} \cdot \mathbf{a}_n(\varphi_{\mathrm{LoS}}^{\mathrm{Rx}}) \cdot (\mathbf{a}_n(\varphi_{\mathrm{LoS}}^{\mathrm{Tx}}))^{\mathrm{H}}, \tag{4.10}$$

$$\mathbf{H}_n^{\mathrm{nLoS}} = \frac{1}{\sqrt{S_{n,c}}} \sum_{c=1}^{C} \sum_{s=1}^{S_{n,c}} \alpha_{n,c,s} \cdot \mathbf{a}_n(\varphi_{c,s}^{\mathrm{Rx}}) \cdot (\mathbf{a}_n(\varphi_{c,s}^{\mathrm{Tx}}))^{\mathrm{H}}, \tag{4.11}$$

where C and $S_{n,c}$ denote the number of clusters and the number of sub-paths in each cluster, respectively. α represents instantaneous complex channel gain for LoS and nLoS components. Moreover, φ indicates the azimuth angle and $\mathbf{a}(\varphi^{\mathrm{Rx}})$, $\mathbf{a}(\varphi^{\mathrm{Tx}})$ respectively, denote angle of

arrival (AoA) array factor at the receiver and angle of departure (AoD) array factor at the transmitter. $(\mathbf{a}(.))^{\mathrm{H}}$ denotes the complex transpose of the antenna array factor.

For the ULA, the antenna array response is defined by,

$$\mathbf{a}(\varphi) = \frac{1}{\sqrt{M}}[1, \ldots, e^{j(m-1)kd_x \sin(\varphi)}, \ldots, e^{j(M-1)kd_x \sin(\varphi)}]^T \tag{4.12}$$

where M is the number of antennas in horizontal axis, k is the wave number which is defined as $k = \frac{2\pi}{\lambda}$. The inter-element spacing (distance between two adjacent antenna elements) is indicated by $d_x = 0.5\lambda$.

4.4 Performance Analysis of Massive MIMO PNC under Jamming Attack

4.4.1 In Sub-6 GHz

In this subsection, we evaluate the error performance of the proposed MIMO PNC scheme against jamming attack in sub-6GHz frequencies. The simulation parameters are listed in Table 4.1. In the simulation, we have a base station with multiple number of antennas communicating with LUEs, and for simplicity, we assume that the number of antennas at each LUE is the same. The jammer is also assumed to have multiple number of antennas and transmitting independently of the LUEs. The objective of the base station is to apply the PNC algorithm in previous, whereas, that of the jammer is to introduce errors in the PNC algorithm execution. In the simulation setup, the jammer has a couple of possibilities to influence the performance of the base station. We simulated various scenarios that include conventional MIMO without PNC, MIMO with PNC, with and without jamming attack. We regulated the transmit power and the number of antennas of the jammer, and then, countered it with regulating the dimension of the received antennas of the base station and also the modulation scheme. cases of MIMO and PNC and the jammer.

Table 4.1 Simulation Parameters

Parameters	***Values***
No. antennas at base station, M	$4,\ldots,16$
No. antennas per UE, K	2
No. UEs, N	$2,\ldots,8$
Channel, H	i.i.d Rayleigh
SNR [dB]	$0,\ldots,50$
Modulation	QPSK, 16QAM
No. iterations	10^4
Channel Coding	Uncoded
Linear Detectors	ZF, MMSE
No. antennas at Jammer, J	$\{1,2\}$
SJR [dB]	$10,\ldots,20$

Fig. 4.2 presents the error performance for all use cases when the modulation scheme is QPSK, employing both ZF and MMSE. The base station has four antennas, and each of the two UEs has two antennas and the jammer has a single antenna with SJR of 10dB. Although the dimension of the antennas at the base station in this setup is not massive MIMO, its worth providing result for completeness. In the simulation result, the BER of MIMO and PNC is comparably better in all use cases. The BER of the MMSE-based use cases performed better than the ZF counterpart, which is as expected, as ZF does not consider noise at the receive antennas in the detection of the transmitte symbols. Among the use cases, it can be seen that non-jammed MIMO and PNC performed better than the non-jammed, but only MIMO. This shows that MIMO and PNC can coexist without any detriment to the performance of the former. It can also be seen that both jammed MIMO and jammed MIMO PNC performed comparatively close to the non-jammed counterpart, until at about 15dB SNR. Further from this SNR, the jammed BER for the usecases starts to remain steady. This is an indication

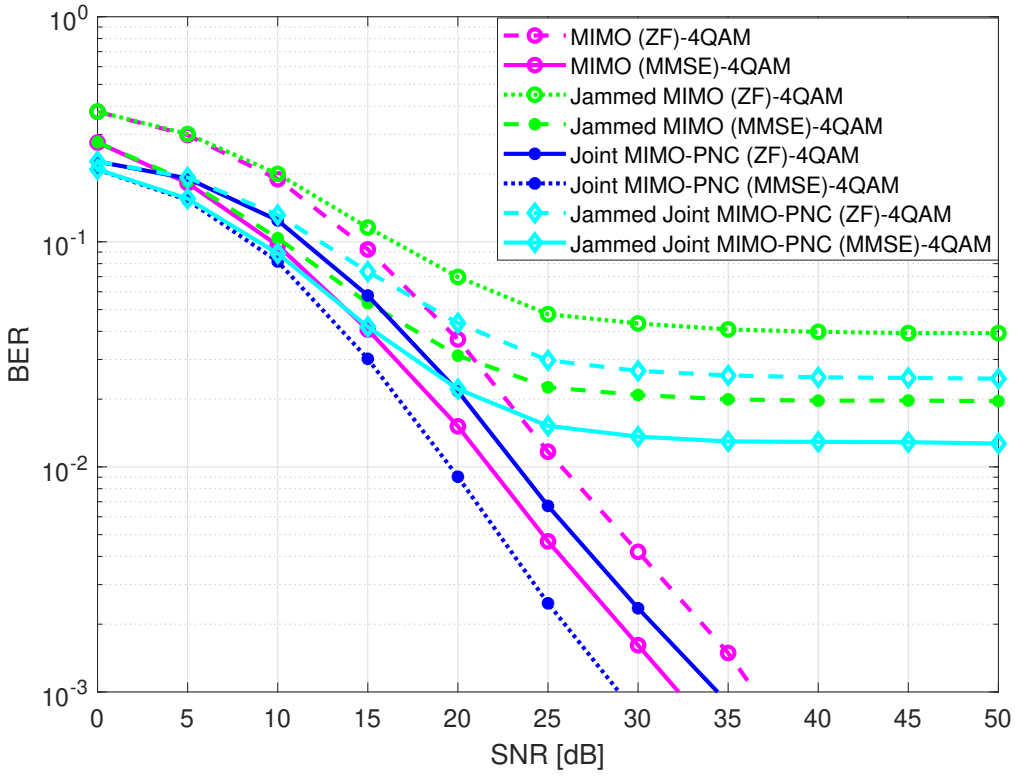

Fig. 4.2 BER performance comparison between i) conventional multi-user MIMO ii) multi-user MIMO with jamming, iii) multi-user MIMO with PNC and iv) multi-user MIMO with PNC and jamming, with 10dB jamming SJR , for M=4, N=2, K=2 and J=1.

of the PNC scheme performing well against jamming in the lower SNR region, and this is achieved at twice the spectral efficiency.

In Fig. 4.3, utilizing the same setup as Fig. 4.2, we doubled the number of antennas of the jammer. The simulation result revealed a degrade in the former compared to the latter. This is an indication that by increasing the number of antennas of the jammer, the jamming signal adversely influences the decoding capabilities of the base station. The jammer may not want to expend extra cost in its quest of impairing the decoding capabilities of the base station, by increasing the number of transmit antennas.

We increased the number of antennas at the base station to sixteen in Fig. 4.4, with the rest of the simulation parameters remaining the same as in Fig. 4.2. The simulation results of the former revealed a similar pattern to that of the latter, except the BER starts to remain

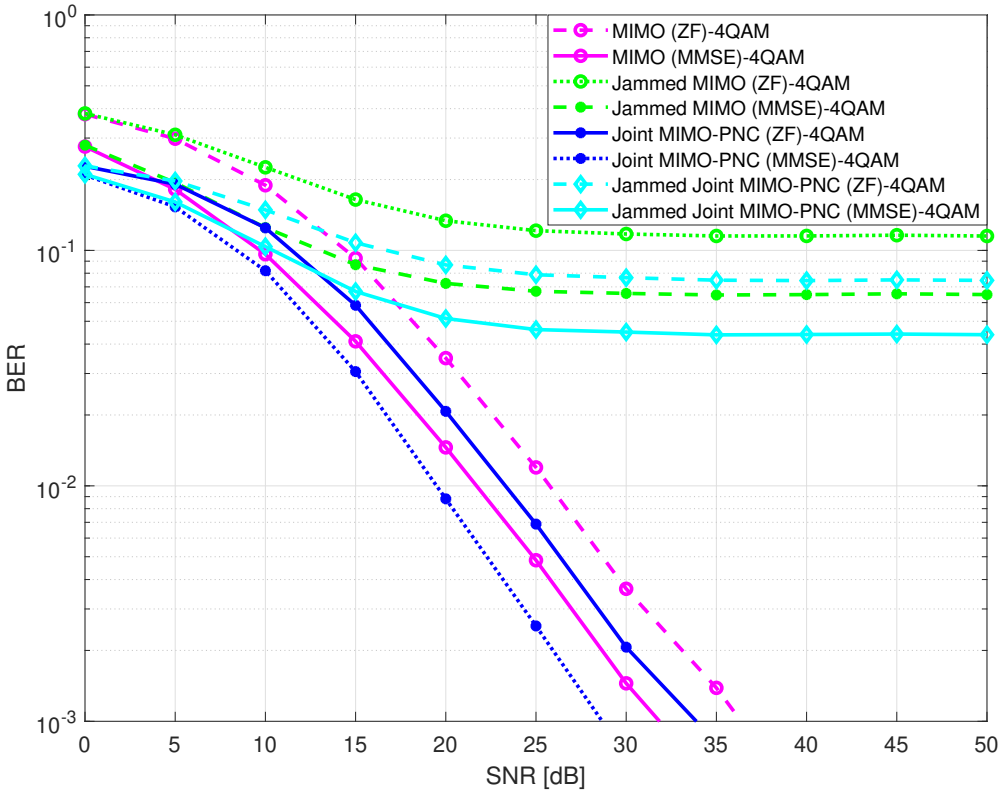

Fig. 4.3 BER performance comparison between i) conventional multi-user MIMO ii) multi-user MIMO with jamming, iii) multi-user MIMO with PNC and iv) multi-user MIMO with PNC and jamming, with 10dB jamming SJR, for M=4, N=2, K=2 and and J=2.

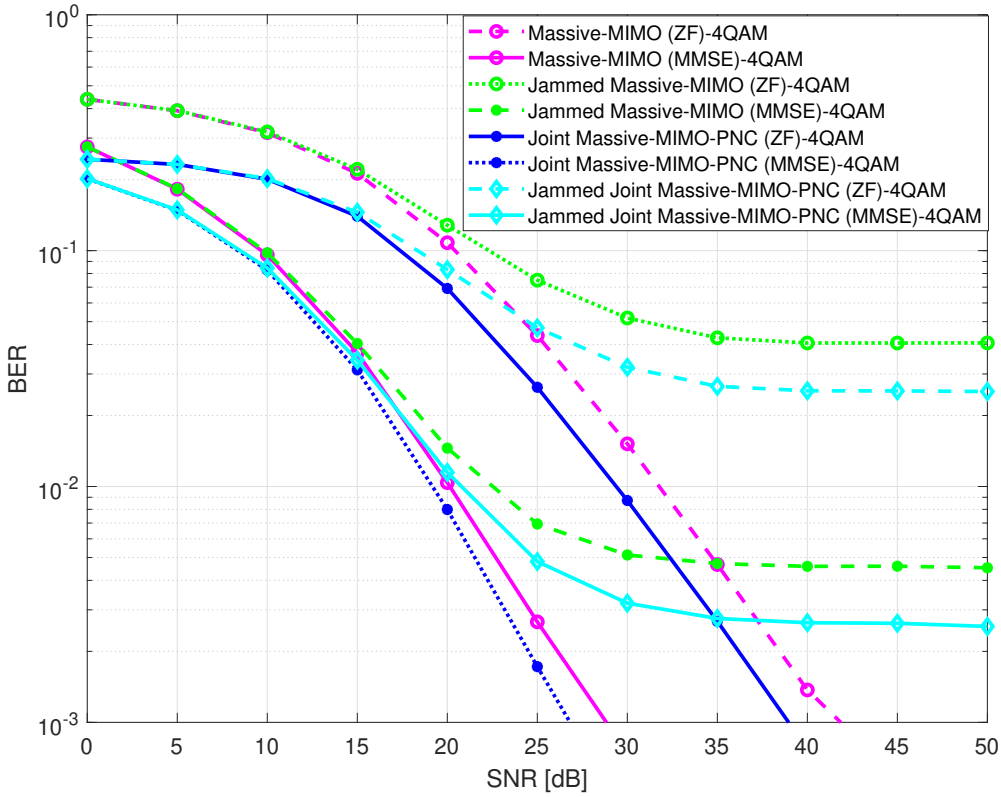

Fig. 4.4 BER performance comparison between i) conventional multi-user MIMO ii) multi-user MIMO with jamming, iii) multi-user MIMO with PNC and iv) multi-user MIMO with PNC and jamming, with 10dB jamming SJR, for M=16, N=8, K=2 and J=1.

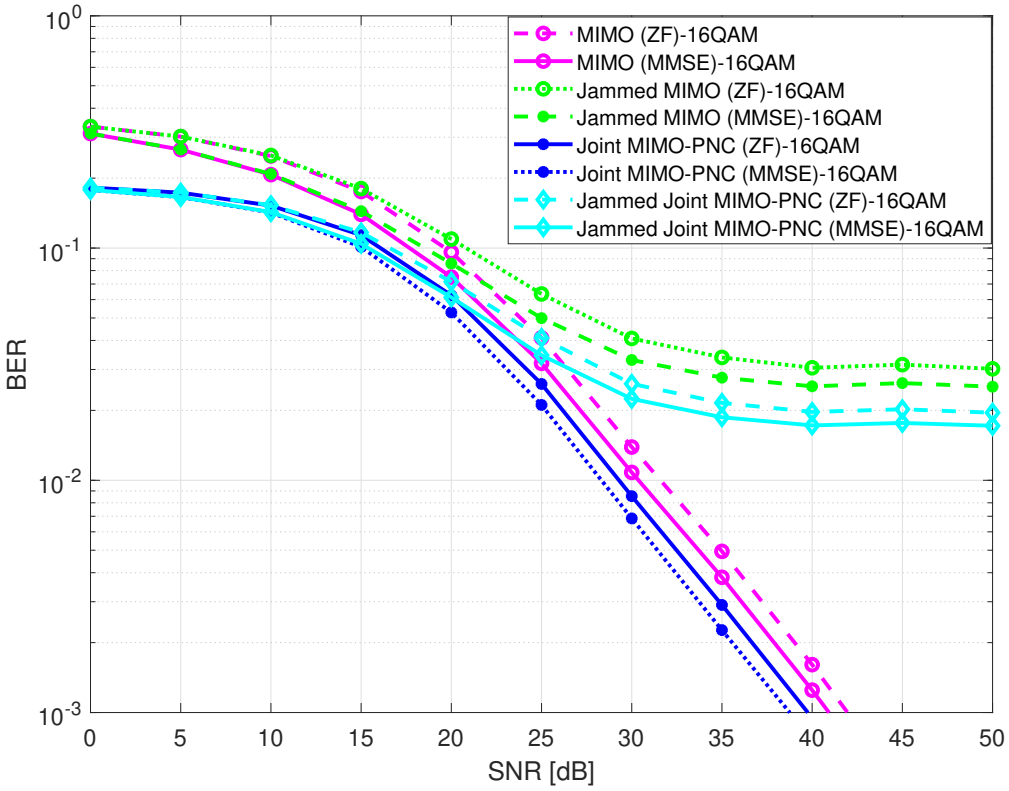

Fig. 4.5 BER performance comparison between i) conventional multi-user MIMO ii) multi-user MIMO with jamming, iii) multi-user MIMO with PNC and iv) multi-user MIMO with PNC and jamming, with 10dB jamming SJR, for M=4, N=2, K=2 and J=1.

steady after 30dB SNR. This is an indication that the more antennas the base station has, the better the resilience against a jamming attack it has in the lower SNR regions.

In Fig. 4.5, we repeated the setup in Fig. 4.2 and Fig. 4.3, respectively, except deploying a higher-order modulation scheme of 16-QAM. The result showed a similar pattern to the QPSK counterpart, except the performance is better, as the BER starts to remain steady at higher SNR, an indication that PNC performs better in the lower SNR regions against jamming attack.

4.4.2 In mmWave

In this subsection, we evaluate the BER performance in the mmWave communications under jamming attacks by employing PNC based on linear detection, which has lower complexity. The mmWave channel parameters described in [83] and [84] are used in our mmWave system simulation, which includes one base station having $M = 16$ antennas and communicating with $N = 16$ legitimate users. The simulation results are shown in Fig. 4.6. It is observed that the mmWave communications by employing PNC through linear detection provides much better performance compared to the conventional mmWave schemes.

4.5 Conclusions

In this section, we outlined the resilience of massive MIMO PNC to jamming attack in both sub-6 GHz and mmWave. In Chapter 3, we showed how the combination of massive MIMO and PNC does not impact the BER any worse than it would in massive MIMO system without PNC. Infact, our results revealed that the BER of massive MIMO and PNC is slightly better than the BER of only massive MIMO. Massive MIMO is generally resilient to jamming attack due to its high degree of freedom. We investigated our proposed work on massive MIMO and PNC against a barraging attack from a jammer, where the jammer is able to use any number of transmit antennas. Over Rayleigh fading channels, our simulation results revealed that massive MIMO PNC performs better in lower SNRs, as opposed to the conventional massive MIMO system, and at twice the spectral efficiency. In addition to that, for mmWave

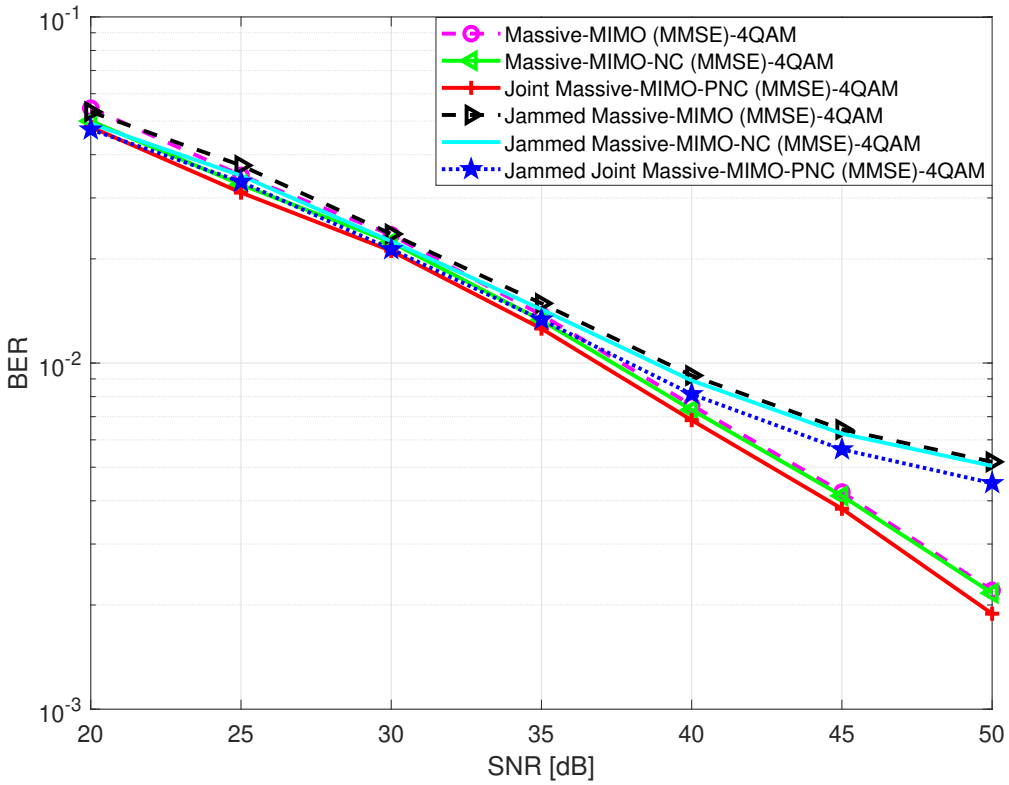

Fig. 4.6 BER performance comparison of mmWave communications for different schemes under jamming attack, with 30dB jamming SJR, for M=16, N=16, K=1 and J=1.

communications under jamming attack, the MIMO-PNC system still provides acceptable BER performance.

Chapter 5

Index Modulation and PNC in Massive MIMO

5.1 Introduction

The concept of Index Modulation (IM) has been introduced in 2.3. Indeed, IM is one of the most promising techniques for 5G and beyond [85]. Whilst the current wireless communication systems require that any information received at the receiver is actually sent by a transmitter, IM has found innovative means to convey information from the transmitter to the receiver without the signal necessarily being transmitted. Rather, it uses the indices of the transmitting resources to convey extra information bits. There have been growing need for techniques that offer a compromise between higher spectral efficiency (SE) and energy efficiency (EE) to be those that get considered in 5G and beyond, and IM shows promising performance gain in both metrics. The resources that IM operates on include sub-carriers, modulation types, time slots, transmit antennas among others [86].

IM introduces an additional dimension to the existing dimensions of wireless transmission that include space, time and frequency. By not using all the available resources to transmit, the communication systems can be designed at a lower cost, lower hardware complexity, reduced energy usage, as few of the resources are actively utilized at any time, and simultaneously guaranteeing high SE and capacity gain.

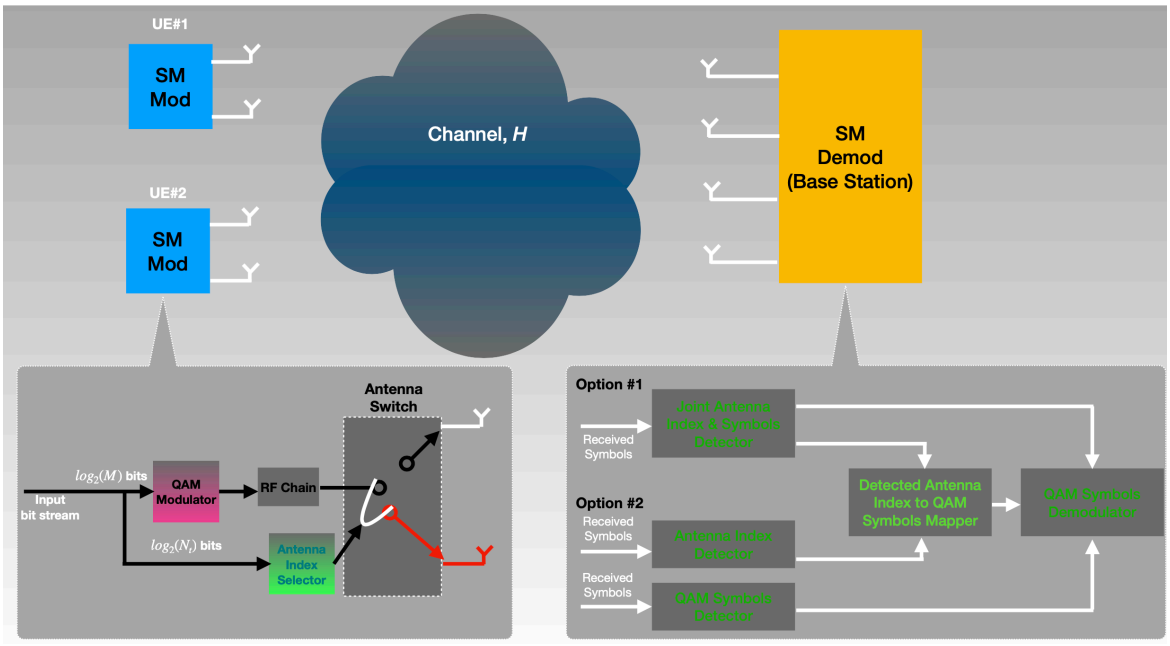

Fig. 5.1 Building functional blocks of a multi-user SM MIMO communication system.

One of the well research variant of IM is the Spatial Modulation (SM) and it will be the main focus in the next sub-section.

5.1.1 Spatial Modulation

While conventional MIMO communication systems leverage on the ability to use all the transmit antennas to increase multiplexing gain, by simultaneously transmitting data on all of them, SM, on the contrary, allows transmission over a single antenna. The stream of data to be transmitted is divided into two groups. One group decides which antenna is selected for transmission, and the other group is transmitted on the selected antenna. The receiver will, not only detect the transmitted data, but also the index of the transmit antenna used for the transmission. MIMO systems usually require one RF chain for each antenna element to be designed at the transmitter. However, such a design is costly, especially when a massive number of antennas are to be implemented. There have been greater strides in mitigating this cost with a blend of digital and analog designs [25]. However, in SM, since only a single antenna is activated at any time, only a single RF chain is therefore needed.

To re-illustrate how SM works, let us take Fig. 5.1 for example. In this figure, there is a base station, with four antennas, communicating with two UEs, each equipped with two antennas. To increase capacity in MIMO communication systems, the UEs would have to exhaust all their transmit antennas to send multiple data streams to the BS. Considering that battery powered communication devices, such as mobile phones, have limitations on the number of antennas they have to be equipped with, it is not scalable and practical, that by virtue of wanting to increase multiplexing gain, the number of antennas are increased. Assuming that the UEs will use QPSK/4-QAM to transmit the bit blocks, using SM, the QPSK bit block will be split into two: one that identifies the antenna that will be selected for transmission, and the other, the actual transmitted bits. For example, in Table 5.1, for QPSK bit block, "01", the bit '0' identifies antenna number one, and the bit '1' is mapped to one BPSK constellation symbol and transmitted on the selected antenna. This, inadvertently, results in a SE of 2bpcu (bits per channel use per user), one coming from the antenna index and the other from the BPSK symbol, although only a single bit is transmitted.

Table 5.1 SM Mapping of 4-QAM Bit block to Antenna Index and 2-QAM symbol.

Bits Block	**Antenna Index**	**Tx Symbol**
00	1	-1
01	1	1
10	2	-1
11	2	1

The main challenge with SM is the detection of the implicitly transmitted antenna index at the receiver or BS. In order to detect the selected antenna for each user, although nothing is transmitted on the non selected antennas, it is still imperative that all antennas are active. It is also important that the BS assumes the totality of both selected and the non selected antennas for the SM. Fig. 5.1 illustrates the building blocks that handle the received messages with the assumption that the transmitting nodes use SM. A joint detection of the antenna index and the transmitted symbols is usually the most common approach. Here, both the antenna index

and the transmitted symbols can be detected at the same time using Maximum Likelihood (ML) estimator. The detected antenna index can then further be decoded by mapping it to the corresponding symbol that was implicitly transmitted. The other alternative will be to use ML to detect the antenna index and use other practical detectors such as Zero-Forcing (ZF) and Minimum Mean Square Error (MMSE) to detect the transmitted symbols. Similar to the joint antenna index and transmitted symbol detection approach, the antenna index is further decoded by mapping it to the implicitly transmitted symbols. In Fig. 5.1, using two antennas, each transmitter is able to transmit QPSK symbols by splitting them into two BPSKs, one that identifies the antenna index and the other, physically transmitted on the selected antenna. By detecting the antenna index, the receiver is able to infer the corresponding bits or symbol at the transmitter. This implicit transmission of the symbols for the antenna index, increases energy efficiency, as half of the energy required to transmit QPSK is needed in SM.

5.2 Proposed Joint PNC and Index Modulation

A joint IM-PNC or SM-PNC is an attractive combination, as each have their unique characteristics, with some complimenting each other. Forexample, SM eliminates inter-channel-interference (ICI), whereas PNC embraces ICI. Therefore, the intriguing question is, how can PNC and IM/SM be combined?

In section 3.2, we showed how PNC and massive MIMO can be combined and the benefits they present. To combine massive MIMO PNC with IM/SM, assuming nothing changes in the architecture of MIMO-IM, as described in section 3.2, then, in uplink, depending on the QPSK bit block, each user uses the first bit to select an antenna and transmits the other half of the bit block on the selected antenna. Since in PNC, there is the need to estimate PNC mapping symbols, without necessarily decoding the individual transmitted symbols, detecting the antenna index alone is sufficient. Once the receiver knows the channel state information, or $\boldsymbol{H}$, our PNC scheme will first estimate the sum-difference of the transmitted symbols, and then use the PNC mapping algorithm to estimate PNC symbols from the estimated sum-difference symbols. In the case of the SM, the channel, $\boldsymbol{H}$, cannot be used by

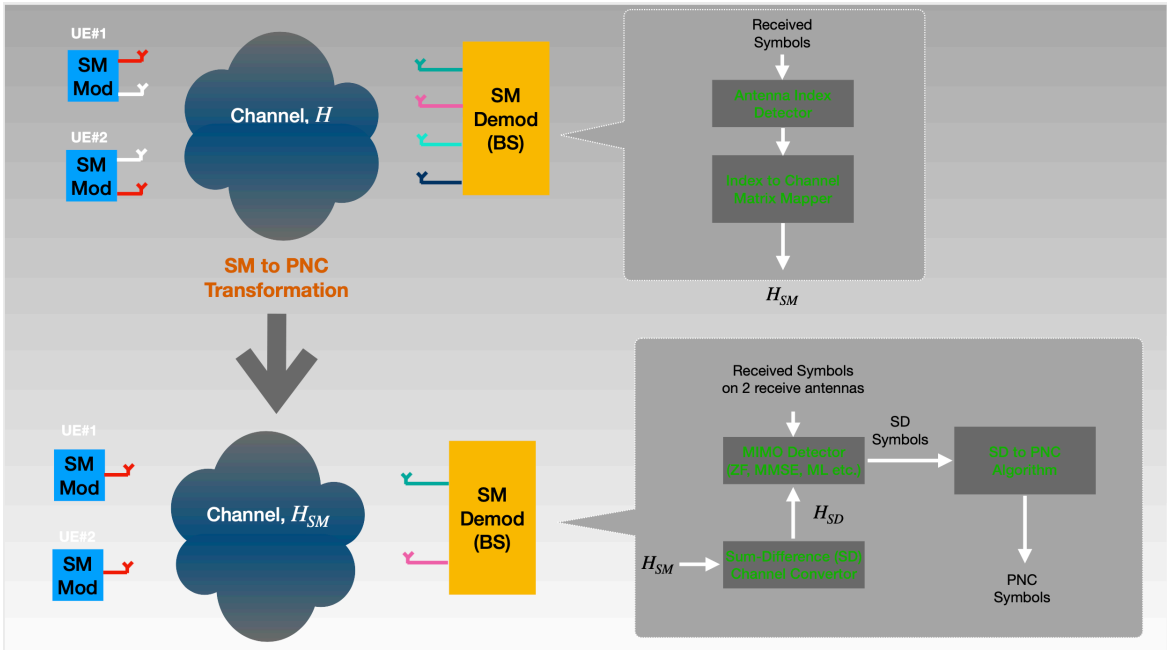

Fig. 5.2 Building functional blocks of a joint multi-user SM MIMO PNC communication system.

the PNC algorithm, because the algorithm operates on the symbols that have been actually transmitted. If the base station considers the antenna section of each user as a black box, it will only see transmissions coming out from a single antenna of each user and infer that only a single channel was used to transmit. Therefore, there is the need for a transformation from the two-antenna UEs to one-antenna UEs and this transformation requires that the channel, $\boldsymbol{H}$, itself is transformed. The transformation of the original channel, $\boldsymbol{H}$, can be achieved by first detecting the antenna index. Knowing the antenna index and the original channel, the columns not related to the antenna index can be masked out and the result will be the actual channels on which active antennas were used, i.e. $\boldsymbol{H}_{\mathrm{SM}}$. The receive symbols as a result of the $\boldsymbol{H}_{\mathrm{SM}}$ is given as,

$$\boldsymbol{r}_{\mathrm{SM}} = (\boldsymbol{H}_{\mathrm{SM}}\boldsymbol{P}_{\mathrm{sd}}{}^{-1})(\boldsymbol{P}_{\mathrm{sd}}\boldsymbol{s}) + \boldsymbol{z} \tag{5.1}$$

$$= \boldsymbol{H}_{\mathrm{sd}}^{\mathrm{SM}}\boldsymbol{s}_{\mathrm{sd}} + \boldsymbol{z}, \tag{5.2}$$

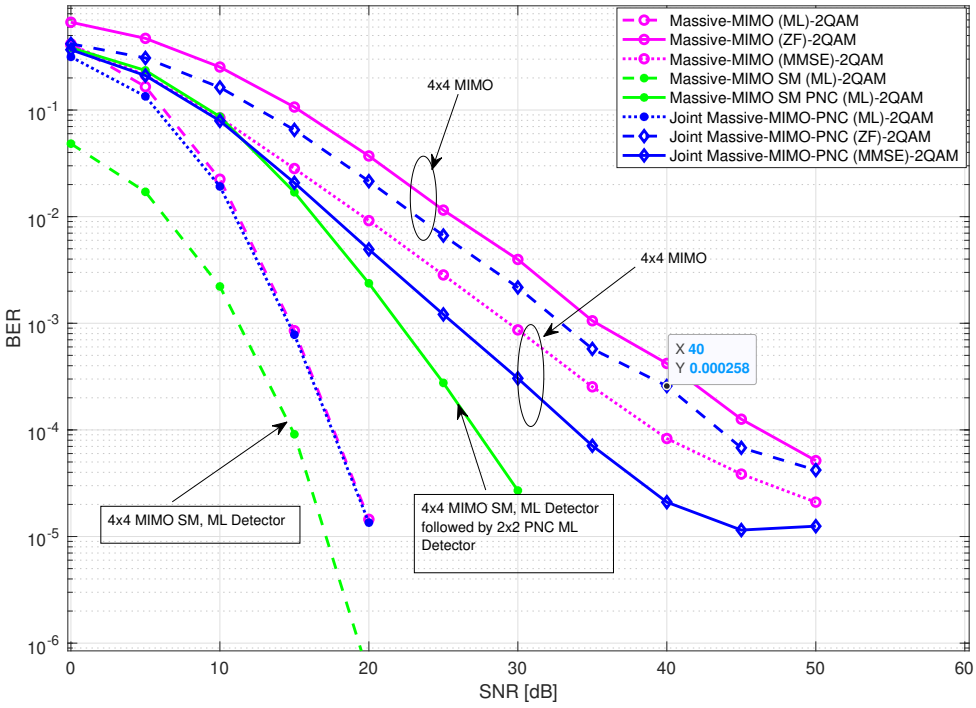

Fig. 5.3 A simulation results of 4 x 4 MIMO System that uses SM to estimate PNC symbols.

where $\boldsymbol{H}_{\text{sd}}^{\text{SM}}$ is the sum-difference channel matrix based on the transformed channel $\boldsymbol{H}_{\text{SD}}$. The equalization channel matrix for ZF and MMSE is further given as

$$\boldsymbol{G}_{\text{sd}} = \begin{cases} (\boldsymbol{H}_{\text{u}}^{\text{H}}\boldsymbol{H}_{\text{u}})^{-1}\boldsymbol{H}_{\text{u}}^{\text{H}}, & \text{for ZF} \\ (\boldsymbol{H}_{\text{u}}^{\text{H}}\boldsymbol{H}_{\text{u}} + \sigma_n^2\text{I})^{-1}\boldsymbol{H}_{\text{u}}^{\text{H}}, & \text{for MMSE} \end{cases}, \tag{5.3}$$

where $\boldsymbol{H}_{\text{u}} = \boldsymbol{H}_{\text{sd}}^{\text{SM}}$. In this example, considering that only two transmit antennas were used collectively by the users, two of the received symbols have to be operated on by the PNC algorithm. After the transformation, the original 4-QAM transforms into a 2-QAM/BPSK.

In Fig. 5.3, a 4 x 4 MIMO system was simulated using spatial modulation. In this setup, each user has two transmit antennas and the BS, four antennas. Each user transmits using QPSK modulation scheme and at any transmit time, because of SM, only a single antenna is utilized by each user. At the receiver, the BS estimates PNC symbols from the QPSK-based SM transmitted symbols using the building block in Fig. 5.2. The simulation results in Fig.

5.3 reveal that it is indeed feasible to combine PNC and SM, where the EE is significantly reduced. The error performance results indicated that the joint MIMO PNC and IM does perform better than the other PNC schemes, but performs a little poorly against the MIMO SM. The reason could be attributed to the fact that in the MIMO SM, the individual symbols are joint detected, whereas with joint MIMO PNC and IM, the antenna index and symbol detection are done independently of each other, with the former involved in the formulating of the channel matrix, which is then used in the PNC estimation algorithm in handling the latter.

In this work, the antenna index and the modulated transmitted symbols are jointly detected using ML [87] as in (5.4)

$$[\widehat{\boldsymbol{s}}, \widehat{\boldsymbol{m}}] = \underset{s, 1<m<M}{\operatorname{argmin}} \|\boldsymbol{r} - \boldsymbol{H}_{\mathrm{SM}}\boldsymbol{s}\|^2, \tag{5.4}$$

where H_{SM} is now an $N \times 1$ channel vector, and m is the m^{th} antenna index that minimises the equation, and whose estimate is then mapped to the transmitted bits which are associated to that index. The detection of $\widehat{\boldsymbol{s}}$ has already been explained in previous sections.

5.3 Conclusions

In this section, we presented a novel approach of combining PNC and SM, a variant of Index Modulation. Individually, each of these physical layer techniques, offer compelling performance benefits that foster a good balance between the EE and SE if combined. PNC leverages on the interference from different transmitters to provide high capacity gain and also increase SE, whereas IM or SM uses few available resources to achieve a similar capacity again, as if all resources were utilized, leading to higher EE. We presented simulation results of the combined techniques and although the performance is good, it would still require further research to make it as practical as possible, by finding joint detecting techniques that have similar or near to, performance of ML detector.

Chapter 6

Conclusions and Future Works

In this thesis, we designed and implemented a practical PNC scheme that operates in a MIMO system. Our MIMO system model can have any antenna dimension, allowing our design to include massive MIMO systems. We considered M-QAM modulation schemes and focused mostly on the square dimension. Similarly, the dimension of the channel matrix considered is square (i.e the matrix has the same number of rows and columns) for the sake of simplicity. We also assumed that the UEs can be equipped with several antennas, but there is a central entity that each of the UEs have to communicate through in order to reach the other end users. The end goal is for the users to exchange information among themselves through this central entity. The central entity can be likened to the modern day cellular base station and is equipped with large number of antennas. Another assumption considered is that there is a perfect synchronisation in transmission by the users to the central station. This is a sharp contrast to real life cellular systems where the transmissions and receptions are not perfectly synchronised, but for simplicity sake, we adopted perfect synchronisation. Furthermore, in simplifying the system model, we also adopted the Rayleigh fading channel model, where the effect of multi-path propagation is factored in.

In our proposed massive MIMO PNC scheme, we grouped the antennas, if multi-antenna UEs, or the individual UEs, if single antenna, into clusters. Each cluster is formulated as a sum and difference of the signals from the antenna pairs of the transmitting UEs. This is achieved with a sum and difference matrix of similar dimension as the the channel matrix.

Therefore, and at the receiver, rather estimating the transmitted symbols from the receive signals, the central station will estimate the sum-difference signals from the receive antennas in each cluster. The estimation of the sum difference symbols is achieved by transforming the known channel matrix with corresponding sum-difference identity matrix. This inherently creates a summation and difference of transmitted symbols at the receiver, one articulated by the proposed PNC scheme. Utilizing linear detectors such as ZF and MMSE, based on the sum-difference linearly transformed channel matrix, the sum-difference symbols can be detected from the received symbols by the central station. Employing Maximum A-posterior (MAP) soft decoding, we mapped the detected sum-difference symbols to the PNC symbols. These PNC symbols are transmitted back to the users in the DL phase, and each user in the cluster can then decode what was transmitted by the other users in the uplink phase. The design is generic enough to handle any number of antennas at the users and also at the central station. But practically, only few antennas can be utilized by each UE.

Considering square M-QAM modulation scheme, several simulations were carried out and the results revealed that using existing MIMO detection schemes, such as ZF and MMSE, our proposed PNC scheme achieves twice the spectral efficiency of conventional massive MIMO. The BER of our scheme was better than the conventional massive MIMO, indicating that our proposed PNC scheme can be deployed without sacrificing the BER of the conventional massive MIMO. Furthermore, the results also revealed that for lower throughput and at low SNR, 4-QAM appears to be the preferred modulation scheme, whereas 64-QAM or higher is the preferred scheme in higher SNR, and for higher throughput.

Having demonstrated the feasibility of a joint PNC and massive MIMO in a single system, we went further to investigate our proposed PNC scheme's resilience against jamming attack. Jamming attack is often intentional and malicious, with the intent of sabotaging a communication system of functioning properly, by bombarding the system with jamming signals or noise. The end result is that the legitimate users are not able to properly decode the receive signals because of the interfering jamming signals. Massive MIMO is noted for its resilience against jamming, due to its high degree of freedom. We simulated our joint massive MIMO and PNC scheme utilizing Rayleigh fading in sub-6GHz, as well as the

mmWave channel. Legitimate users communicate through the central station, whilst lurking in this is a jammer sending jamming signals. The jammer is able to use any number of transmit antennas. Our simulation results reveal that our proposed PNC scheme in massive MIMO system does not deteriorate the latter's resilience to jamming, whist still increasing the spectral efficiency by two. Infact, our results revealed that the BER of the joint massive MIMO and PNC is slightly better than the BER of only massive MIMO. Over Rayleigh fading channels, our simulation results revealed that massive MIMO PNC performs better in lower SNRs, as opposed to the conventional massive MIMO system, and at twice the spectral efficiency. In addition to that, for mmWave communications under jamming attack, the MIMO-PNC system still provided acceptable BER performance.

IM is a novel physical layer technique that boosts energy efficiency by utilizing fewer resources than usual, to transmit. However, the indices of the utilized resources inherently carry information, if the receiver can detect them. A joint IM and massive MIMO PNC, if feasible, is expected to create a good balance between the spectral and energy efficiencies. In this thesis, we considered the Spatial Modulation (SM) variant of the IM, where a single antenna has to be selected for transmission, and besides detecting the actual transmitted symbols, the receiver has to also detect the index of the antenna utilized for transmission. By so doing, the receiver would have inferred the information bits or symbols used to select the antenna. In our proposed PNC-IM scheme, we showed how to transform the original channel matrix for the IM to the channel matrix suited for the estimation of the PNC symbols. We simulated the joint IM and massive MIMO PNC scheme and our simulation results revealed that, although the performance is relatively good, it would still require further research to make it as practical as possible. Further research effort would be required in designing joint detecting techniques that avoid detecting the antenna index separately from detecting the transmitted symbols.

We have shown the feasibility of a joint massive MIMO and PNC, a joint IM and PNC and also shown the resilience that the joint massive MIMO and PNC have on jamming attack. However, further research will be required to bring this work closer to its realization in the practical systems. The following are some of the proposed future derivative works:

- We believe asynchronisation of transmissions would have to be addressed. In practical cellular networks, users can transmit at anytime and there is no synchronisation in their transmissions. In our work, we had to adopt a synchronised system model to simplify the modeling. However, asyncrhonisation has to be considered to realize its practically.

- Similarly, the modulation scheme for our proposed PNC scheme in this thesis work is M-QAM. We assumed that the users adopts the same modulation scheme and transmission for simplicity sake. However, in real wireless communication networks, users can be configured to use different modulation schemes and can be at different distances to the central station, and therefore experiencing different fading. We believe further research in having users use different modulation schemes for our proposed PNC scheme would shed some light into how this scheme would operate in real systems.

- The same goes for non-square channel matrix, here the matrix's rows and columns have different dimensions. Although, we adopted a square channel matrix in our modeling and simulation, this is not always true in real systems. We believe our proposed PNC scheme would work well with non-square channel matrices. However a thorough investigation and performance analysis are needed.

- Finally, we believe the relatively good results we have had for the joint IM and the PNC is the fact that we adopted detectors not fully aligned with the joint scheme. The detectors for the indices and that of the received sum-differences should be joint designed and we believe further research is required here to design and analyze the performance of such detectors.

References

[1] G. Fodor, N. Rajatheva, W. Zirwas, L. Thiele, M. Kurras, K. Guo, A. Tolli, J. H. Sorensen, and E. Carvalho. An Overview of Massive MIMO Technology Components in METIS. *IEEE Commun. Mag.*, 6:155–161, 2017.

[2] E. G. Larrson, O. Edfors, F. Tufvesson, and T. L. Marzetta. Massive MIMO for Next Generation Wireless Systems. *IEEE Commun. Mag.*, 52:186–195, 2014.

[3] P. Chen, Z. Xie, Y. Fang, Z. Chen, S. Mumtaz, and J. J. P. C. Rodrigues. Physical-Layer Network Coding: An Efficient Technique for Wireless Communications. *IEEE Network*, 34(2):270–276, 2020.

[4] Y. Arjoune and S. Faruque. Smart Jamming Attacks in 5G New Radio: A Review. *Comput. and Commun. Workshop and Conf.*, pages 1010–1015, 2020.

[5] Z. Feng and C. Hua. Machine Learning-based RF Jamming Detection in Wireless Networks. *Int. Conf. on Sec. of Smart Cities*, pages 1–6, 2018.

[6] S. Doğan Tusha, A. Tusha, E. Basar, and H. Arslan. Multidimensional Index Modulation for 5G and Beyond Wireless Networks. *Proceedings of the IEEE*, 109(2):170–199, 2021.

[7] S. Zhang and S.C. Liew. Physical Layer Network Coding with Multiple Antennas. *IEEE Wireless Commun. and Net. Conf.*, pages 1–6, 2010.

[8] G. J. Foschini. Layered space-time architecture for wireless communication in a fading environment when using multi-element antennas. *Bell Labs Technical Journal*, 1(2):41–59, 1996.

[9] P. W. Wolniansky, G. J. Foschini, G. D. Golden, and R. A. Valenzuela. V-BLAST: an architecture for realizing very high data rates over the rich-scattering wireless channel. *Int. Symposium on Sign., Sys., and Elec.*, page 295–300, 1998.

[10] G. D. Golden, G. J. Foschini, R. A. Valenzuela, and P. W. Wolniansky. Detection algorithm and initial laboratory results using V-BLAST space-time communication architecture. *Elec. Letters*, 35(1):14–16, 1999.

[11] D. Senaratne and C. Tellambura. Spatial Multipath Resolution for MIMO System. *IEEE Wireless Commun. Letters*, 1(1):10–13, 2012.

[12] M. El-Hajjar and L. Hanzo. Multifunctional MIMO systems: A combined diversity and multiplexing design perspective. *IEEE Wireless Commun.*, 17(2):73–79, 2010.

[13] C. X. Wang, X. Hong, X. Ge, X. Cheng, G. Zhang, and J. Thompson. Cooperative MIMO channel models: A survey. *IEEE Commun. Mag.*, 48(2):80–87, 2010.

[14] A. M. Shteiman, S. Galli, L. Mailaender, and X. F. Qi. The Effect of Diversity Combining on ISI in Massive MIMO. *IEEE Vehicular Techn. Conf.*, pages 1–6, 2018.

[15] G. J. Foschini and M. J. Gans. On limits of wireless communications in a fading environment when using multiple antennas. *Wireless Pers. Commun*, (3):311–315, 1998.

[16] T.M. Cover and J.A. Thomas. *Elements of Information Theory*. Wiley, Germany, 2012.

[17] T. Alexander, W. Mazurczyk, A. Mishra, and A. Perotti. Mobile Communications and Networks. *IEEE Commun. Mag.*, 57:42–42, 2019.

[18] Q. H. Spencer, C. B. Peel, A. L. Swindlehurst, and M. Haardt. An introduction to the multi-user MIMO downlink. *IEEE Commun. Mag.*, 42(10):60–67, 2004.

[19] A. Kurve. Multi-user MIMO systems: the future in the making," in IEEE Potentials. *IEEE Potentials*, 28(6):37–42, 2009.

[20] F. Rusek, D. Persson, B. K. Lau, E. G. Larsson, T. L. Marzetta, O. Edfors, and et al. Noncooperative Cellular Wireless With Unlimited Numbers of Base Station Antennas. *IEEE Trans. Wireless Commun.*, 9(1):3590–3600, 2010.

[21] F. Rusek, D. Persson, B. K. Lau, E. G. Larsson, T. L. Marzetta, O. Edfors, and et al. Scaling up MIMO: Opportunities and Challenges With Very Large Arrays. *IEEE Signal Process. Mag.*, 30(1):40–60, 2013.

[22] T. L. Marzetta. Massive MIMO: An Introduction. *Bell Labs Technical Journal*, 20:11–22, 2015.

[23] C. Studer and E. G. Larsson. PAR-Aware Large-Scale Multi-User MIMO-OFDM Downlink. *IEEE J. Sel. Areas Commun.*, 31(2):303–313, 2013.

[24] F. W. Vook, A. Ghosh, E. Diarte, and M. Murphy. 5G New Radio: Overview and Performance. *Conference on Signals, Systems, and Computers*, pages 1247–1251, 2018.

[25] S. A. Busari, K. M. S. Huq, S. Mumtaz, L. Dai, and J. Rodriguez. Millimeter-Wave Massive MIMO Communication for Future Wireless Systems: A Survey. *IEEE Commun. Surveys and Tuts*, 20(2):836–869, 2018.

[26] M. A. M. Albreem. 5G wireless communication systems: Vision and challenges. *Int. Conf. on Computers, Commun., and Contr. Technol.*, page 493–497, 2015.

[27] H. Yang and T. L. Marzetta. Performance of Conjugate and Zeroforcing Beamforming in Large-Scale Antenna Systems. *IEEE J. Sel. Areas Commun.*, 31(2):172–179, 2013.

[28] S. Buzzi and C. D'Andrea. Are mmWave Low-Complexity Beamforming Structures Energy-Efficient? Analysis of the Downlink MU-MIMO. *IEEE Globecom*, 2016.

[29] A. Faisal, H. Sarieddeen, H. Dahrouj, T. Y. Al-Naffouri, and M. S. Alouini. Ultramassive MIMO Systems at Terahertz Bands: Prospects and Challenges. *IEEE Vehicular Techn. Mag.*, 15(4):33–42, 2020.

[30] A. A. Esswie, M. El-Absi, O. A. Dobre, S. Ikki, , and T. Kaiser. A novel FDD massive MIMO system based on downlink spatial channel estimation without CSIT. *IEEE Int. Conf. Commun.*, pages 1–6, 2017.

[31] Chockalingam A and B. Rajan. *Large MIMO Systemss*. Cambridge University Press, Cambridge UK, 2014.

[32] E. G. Larsson. MIMO Detection Methods: How They Work [Lecture Notes]. *IEEE Sign. Proc. Mag.*, 26(3):91–95, 2009.

[33] I.E. Telatar. Capacity of Multi-antenna Gaussian Channels. *European Trans. on Telecommun.*, 10(3):585–595, 1999.

[34] V. Tarokh, N. Seshadri, and AR Calderbank. Space-time codes for high data rate wireless communication: performance criterion and code construction. *IEEE Trans. Infor. Theory*, 44(2):744–765, 1998.

[35] J.C. Guey, M.P. Fitz, M.R. Bell, and W.Y. Kuo. Signal design for transmitter diversity wireless communication systems over Rayleigh fading channels. *IEEE Trans. on Commun.*, 47(4):527–537, 1999.

[36] S. M. Alamouti. A Simple Transmit Diversity Technique for Wireless Communication. *IEEE Journal on Sel. Areas in Commun.*, 16(8):1451–1454, 1998.

[37] M. A. Albreem, M. Juntti, and S. Shahabuddin. Massive MIMO Detection Techniques: A Survey. *IEEE Commun. Surveys Tut.*, 21(4):3109–3132, 2019.

[38] R. Ahlswede, N. Cai, S.Y. Li, and R. Yeung. Network information flow. *IEEE Trans. Inf. Theory*, 46(4):1204–1216, 2000.

[39] S.Y. Li, R. Yeung, and N. Cai. Linear network coding. *IEEE Trans. Inf. Theory*, 49(2):371–381, 2003.

[40] R. Koetter and M. Medard. An algebraic approach to network coding. *IEEE Trans. Netw.*, 11(5):782–795, 2003.

[41] S. L. Zhang, S. C. Liew, and P. P. Lam. Hot Topic: Physical-layer Network Coding. *Int. Conf. on Mobile Computing and Networking*, pages 358–365, 2006.

[42] B. Nazer and M. Gastpar. Computing over multiple-access channels with connections to wireless network coding. *IEEE Int. Symp. Inf. Theory*, page 1354–1358, 2006.

[43] P. Popovski and H. Yomo. The anti-packets can increase the achievable throughput of a wireless multi-hop network. *IEEE Int. Conf. Commun.*, page 3885–3890, 2006.

[44] T. Yang and I. B. Collings. On the Optimal Design and Performance of Linear Physical-Layer Network Coding for Fading Two-Way Relay Channels. *IEEE Trans. Wireless Commun.*, 13(2):956–967, 2004.

[45] D. H. Vu and X. N. Tran. Physical network coding for bidirectional relay MIMO-SDM system. *Int. Conf. on Advanced Techno. for Commun.*, pages 141–146, 2013.

[46] L. Shi, T. Yang, K. Cai, P. Chen, and T. Guo. On MIMO Linear Physical-Layer Network Coding: Full-Rate Full-Diversity Design and Optimization. *IEEE Trans. on Wireless Commun.*, 17(5):3498–3511, 2018.

[47] T. Yang, X. Yuan, L. Ping, I.B. Collings, and J. Yuan. Eigen-Direction Alignment Aided Physical Layer Network Coding for MIMO Two-Way Relay Channels. *IEEE Int. Symp. on Information Theory*, pages 2253–2257, 2011.

[48] T. Yang, X. Yuan, L. Ping, I.B. Collings, and J. Yuan. A new physical-layer network coding scheme with eigen-direction alignment precoding for MIMO two-way relaying. *IEEE Trans. Commun.*, 61(3):973–986, 2013.

[49] D. G. M. Mitchell, M. Lentmaier, and D. J. Costello. Spatially Coupled LDPC Codes Constructed From Protographs. *IEEE Trans. on Information Theory*, 61(9):4866–4889, 2015.

[50] Y. Fang, P. Chen, G. Cai, F. C. M. Lau, S. C. Liew, and G. Han. Outage-Limit-Approaching Channel Coding for Future Wireless Communications: Root-Protograph Low-Density Parity-Check Codes. *IEEE Vehicular Techn. Mag.*, 14(2):85–93, 2019.

[51] Z. Ding, I. Krikidis, J. Thompson, and K. K. Leung. Physical layer network coding and precoding for the two-way relay channel in cellular systems. *IEEE Trans. Signal Process.*, 59(2):696–712, 2011.

[52] S. Liew, S. Zhang, and L. Lu. Physical-layer network coding: Tutorial survey and beyond. *Phys. Commun.*, 6(1):4–42, 2013.

[53] M. Huang, J. Yuan, and T. Yang. Error probability of physical-layer network coding in multiple-antenna two-way relay channel. *IEEE Global Commun. Conf.*, 2012.

[54] M. Huang, J. Yuan, and T. Yang. Physical-layer network coding with Alamouti scheme for the TWRC with linear decoder. *Australian Commun. Theory Workshop*, 2014.

[55] M. Huang, J. Yuan, and T. Yang. Error Performance of Physical-Layer Network Coding in Multiple-Antenna TWRC. *IEEE Trans. Vehicular Tech.*, 63:3750 – 3761, 2014.

[56] S. Zhang, Q. F. Zhou, C. Kai, and W. Zhang. Full Diversity Physical-Layer Network Coding in Two-Way Relay Channels With Multiple Antennas. *IEEE Trans. Wireless Commun.*, 13:4273–4282, 2014.

[57] J. S. Lemos and F. A. Monteiro. Full-duplex massive MIMO with physical layer network coding for the two-way relay channel. *IEEE Sensor Array Multichannel Signal Process. Workshop*, pages 1–5, 2016.

[58] T. Mao, Q. Wang, Z. Wang, and S. Chen. Novel Index Modulation Techniques: A Survey. *IEEE Commun. Surveys Tutorials*, 21(1):315–348, 2019.

[59] S. Dogan-Tusha, A. Tusha, E. Basar, and H. Arslan. Multidimensional Index Modulation for 5G and Beyond Wireless Networks. *arXiv:2010.00850*, 2020.

[60] M. Di Renzo, H. Haas, , and P. M. Grant. Spatial modulation for multiple-antenna wireless systems. *IEEE Commun. Mag.*, 49(12):182–191, 2011.

[61] H. S. Hussein, M. Elsayed, U. S. Mohamed, H. Esmaiel, and E. M. Mohamed. Spectral Efficient Spatial Modulation Techniques. *IEEE Access*, 7:1454–1469, 2019.

[62] Y. Wu and W. Y. Zou. Orthogonal frequency division multiplexing: A multi-carrier modulation scheme. *IEEE Trans. Consum. Electron.*, 41(3):392–399, 1995.

[63] C. B. Barneto et al. Full-Duplex OFDM Radar With LTE and 5G NR Waveforms: Challenges, Solutions, and Measurements. *IEEE Trans. on Microwave Theory and Techniques*, 67(10):4042–4054, 2019.

[64] E. Basar, U. Aygolu, E. Panayirci, and H. V. Poor. Orthogonal frequency division multiplexing with index modulation. *IEEE Trans. Signal Process.*, 61(22):5536–5549, 2013.

[65] R. Abu-alhiga and H. Haas. Subcarrier-index modulation OFDM. *IEEE Int. Symp. Pers., Indoor Mobile Radio Commun.*, page 177–181, 2009.

[66] D. Tsonev, S. Sinanovic, and H. Haas. Enhanced subcarrier index modulation (SIM) OFDM. *IEEE Global Telecommun. Conf. Workshops*, page 728–732, 2011.

[67] E. Basar. Multiple-input multiple-output OFDM with index modulation. *IEEE Signal Process. Lett.*, 22(12):2259–2263, 2015.

[68] E. Basar. On multiple-input multiple-output OFDM with index modulation for next generation wireless networks. *IEEE Trans. Signal Process.*, 64(15):3868–3878, 2016.

[69] M. Nakao, T. Ishihara, and S. Sugiura. Single-carrier frequency domain equalization with index modulation. *IEEE Commun. Lett.*, 21(2):298–301, 2017.

[70] M. Nakao, T. Ishihara, and S. Sugiura. Dual-mode time-domain index modulation for Nyquist-criterion and faster-than-Nyquist single-carrier transmissions. *IEEE Access*, 5:27659–27667, 2017.

[71] S. Jacob, T. L. Narasimhan, and A. Chockalingam. Space-time index modulation. *WCNC*, pages 1–6, 2017.

[72] H. Zhang and L. Cai. Design of Channel Coded Heterogeneous Modulation Physical Layer Network Coding. *IEEE Trans. Vehicular Techn.*, 67(3):2219–2230, 2018.

[73] F. A. P. Figueiredo, J. P. Miranda, F. L. Figueiredo, and F. A. C. M. Cardoso. Uplink performance evaluation of massive mu-mimo systems. *ArXiv*, abs/1503.02192, 2015.

[74] A. J. Viterbi. An Intuitive Justification and a Simplified Implementation of the MAP Decoder for Convolutional Codes. *IEEE Select. Areas Commun.*, 16:260–264, 1998.

[75] L. Shi and S. C. Liew. Complex Linear Physical-Layer Network Coding. *IEEE Trans. Info. Theory*, 63(8):4949–4981, 2017.

[76] E. Bout, V. Loscri, and A. Gallais. Energy and Distance evaluation for Jamming Attacks in wireless networks. *Int. Symp. on Distr. Sim. and Real Time Appl.*, pages 1–5, 2020.

[77] Y. Zou, J. Zhu, X. Wang, and L. Hanzo. A Survey on Wireless Security: Technical Challenges, Recent Advances, and Future Trends. *In Proceedings of the IEEE*, 104(9):1727–1765, 2020.

[78] A. Mpitziopoulos, D. Gavalas, C. Konstantopoulos, and G. Pantziou. A survey on jamming attacks and countermeasures in wsns. *In Proceedings of the IEEE*, 11:42–56, 2009.

[79] J. Gao, S. A. Vorobyov, H. Jiang, and V. H. Poor. Worst-case jamming on MIMO Gaussian channels. *IEEE Trans. Sign. Proc.*, 63:5821–5836, 2016.

[80] Z. Xiao, B. Gao, S. Liu, and L. Xiao. Learning based power control for mmWave massive MIMO against jamming. *GLOBECOM*, 63:1–6, 2018.

[81] J. Zhu, Z. Wang, Q. Li, H. Chen, and N. Ansari. Mitigating Intended Jamming in mmWave MIMO by Hybrid Beamforming. *IEEE Wireless Commun. Let.*, 8(6):1617–1620, 2019.

[82] S. N. Diggavi and T. M. Cover. The worst additive noise under a covariance constraint. *IEEE Trans. Inf. Theory*, 47(7):3072–3081, 2001.

[83] M. K. Samimi and T. S. Rappaport. 3-D millimeter-wave statistical channel model for 5G wireless system design. *IEEE Trans. on Micro. Theory and Techn.*, 64(7):2207–2225, 2016.

[84] I. A. Hemadeh, K. Satyanarayana, M. El-Hajjar, and L. Hanzo. Millimeter-wave communications: Physical channel models, design considerations, antenna constructions, and link-budget. *IEEE Commun. Surv. and Tut.*, 20(2):870–913, 2018.

[85] E. Basar. Reconfigurable Intelligent Surface-Based Index Modulation: A New Beyond MIMO Paradigm for 6G. *IEEE Trans. on Commun.*, 68(5):3187–3196, 2020.

[86] E. Basar, M. Wen, R. Mesleh, M. Di Renzo, Y. Xiao, and H. Haas. Index Modulation Techniques for Next-Generation Wireless Networks. *IEEE Access*, (5):16693–16746, 2017.

[87] A. Younis, N. Serafimovski, R. Mesleh, and H. Haas. Generalised spatial modulation. *Asilomar Conf, on Signals, Systems and Computers*, pages 1498–1502, 2010.